FACULTY OF SCIENCE AND TECHNOLOGY

MASTER'S THESIS

Study programme / specialisation: Petroleum Engineering / Drilling & Well Engineering	Spring semester, 2020 Open
Author: Andreas Sandvik Jakobsen Håkon Hagen	*Andreas Sandvik Jakobsen* .... *Håkon Hagen* .... (signature of author)
Programme coordinator: Anita Malde Supervisor(s): Dan Sui	
Title of master's thesis: Design and Optimization of an Autonomous Laboratory-Scale Drilling Rig and Bit Design for Directional Drilling	
Credits (ECTS): 30	
Keywords: Drilling Automation Downhole Sensor Bit Design ROP Optimization Drillbotics Directional Drilling Drill String Mechanics	Number of pages: 168 + supplemental material/other: 57 Stavanger, 03. July 2020
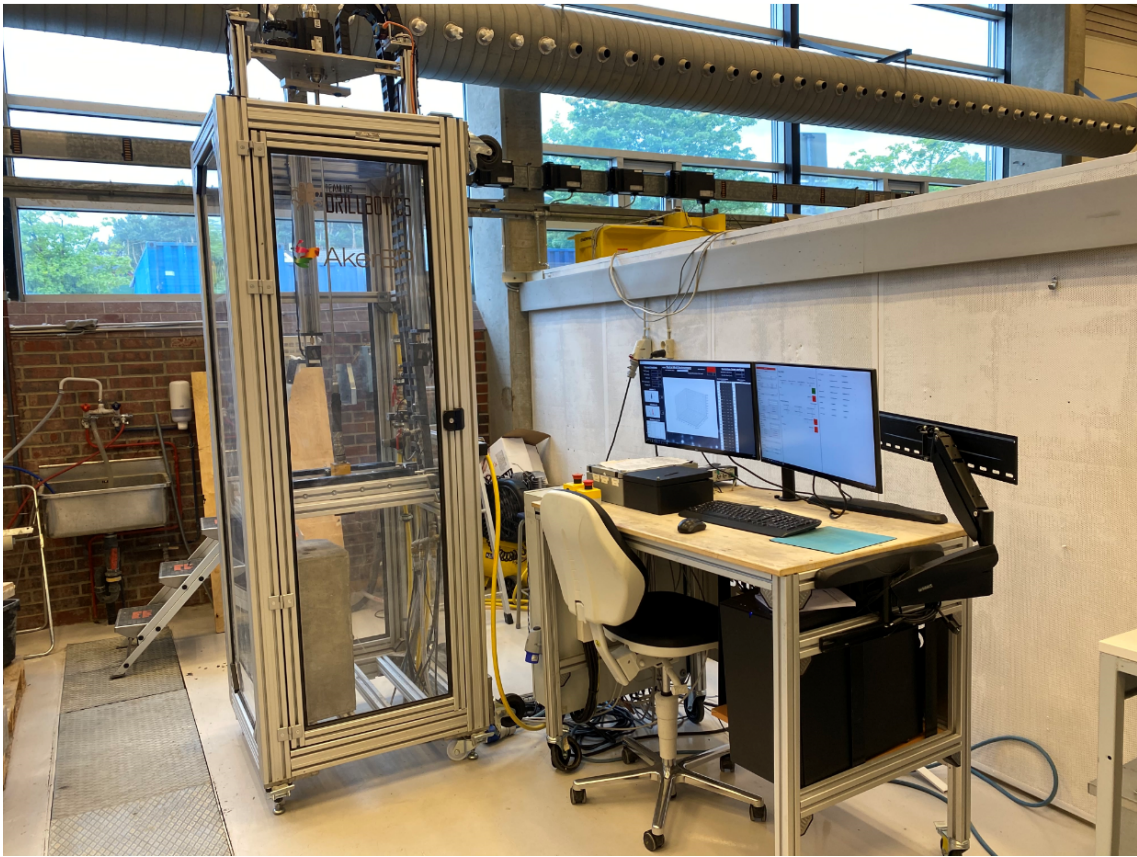
Constructed and Improved Autonomous Laboratory-Scale Drilling Rig

Abstract

This report documents the work that has gone into the design and optimization of a laboratory-scale drilling rig and bit design for the purpose of directional drilling and to participate in the Drillbotics competition. Drillbotics is an international competition organized by SPE's Drilling Systems Automation Technical Section (DSATS) that challenges university teams to build an autonomous laboratory-scale drilling rig. Each year a different challenge is introduced and autonomous directional drilling, steering and downhole measurements are the main focus for this year's competition.

A brand new Bottom Hole Assembly (BHA) was designed and manufactured at the University of Stavanger to accommodate the improvements identified during the 2019 Drillbotics competition. One of the recognized challenges was the pneumatic motor in the BHA breaking at the connection point. The addition of bushing, bearings, a motor shaft and motor sleeve provided the pneumatic motor with the necessary protection, and no motors broke during this year's testing.

A proprietary bit design has been 3D-printed at the University and designed with the assistance from Lyng Drilling, a Schlumberger company. The UiS bit is optimized for directional drilling and was made to enhance performance and ensure good borehole quality. The results from the tests performed show great potential for the UiS bit, and compared with the other drill bits it had the greatest horizontal displacement built, reduced vibrations and excellent hole quality.

The implementation of a 9-axis Inertial Measurement Unit (IMU) on a custom flexible Printed Circuit Board (PCB) allowed the team to fit the sensor closer to the bit, providing more accurate data regarding the current bit position. The testing of the downhole sensor was limited due to unforeseen incidents, however the sensor has been assembled, calibrated and debugged. The results from the limited testing showed great potential and the position of the IMU in the x-, y- and z-axis could be measured. The code will be handed over to the team competing in the 2021 competition for further development.

Limited time for testing and a complicated BHA design resulted in countless hours spent on making slight adjustments to overcome challenges and practicalities to ensure a functional drilling assembly. The challenges, lessons learned and future recommendations for the 2021 competition are thoroughly explained in the final chapter of the report.

The competition day for the 2020 competition should have been on June 24th in Celle, Germany. Unfortunately, the competition was cancelled due to the global pandemic and this report could not include the rig performance at the competition.

Acknowledgments

Contents

List of Figures

List of Tables

List of Abbreviations

AHRS Attitude and Heading Reference System.

ALM Additive Layer Manufacturing.

BHA Bottom Hole Assembly.

DIFF Differential Inputs.

DLS Dogleg Severity.

DOC Depth of Cut.

DOF Degrees of Freedom.

DSATS Drilling Systems Automation Technical Section.

EMI Electromagnetic Interference.

FEA finite element analysis.

FEM finite element method.

HBM High Bandwidth Memory.

HSE Health, Safety and Environment.

I2C Inter-Integrated Circuit.

IDE the Institute of Computer Science and Electro-Technology.

IEP the Institute of Energy and Petroleum.

IMBM the Institute of Mechanical and Structural Engineering and Material Science.

IMU Inertial Measurement Unit.

lpm Liters Per Minute.

MARG Magnetic, Angular Rate, and Gravity.

MCU Microcontroller Unit.

MD Measured Depth.

MEMS Microelectromechanical system.

NDT Nondestructive testing.

PCB Printed Circuit Board.

PDC Polycrystalline Diamond Compact.

PDM Positive Displacement Motor.

PID proportional–integral–derivative.

PLA Polyactic Acid.

PLC Programmable Logic Controller.

PWM Pulse-Width Modulation.

RMS Root Mean Square.

ROP Rate Of Penetration.

RSS Rotary Steerable Systems.

SCL Serial Clock.

SDA Serial Data.

SE Single-Ended.

SPE Society of Petroleum Engineers.

TC Tungsten Carbide.

TD target depth.

TSP Thermally Stable Polycrystalline.

UCS Uniaxial Compressive Strength.

UiS University of Stavanger.

USB Universal Serial Bus.

WOB Weight On Bit.

Chapter 1

Introduction & Overview

1.1   The Drillbotics Competition & Objectives

The Drillbotics competition is an international competition between teams from universities from around the world. The goal is to design and build the best fully automated miniature drilling rig. The University of Stavanger (UiS) participated for the first time in 2017, and has since then acquired a 3rd and 2nd place finish in the Drillbotics competition. The challenge for the first two years was to drill a vertical well through an unknown heterogeneous rock sample. Since the 2019 competition, the challenge has been to drill a deviated well in a sandstone of known strength. To facilitate for autonomous drilling operation, the rig must be equipped with sensors. As of last year, the combination of surface and downhole sensors is mandatory, and to avoid disqualification for sensor failure, redundant or immediately replaceable items should be part of the design and implementation. The teams can drill a vertical pilot hole not more than 1" deep from the rock´s top face. When the test begins, the teams will start drilling autonomously by continuing to drill the pilot hole, keeping the wellbore as vertical as possible until reaching the kick-off point. The teams will kick off from vertical at any depth below the 4" vertical surface hole.

The problem statement for the 2019-2020 competition is "Design a rig and related equipment to autonomously drill a well, using downhole sensors, that is able to hit multiple directional targets, as quickly as possible while maintaining borehole

quality and integrity of the drilling rig and drillstring." [12] Directional steering is a more critical part of the competition for 2020, and the team score more points based on how accurately each directional target is hit. Furthermore, to evaluate the drilling operation the following criteria shall be considered (the following pages are extracted from the 2019-2020 Drillbotics Guidelines).

Due to the global pandemic multiple universities shut down or severely restricted student access to labs and team meetings. As a result, a lot of teams were unable to make progress towards the final demonstration and the 2020 competition was cancelled. The UiS team was unable to access the rig for the duration of 7 weeks, and in the aftermath of the lockdown access was limited. Due to these circumstances, the scope had to be reduced and limited testing could be performed.

1.1.1 Project Timeline

Phase I - Design:	Fall 2019
Submit monthly reports	On or before the final day of each month
Submit final design to DSATS	30 Nov 2019, midnight UTC
Submit an abstract to DSATS*	30 Nov 2019, midnight UTC

*DSATS will submit an abstract to the SPE that will include excerpts from the student abstracts by the conference paper-submittal deadline, typically in mid-summer, for consideration of a paper by the conference program committee.

Phase II – Construction and Testing	Spring 2020
DSATS to announce finalists	On or about 15 Jan 2020
Construction	Spring 2020
Monthly reports	On or before the final day of each month
Drilling Test	Specific on-site test locations and dates for the North American and European locations to be arranged not later than 31 March 2020. The testing will typically occur in late May or early June.
The timeline for the Phase II tests:	Day 0 Students arrive
	Day 1 Students rig up; judges arrive
	Day 2 Students present to judges
	Day 3 Performance tests
	Day 3 pm/Day 4 Students rig down and depart

Figure 1.1: Project Timeline taken from the 2020 Competition Guidelines. [12]

1.2   Team Drillbotics

Over the course of the last years, the awareness of the Drillbotics competition and student organization at the University of Stavanger, UiS Drillbotics, has grown. Due to an increasing demand for multi-disciplinary knowledge in project teams and benefits by involving so-called subject matter experts, the student team at the University is now comprised of seven (7) Bachelor of Science and Master of Science students from the Institute of Energy and Petroleum (IEP), the Institute of Computer Science and Electro-Technology (IDE) and the Institute of Mechanical and Structural Engineering and Material Science (IMBM)

Team members:

- Andreas Sandvik Jakobsen, MSc Student IEP

- Håkon Petersen Hagen, MSc Student IEP

- Magomed Khadisov, MSc Student IEP

- Joakim André Alsaker-Haugen, MSc student IDE

- Jonatan Byman, BSc student IMBM

- Jon E. Karlsen, BSc student IMBM

- Joachim Nygaard, BSc student IMBM

1.3   Project Management

The Drillbotics competition is divided into two phases; Phase I includes the detailed engineering and plan for mechanical upgrades, control system architecture, HSSE and cost analysis. Phase II is the execution of the plan, ordering of components and construction of the rig. Phase II culminates with an event in Celle, Germany hosted by the Society of Petroleum Engineers (SPE)'s Drilling Systems Automation Technical Section (DSATS). All the universities that participate in the Drillbotics competition in Europe, Africa or Asia are invited to this event where the teams share experiences, present their work and compete in a rig performance test. The

reward for winning is to publish a SPE paper, present their paper and exhibit their rig at the IADC/SPE International Drilling Conference.

During these phases a continuous flow of information among team members is essential. To ensure short communication channels all team members are urged to use the Drillbotics office even when working on individual tasks. To make sure we remain flexible the team has followed an agile methodology approach. Agile methodology is a type of project management process where our demands and solutions evolve through the collaborative effort of the cross-functional team. Some of the important routines are described below:

Weekly Sprint meetings Each week, throughout both phases, all team members, supervisors and involved personnel met to get feedback on the progress and discuss solutions to various issues that may have occurred. The meeting would start with a sprint retrospective where the team reflects on their tasks from the previous week, and set new goals for the coming week. During the home office period these weekly meetings were replaced by daily 30-minute meetings to ensure full transparency.

Project Planning - Trello Trello is the collaboration tool we used to organize our projects and tasks. This helped each team member keep track of the different parallel activities at hand, plan ahead and stay up to date.
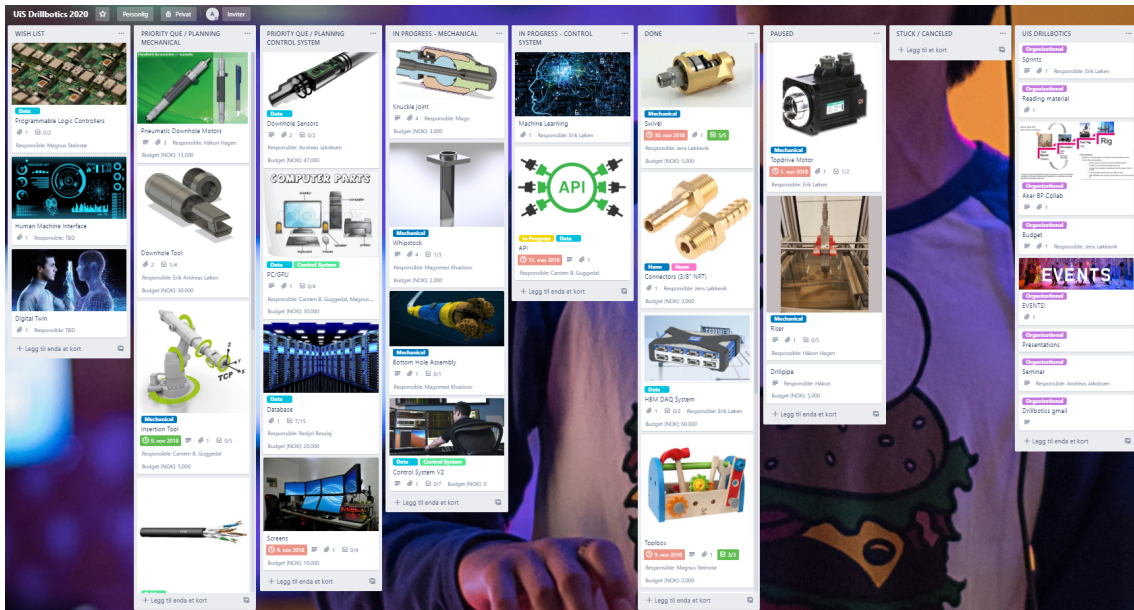
Figure 1.2: Snapshot of UiS Drillbotics' project planner Trello.

Budget The Drillbotics guidelines state that any team spending more than US$ 10,000, or its equivalent in other currencies, may be penalized for running over budget. [12] To make sure the team stayed under budget, all inventory and new orders were listed in an excel sheet to keep track of the budget.

OneDrive cloud storage was set up for the 2017-2018 competition and has been actively used since. All notes from meetings, theses, theoretical papers and other documentation can be found here.

GitHub is a Git repository hosting service, but it adds many of its own features. While Git is a command line tool, GitHub provides a Web-based graphical interface. It also provides access control and several collaboration features, such as a wikis and basic task management tools for every project. All code developed for the control system, graphical user interface and downhole sensor can be found in the UiS Drillbotics GitHub repository.

1.4   Safety & Hazards

To ensure that safety is a priority it was of utmost importance that the team was dedicated to embedding safety into the project. Each and every team member will hold each other accountable for safety to make sure everyone follows the right processes.

In accordance with HSE regulations and good practice, all high-voltage components are placed within a fuse box cabinet. This cabinet houses both the fuses for single-phase and 3-phase power systems as well as all motor drivers, power supplies and so on. Good space in the electrical cabinet will allow additions to next year's competition to be integrated into this cabinet. All micro-controllers, amplifiers and so on have been installed in a Faraday Cage; to protect the systems within and to reduce the electromagnetic interference caused by the 3-phase top drive, driver and 3-phase grid at the University.
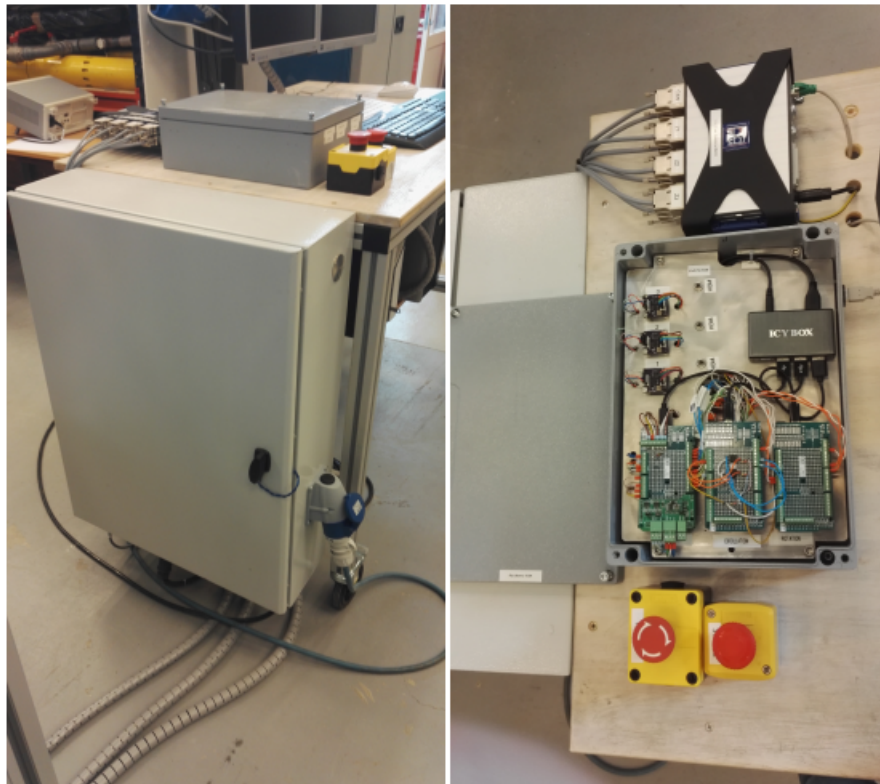
(a) *High volatge system.* **(b)** *Low voltage system.*

Figure 1.3: The rig's electrical setup, ensuring safety for the equipment and team.

Chapter 2

Smart Rig Design & Key Systems

2.1 Drilling Rig

2.1.1 Rotational Systems

Top Drive

This year the drilling rig will utilize both the hollow-shaft electric top drive motor and the pneumatically driven down-hole motor in conjunction. The currently installed top drive transfers torque directly to the drill string and provides a rated torque of 2.86 Nm and a maximum instantaneous torque of 8.59 Nm. The hollow shaft allows the mud injection hose to travel up the derrick and to be connected to the top drive from above, using a swivel (rotary union). Hence, the drilling fluid can be circulated through the rotating shaft of the motor and into the pipe at any time. The decision to attach the mud injection hose from above the top drive, rather than beneath, was made due to difficulties in locating small-scale rotary unions that would not produce considerable amounts of viscous friction when the motor rotates at a high rotational speed in a low-pressure surface environment.

The main role for the top drive is to set toolface while drilling and to hold angle whilst following a pre-calculated trajectory. The pneumatic system will be used as primary motor for drilling. Experiences from the 2019 competition gave insight in how challenging it is to build angles in such an environment. One can easily

believe that the majority of drilling time will be used to build angle while drilling to be able to reach the targets. While building angle, only the bit will be rotating. Rotation will be applied from a downhole pneumatic motor which will drive either a flexible wire connected to the bit or a universal joint. This will be more thoroughly explained in later sections.

This year downhole measurement should be incorporated into the closed loop control and one challenge has been EMI from the 3-phase top drive motor. Sensors have performed perfectly in laboratory conditions, but as soon as they are in proximity of the top drive the signals disappear completely. This issue has been addressed and alternatives for the top drive motor is on the drawing board. One suggestion is to make use of relays to turn off the top drive during drilling, and solely rely on the downhole motor. The top drive is turned on when an azimuth-change is to be made, allowing the control system to change the mechanical angle of the top drive and thus orientation of bit. Another suggestion is to continue using the top drive motor and do extensive EMI compensating measures. One can also take survey points in certain intervals, like they do in the industry while making up stands. The top drive will be turned off and a survey point will be taken, which should ensure good quality data.

(a) Motor.   (b) Driver.

Figure 2.1: Top drive system, consisting of the motor and the driver. [23]

Pneumatic Motor

The idea is based on just rotating the bit using a downhole motor. Air motors have several different designs available to serve a wide variety of needs; using an air motor allows us to have enough torque and rotational motion. Air-driven motors generally have a higher power density, so a smaller air-driven motor can deliver the same power as its electrical counterpart. Air motor speed can be regulated through simple flow-control valves instead of expensive and complicated electronic speed controls. Air motor torque can be varied simply by regulating pressure. [1]

There are many different types of pneumatic motors, however the team believe that an air vane motor will be the most suitable for drilling. Vane motors essentially consist of a rotor which revolves in an eccentrically offset perforation of the rotor cylinder. The vanes form working chambers, the volume of which increases in the turn direction. As the compressed air expands, the pressure energy subsequently transforms into kinetic energy, thereby producing the rotary motion.

Figure 2.2: DEPRAG Pneumatic Motor.

The pneumatic motor from DEPRAG is rated for 2.1 Nm nominal torque and 1500 RPM. Based on previous well logs and experience drilling with the laboratory-scale

rig, these performance numbers related to rotation and torque should be efficient. However, the size of an air vane motor with these specs is quite large. With a length of 20 cm and it being rigid stainless steel, there might be problems when trying to kick-off from vertical. In addition, connections to connect the universal joint or wire and air vane motor will have to be manufactured.

2.1.2 Hoisting System

The construction is equipped with a complete hoisting system consisting of actuators, stepper motors and brakes. The top plate is where the top drive and other components are mounted. The top plate is positioned between three tri-axial load cells connected to the actuators with self-manufactured brackets. The decision was made to use three actuators based on providing enough lifting force and for proper stabilization. Another benefit of using three actuators is the resolution of weight setpoints inputted into the system giving the possibility to have small incremental changes in WOB. The brakes have been implemented to be able to stop hoisting/lowering of the top plate if necessary, as well as to reduce the holding torque on the stepper motors when the system is not running. To avoid the breaks being mistakenly opened or closed, a solid-state relay open and close the breaks simultaneously. This eliminates the risk of an individual actuator braking. Communication between the actuators, brakes, relays and motor is established with the help of the microcontrollers (e.g. Arduinos). New to this year is the addition of HBM single-axis load cells, that can sustain -200N (tension) to 200N (compression) force. These load cells were purchased last spring, but not installed – seeing as making changes to key sensors just prior to competition date is not considered a viable practice.

Each actuator is controlled by a dedicated stepper motor with a step-angle of 1.8 degrees, in which each step-angle consists of 10 micro steps, i.e. 2000 steps/rev. Each lead-screw revolution corresponds to 8mm travel length, i.e. the system operates with an elevation resolution of 4 µm. Very high actuator precision is required for optimal WOB control, which has been a key design criterion upon constructing the system. During the 2018-2019 competition the team decided to go for more powerful stepper motors translating even more load to the drilling system. Previous years the team has observed that the stepper motors work at the upper limit of what

they can endure, increasing the chance of overheating and failure. The new load cells and more powerful stepper motors allow the system to increase the maximum WOB from approximately 300N WOB up to 600N WOB. To address our vibration challenge, the spring loaded couplings between the actuators and stepper motors were replaced with rigid couplings.
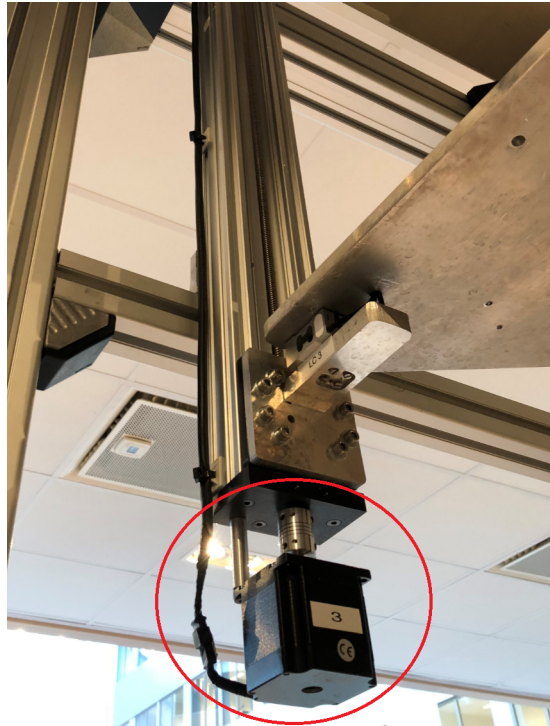
Figure 2.3: One of three (3) stepper motors (Highlighted with red circle) and linear actuators

2.1.3 Pneumatic System

The pneumatic motor requires a flow rate of 300 lpm and 6.5 bar in order to deliver its maximum torque output to the bit. The compressor in use is able to deliver up to 10bar. The plan was to split the air flow from the compressor to divert flow through both the pneumatic motor and the cuttings transport system described in the next section. However, during testing it was observed that the pressure required from the cuttings transport system would interfere with the inlet pressure at the solenoid valve. To solve this the cuttings transport system is connected to the University's pneumatic line.

1) Outlet (to pneumatic motor)

2) Pressure Transmitter

3) Manual choke valve

4) Manual pressure relief valve
5) Solenoid valve

6) Manual pressure relief valve
7) Passive pressure relief valve
8) Hydraulic Maintenance unit

9) Inlet (from compressor outle
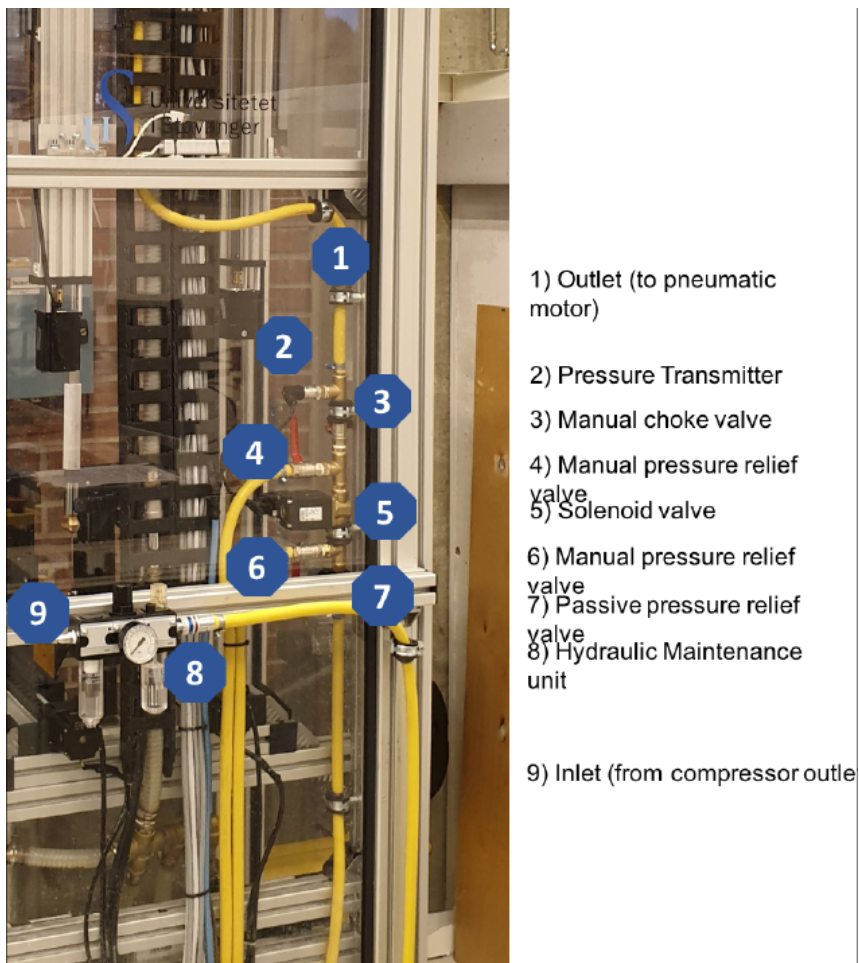
Figure 2.4: Pneumatic system comprised of various components to regulate the air inflow, monitor pressure and lubricate the system [24].

Solenoid Valve

The solenoid valve is a 2-way normally closed control valve. The valve control takes place through the control electronic which coverts an analogue input signal into a Pulse-Width Modulation (PWM) signal. The duty cycle of the PWM signal determines the coil current and hence the position of the plunger. [33] It is used to throttle the inlet pressure from 0-100% to control the rotational speed of the motor. Table 2.1 represents the various bit RPM at different valve opening positions.

Solenoid Valve Position	0Nm Torque [RPM]	0.5Nm T [RPM]	1.0Nm T [RPM]	1.5Nm T [RPM]	2.1Nm T [RPM]
60%	420	370	320	270	210
70%	732.6	645.4	558.4	471	366.3
80%	924.6	814.5	704.5	594.4	462.3
90%	1038.6	915	791.3	667.7	519.3
100%	1074.6	946.7	818.7	690.8	537.3

Table 2.1: Bit RPMs for solenoid valve openings ranging from 60 to 100%, corrected for 0 to 2.1 Nm torque. The data is taken from experiments performed by Løken and Løkkevik. [24]

Pressure Transmitter

The pressure sensor used to measure the inlet pressure in the pneumatic system is a 3100 Series Pressure Sensor from Gems. The high output pressure transducer is fitted with an Asic providing 8 to 30V dc voltage output, and a 4 to 20 mA current output capable of being used in control and indicating loops without further amplifications. [11]

Figure 2.5: Type 8605 solenoid valve from Bürkert, rated for 0 to 10 bar.

Figure 2.6: 3100 Series Pressure Sensor from Gems Sensors & Controls, rated for 0 to 16 bar.

2.1.4 Cuttings Transport System

In order to not fill the entire lab area with airborne dust particles from the drilling, an efficient cuttings transport system is imperative. Experience shows that drilling with the pneumatic motor creates extremely fine cuttings which easily becomes airborne from the 300 liter per minute flow of air. Cement and sandstone particles should not be inhaled, so for HSE reasons require a complete collection of cuttings.

To accommodate the fine particle collection, two ash vacuums are used to collect the particles. Since most of the particles travel with the same velocity as the air, the cuttings must be confined in a space where it can be extracted from the air. Therefore, a confinement box was designed to be 3D-printed in ABS.
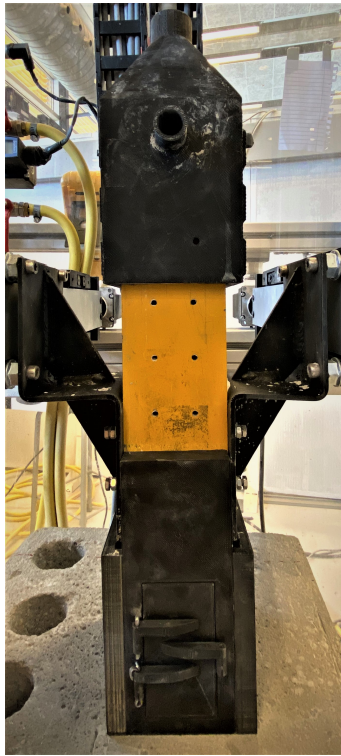
Figure 2.7: 3D-printed cutting transport system.

The cuttings transport system is designed such that the cuttings will be confined within the riser area. The bottom part of the system is placed on top of the formation and is extended onto the riser wall (yellow). A door has also been included to be able to inspect the drilling assembly while drilling. The top part of the system is slid down on top of the riser. There is an internal seal which clamps around the pipe confining the cuttings. The cuttings are collected by the use of two ash vacuum cleaners which are attached to the 3D-printed parts.

Manufacturing of the cuttings transport system was done using a Fortus 450mc industrial plastic printer to ensure the best available quality.

2.2 Advanced Bottom-Hole Assembly

The experiences from the 2018-2019 competition led to the decision to remake the Bottom Hole Assembly (BHA) for this year's Drillbotics competition. Key chal-

lenges were highlighted such as; pneumatic motor connection breaking due to radial loading, sensor sub being too far behind the bit and not being able to control the bend in the knuckle joint. The additions of a thrust roller bearing, brass bushings, a flexible Printed Circuit Board (PCB), flexible bend and 3D printed stainless steel motor sleeve are all new to this year's design. The design criteria and role of each component will be described in this section.

2.2.1   Additive Manufacturing

Additive Layer Manufacturing (ALM), also called 3D printing, is gradually finding practical applications in the oil and gas industry. The industry has shown slow but steady adoption of this technology in recent years. Though 3D printing technology was largely limited to polymer-based products like Polyactic Acid (PLA) in its infancy, advancements in metal-based 3D printing is making this technology more relevant. 3D printing reduces the time it takes to produce complex prototypes, an advantage the team has made the most of. Most of the following components in this chapter have been 3D printed in PLA to discover design flaws and unforeseen issues. Metal-based 3D printing allows the team to print fully functional components for use in operation.

Figure 2.8: Markforged Metal X 3D Printer

There are several advantages and opportunities with 3D printing technology. In the coming years, these are the areas we believe 3D printing will create value.

- One can print prototypes or models to improve efficiency and improve decision making by visualization.

- The option to 3D scan components and print them. Old oil fields may have a lot of components that are no longer manufactured. With 3D printing one is able to replace the faulty component at a reduced cost.

- Cost and lead time is reduced as the 3D printer does not require a mold. It can print different components in sequence, in addition to having it on-site which removes the delivery time.

- Digital storage with technical drawings that can be printed as required, rather than a large physical storage with reserve parts.

2.2.2 Universal Joint

The universal joint concept is one of two proposed solutions to this year's directional drilling challenge. The main objective of the universal joint is to transfer the required torque between the pneumatic motor and the motor shaft without the possible problems caused by a wire. A number of key factors regarding the universal joint concept were identified.

- It will be able to handle the horizontal and vertical stresses.

- Handle shear stress and vibrations with respect to external forces translated from the drill bit.

- Keep the joint as compact as possible and still maintain the structural integrity of the design.

- It will be able to meet the required rotational speeds from the motor.

- Manufacturing capability, able to order off the shelf component.

The design of the joint is a common method of transferring torque in other machinery such as cars and trucks, though the dimensions differ. The Drillbotics team discussed the advantages of this design relative to the wire concept and the pros recognized are listed below.

- Immediate torque on bit.

- Reduced BHA length.

- High operating speeds.

- Eliminates the possible wear on the inner wall of the sleeve made by the wire.

The universal joint connection to the pneumatic motor are M8x0.75 threads and M8x1.25 threads to the motor shaft. Two universal joints in different sizes were prepared for the experiments. The learnings from using the universal joint are summarized in Chapter 8.
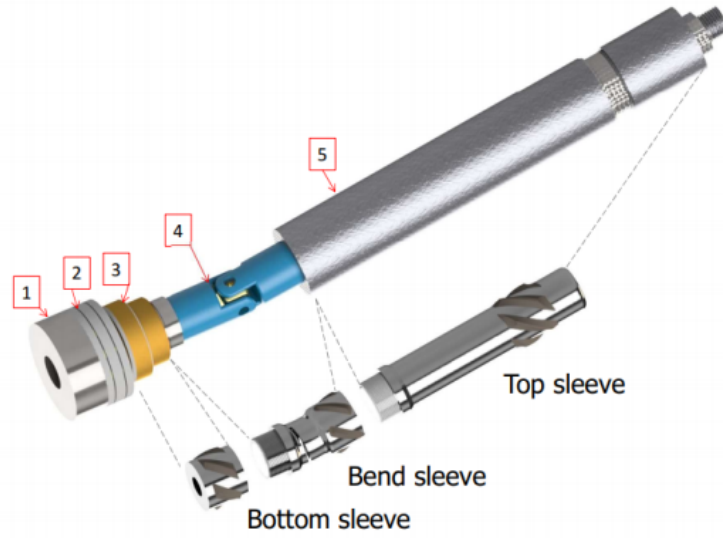
Figure 2.9: The BHA with the motor shaft (1), thrust roller bearing (2), bushings (3), universal joint (4) and pneumatic motor (5). The sleeve is represented next to the components in the figure.

The downside of the universal joint concept is the variation in the velocity out of the joint to the bit, this will add some vibration and stresses to the design. There are some ways to minimize this effect by using a double universal joint or decreasing the angle of the existing joint. If the angle is smaller, the effect of the different velocities of the two axles will decrease.

ω_2 = angular velocity out (bit)

ω_1 = angular velocy in (motor, max rpm is 1500) = 157 Rad/s

β = the axle angels relative to eachother (8 degree bend) = 0.139626 radians

γ_1 = the rotation angle for axle 1 (one rotation around the axle) = 2π

$$\omega_2 = \frac{\omega_1 \cdot cos\beta}{1 - sin\beta^2 \cdot cos\gamma_1} = \frac{157 \cdot cos(0.139626)}{1 - sin^2(0.139626) \cdot cos^2(2\pi))} = 158.5 Rad/s \qquad (2.1)$$

The ratio between the input and the output of the angular velocities' balances around one percent from the angular input. This means in theory that it will not have any immediate effects on the design itself.

2.2.3 Wire

The steel wire concept is the alternative solution to the universal joint concept. Using the wire could potentially reduce the length of the BHA as the motor placement would be more flexible. Removing the pneumatic downhole motor and running the wire through the drill pipe from the top drive would be an alternative solution that would reduce the BHA length drastically. However, doing this with the current design would result in minimal directional control. The key factors for the wire concept were:

- Flexible motor placement

- Able to handle high RPM

- Of the shelf wire and connections

The downsides were identified as a risk for tangled wire and wear on the inside of the sleeve.
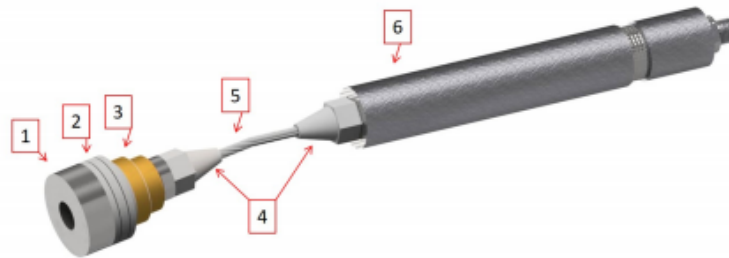
Figure 2.10: The BHA with the swageless studs (4) and steel wire (5).

2.2.4 Bushings

Bushings, also called plain bearings or sleeve bearings, reduce friction between two surfaces sliding against each other. In this year's design, straight cylindrical brass

21

bushings are used to accommodate loads experienced during directional drilling. The bushings sit on the motor shaft and need to be carefully manufactured to ensure the correct fit. If the bushings are too large, torque from the motor will be lost to friction on the motor shaft. If the bushings are too small it will allow the motor shaft to wiggle, making the drill bit unstable and bit walking may occur. The bushings are held in place by the use of a retaining ring. It is important that the cross-sectional area of the bushings are unharmed as any damage to them may cause issues with rotation. If the bushings do not spin freely, bit torque and drilling efficiency is reduced.
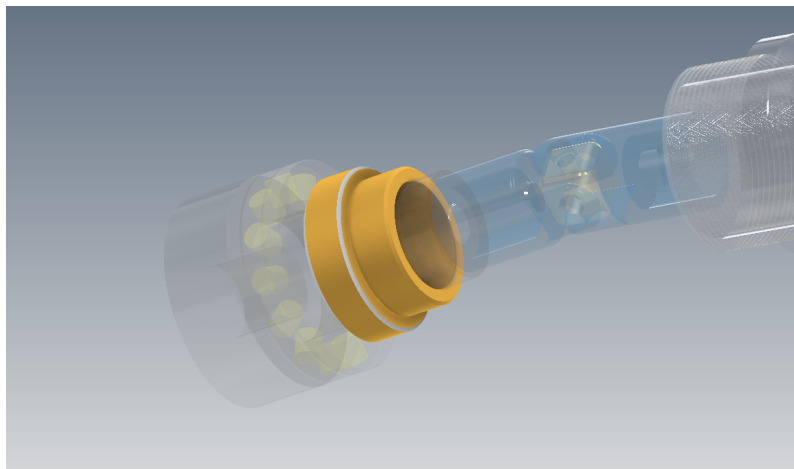
Figure 2.11: Bushings.

2.2.5   Thrust Roller Bearing

The thrust roller bearing used in the BHA is designed to accommodate axial loads only and must not be subjected to any radial load. The thrust roller bearing is rated for 18.6 kN dynamic loading and 48 kN for static loading at 3800 RPM. Thus, it should be able to handle the drilling operation with ease. The bearing sits between the motor shaft and lower stabilizer and is what enables the shaft to rotate while the stabilizer remains stationary.
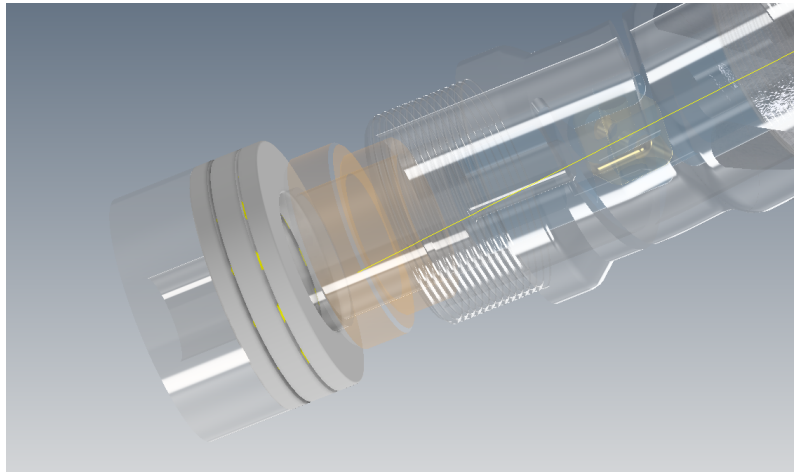
Figure 2.12: SKF Thrust Roller Bearing.

2.2.6 Motor Shaft

The motor shaft connects the universal joint and bit, its job is to transfer the torque from the pneumatic motor to the drill bit. It will rotate at the same rotational speed as the drill bit. Press-fitted onto the motor shaft by the use of a hydraulic press is the lower bearing ring, the outer diameter of this part of the shaft should be 0.02 mm larger than the bearing ring. A large quantity of motor shafts were CNC-machined in the workshop at the University and prepared for different bit connections (M14, M16 and 1/4" NPT threads) and M8 threads for the universal joint connection. The bearing is installed on the motor shaft followed by the lower stabilizer, two brass bushings and finally a retaining ring to hold the components in place. The OD of the lower part of the motor shaft is close to on gauge with the bit, acting as a gauge pad.
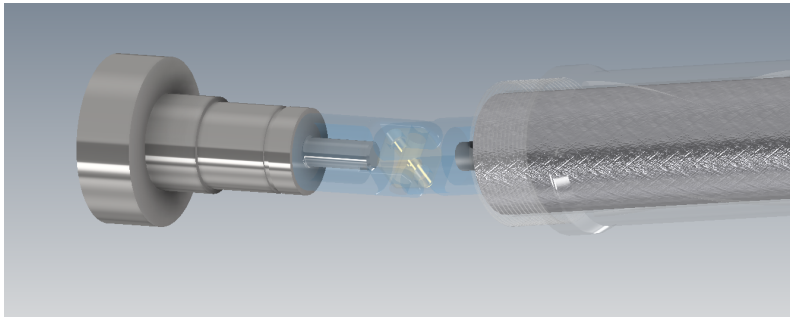
Figure 2.13: Motor Shaft.

2.2.7 Motor Sleeve

The motor sleeve is printed in 17-4 ph stainless steel at the University of Stavanger. Post-machining of threads and removal of support structure is done by the team members in the workshop. The purpose of the sleeve is to protect the components inside, specifically the pneumatic motor, universal joint and motor shaft. There is also a dedicated slot for the custom Printed Circuit Board (PCB) above the middle stabilizer. The air from the exhaust on the pneumatic motor travels down the motor sleeve and out of an air conduit angled at 45°to ensure sufficient hole cleaning. From previous experience, the particles generated with the pneumatic motor are very fine and easy to transport even with air.
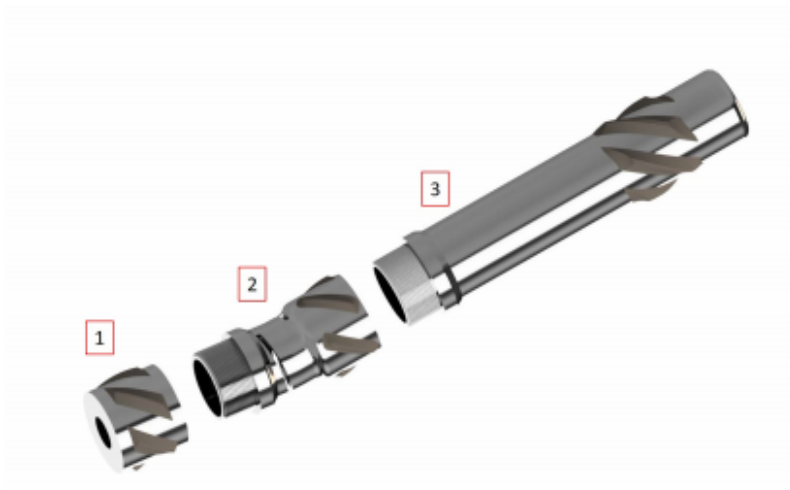
Figure 2.14: Motor Sleeve.

2.2.8 Bent Sub

The bend sleeves play an important role in the process, as they are designed to provide an angle for directional drilling. The design of the bend sleeve has therefore received a lot of attention this year. Three different concepts for the bent sub geometry was proposed; a "Lego" cut, a helical cut and a solid bend with no cutout. The purpose of the cutouts are to allow the bend to straighten if enough WOB is applied. Consequently, the rig is able to drill straight when required to. Having a flexible bend in the system would also make it easier to trip out of the borehole and preventing any stuck pipe issues.

The results of a finite element analysis (FEA) in the Ansys Mechanical software was used to determine the downward force required to straighten the bent subs. The results and process are described thoroughly in (Byman, 2020) [8]. The "Lego" cut was considered to be the most promising concept. It is able to be straightened at a force of 185 N, compared to the helical cut which needed a force of 2690 N to straighten. The rig is able to provide a downward force (WOB) of 600 N, and the optimal parameter during past experiments have been between 100-200 N. By using this geometry, directional steering is improved as the rig is able to both build angle and drill a straight hole, depending on the forces applied.

Figure 2.15: 3D printed stainless steel bent subs with different geometries. From left to right; "Lego" cut, no cutout and helical cut.

2.3   Downhole Sensor Setup

The use of both surface and downhole measurements to control the drilling process in real-time is mandatory, and failure to do so will result in a failing grade for this year's competition. [12] The purpose of the downhole sensor is to track the position of the drillbit in real time. The robotics and signal processing master student, Joakim Andrè Alsaker-Haugen, has had the primary responsibility for the downhole sensor. A more comprehensive overview of theory, programming and testing of the downhole sensor can be found in his master thesis. [5] The downhole sensor requirements identified in the design phase were as follows:

- Measure downhole position (azimuth and inclination)

- Measure vibrations

- Measure tripping acceleration

- Custom made to reduce the dimensions

- Easily replaceable in case of malfunction

- High frequency communication with the control system

The following terms are used throughout this thesis and are defined here to aid in clarity.

Accelerometer - A sensor that measures linear acceleration.

Gyroscope - A sensor that measures rotational velocity.

Magnetometer - A sensor that measures changes in magnetic field strength.

Inertial Measurement Data - Any data collected from the inertial measurement unit, four our purpose this will be: Rotational velocity, linear acceleration, magnetic field strength and temperature.

Inertial Measurement Unit (IMU) - A device used to collect inertial measurement data.

2.3.1 Inertial Measurement Unit - ICM-20948

The downhole sensor chosen by the team for this year's competition is the Inertial Measurement Unit (IMU) ICM-20948 from TDK InvenSense, shown in Figure 2.16. It is a 9-axis MotionTracking device and contains a 3-axis gyroscope, 3-axis accelerometer and a 3-axis compass (magnetometer). With the measurements from these components, one can calculate azimuth, inclinations and also vibrations. The ICM-20948 features I^2C and SPI serial interfaces, on-chip 16-bit ADCs, programmable digital interrupts and an embedded temperature sensor. The device features an operating voltage range from 1.71V to 1.95V. The gyroscope has a programmable full-scale range of +-250 dps, +-500 dps, +-1000 dps, and +-2000 dps. The accelerometer has a user-programmable accelerometer full-scale range of +-2g, +-4g, +-8g and +-16g. Communication with all registers of the device is performed using I^2C at up to 100 kHz (standard-mode) or up to 400 kHz (fast-mode). [21]

Figure 2.16: ICM-20948, TDK InvenSense 9-Axis MotionTracking device.

2.3.2 Sensor Positioning

In previous years, a versatile sensor sub design has been utilized. It allowed for easy access and it was independent of the other parts of the BHA. One of the disadvantages with the sensor sub was the distance between the sensors and the bit.

It was connected behind the bit, bit sub, pneumatic motor and knuckle joint. This resulted in the position of the bit to be tracked to be around 30 cm ahead of the sensor, making real-time steering difficult. To improve this, a flexible Printed Circuit Board (PCB) is introduced. This enabled the team to find room for the sensor package much closer to the bit. Due to an already crowded BHA, it was decided to incorporate a slot for the sensor package on the motor sleeve, just above the second stabilizer. The outer diameter of the sensor slot is lower than the stabilizers to reduce excessive vibrations. The downhole sensor slot is presented on the motor sleeve in Figure 2.17. The USB sensor wire will exit above the motor through a spiralled channel in the motor sleeve.
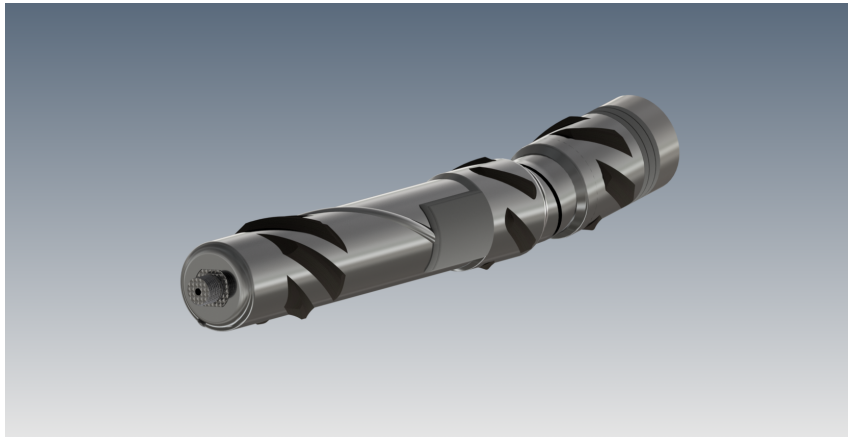
Figure 2.17: The 32.5x24x2.9mm curved sensor slot featured on the motor sleeve.

2.3.3   Printed Circuit Board

Due to the space limitations the team designed a custom flexible PCB. To overcome the challenges with space limitations in our BHA, all the components are surface mounted. The PCB includes the ATMEGA328P-AU MCU, ICM-20948 9-Axis IMU, a Gauge Pressure Sensor and FT232RQ-Reel USB to serial UART interface as the main components.

(a) Left side components.   (b) Right side components.
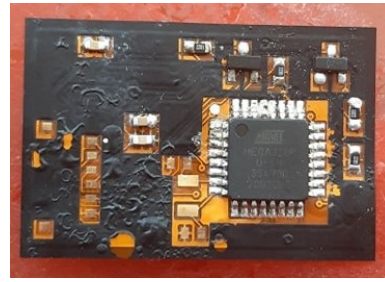
Figure 2.18: Printed Circuit Board with component placement

2.3.4 Microelectromechanical system sensors

The magnetometer and accelerometer sensor used in the sensor package are Microelectromechanical system (MEMS) sensors. For a laboratory-scale drilling rig with a steel frame (magnetic material), with internal rotating parts and electrical equipment within close proximity to the magnetic sensor, it can be expected that the drilling operation will happen in a highly non-constant magnetic distorted environment. The drilling process itself will also produce vibrations. Therefore, it is important to understand how the two sensors work and how distortion will affect the measurements. Below, the working principle of the magnetometer, accelerometer and magnetic distortion will be described. This section is inspired by the work done by M.B. Nåmdal for his master thesis written in affiliation with the NTNU Drillbotics 2019 team. [27]

2.3.5 MEMS Accelerometer

The MEMS accelerometer is used to measure linear acceleration in x-, y- and z-direction by using the change in capacitance together with a known spring constant. Each axis has separate proof masses which is suspended with springs in a base structure. A movable plate in the proof masses is placed between the base structure and the fixed plate and represents capacitors. The deflection of proof masses is measured by the use of the capacitance difference, and multiple movable and fixed plates are added to amplify the difference. This is illustrated in Figure 2.19. The linear acceleration is measured by the use of the known spring constant together

with the measured capacitance difference. [6]
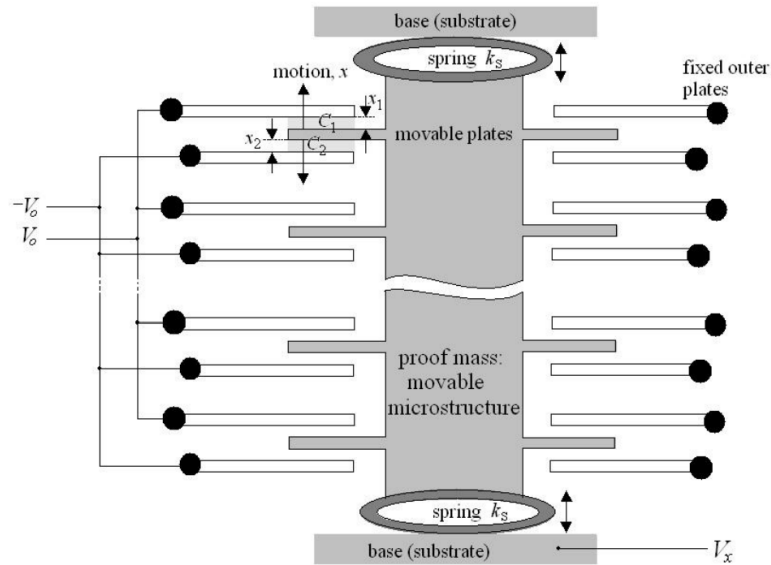
Figure 2.19: Accelerometer structure with proof masses [6].

Measurement noise

High frequent oscillations occur on the measurement signal due to electrical disturbance from electrical equipment or Electromagnetic Interference (EMI). A kalman filter should be implemented to deal with the measurement noise.

Process noise

Heavy vibrations are generated during a drilling operation with the current rig setup, the vibrations propagate up the drillstring to the rest of the rig. These dynamic movements are defined as process noise. While drilling the team varies the drilling parameters to break the oscillations in an attempt to reduce vibrations. The vibration process noise should be dealt with by the implementation of a kalman filter.

Earth's Gravitation

The earth's gravitational acceleration have a constant direction and magnitude of approximate $9.81 m/s^2$ or 1g perpendicular the the earth's surface (with small variations dependent on location). This constant acceleration can be used as a reference direction to determine up or down for the accelerometer.

2.3.6 MEMS Magnetometer

To measure the magnetic field strength, the MEMS magnetometer uses the hall effect. The hall effect takes advantage of two magnetic characteristics; the flux density and polarity to measure the magnetic field strength. A closed loop circuit consisting of a p-type semiconductor and a DC power supply is utilized to send low current through the semiconductor. When the hall element (semiconductor) is placed in a magnetic field, the passing electrons will be diverted to the corresponding side of the semiconductor. If the electron density is higher on one side, a potential difference can be measured and defined as the hall voltage and used to determine the strength of the magnetic field. [34] The hall effect is illustrated in Figure 2.20.
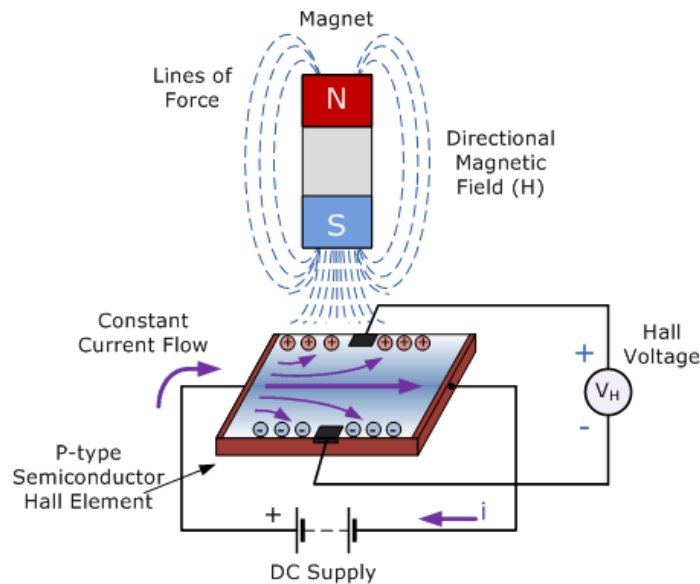
Figure 2.20: Hall Effect Illustration [34]

Measurement noise

The high frequent oscillations is the same as for the accelerometer and will be handled correspondingly.

Process noise

Distortions of the earth's magnetic field are a result of external magnetic influences generally classified as either a hard- or soft-iron effect. If no distorting effect are present, rotating a magnetometer through a minimum of 360°and plotting the resulting data as x-axis vs. y-axis will result in a circle centered around (0, 0). [13] The hard-iron effect may produce an offset of the circle from the (0,0) reference point. A In the case of soft-iron effect, it may cause the circle to deform and produce an ellipsis.

Hard-Iron Distortion is produced by materials that produce a magnetic field. As long as the orientation and position of the magnet relative to the sensor is constant, the produced offset will also be constant. While performing a survey the downhole sensor will be in a set orientation, however some material such as the rig frame will not move relative to the sensor. In an attempt to improve this, all parts of magnetic materials and electrical equipment with close proximity to the sensor should be replaced by a non-magnetic material. Through testing the team discovered that the stainless steel material used for the BHA is also magnetic. The workshop at the University has the necessary tools to demagnetize the components that will create magnetic distortion in the system. This process should be performed prior to calibration of the IMU.

Soft-Iron Distortion is the result of material that distorts a magnetic field, but does not necessarily generate a magnetic field itself. Material such as iron and nickel will create a soft-iron distortion [13]. Unlike the hard-iron distortion where the influence is constant regardless of orientation, the distortion produced by soft-iron materials is dependent upon the orientation of the material relative to the sensor and the magnetic field. Therefore, it cannot be compensated for by the use of a constant. In the case of a soft-iron distortion a more complicated procedure would be required.

Figure 2.21 displays ideal distortion-free magnetometer data, where the output is centered around (0,0) and circular in shape, as blue. The magnetometer data displaying hard-iron distortion which exhibits a constant offset for both the x- and y-axis is shown as the red circle. Soft-iron effect distorts the ideal circle into an elliptical shape, it is represented in Figure 2.21 as the black ellipsis.
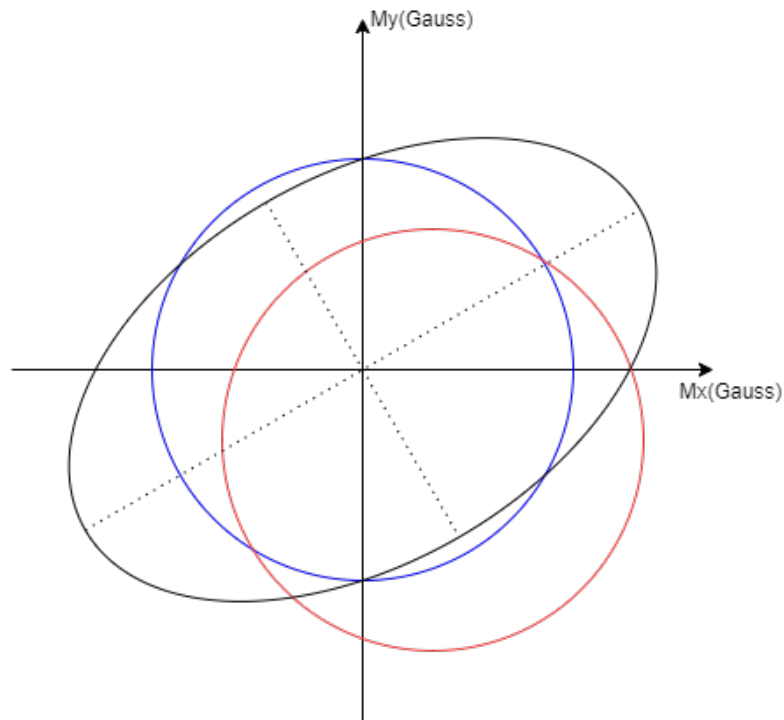
Figure 2.21: Magnetic Distortion affecting the magnetometer data.

2.3.7 Communication Protocols

The downhole setup uses two different communication protocols for the serial communication. Inter-Integrated Circuit (I2C) between the IMU and Microcontroller Unit (MCU), and Universal Serial Bus (USB) from the MCU to the topside computer.

Inter-Integrated Circuit (I2C)

Inter-Integrated Circuit (I2C) is a master-slave communication protocol that uses a bidirectional open drain lines; Serial Data (SDA) and Serial Clock (SCL). I2C is not only used on single boards, but also to connect components which are linked via cable. Simplicity and flexibility are key characteristics that make this bus attractive to many applications. With I2C you can connect multiple slaves to a single master, and you can have multiple masters controlling single, or multiple slaves. [7] The team uses I2C communication between the IMU and pressure sensor to the MCU on the circuit board. The IMU is a 8-bit chip that stores the sensor measurements in 16-bit series on both high and low registers. This makes it practical to use the i2c-read-register to read both high- and low-bits of the measurements before combining them to a 16-bit signed integer.

Universal Serial Bus (USB)

Universal Serial Bus (USB) is one of the most common interfaces for connecting a variety of peripherals to computers. USB provides a sufficiently fast serial data transfer mechanism for data communications, and provides the team with a simple and effective means of connectivity from the computer to the downhole tool.

2.4   Survey Calculations

To track the well trajectory a 9 Degrees of Freedom (DOF) Magnetic, Angular Rate, and Gravity (MARG) sensor consisting of 3-axis gyroscope, accelerometer and magnetometer will be used. Data generated from this sensor will be used in an Attitude and Heading Reference System (AHRS) that will provide a 3D orientation of the drill bit. This is done by integrating the gyroscope and fusing this data with accelerometer and magnetometer data. With these sensors the drift from integrating the gyroscope is compensated for by reference vectors, gravity, and the earth magnetic field. This will give the roll, pitch, and yaw for the drilling bit, that will be used to calculate the bit position. The bit position will be tracked by using the attitude heading reference together with the vertical drilling speed of the top plate. As the drilling assembly is a rigid object the vertical drilling speed should be the same

speed as the drill bit's heading. Thus, by knowing the bits attitude and heading the Distance can simply be calculated using *speed · time* to calculate its position from a known point in space. The direction the bit is traveling in will be based on the orientation of the bit, the attitude and heading reference will tell which orientation the bit is pointed in. The calculated position based on the AHRS will then be compared and used together with the position calculated from using forward kinematic to estimate the most likely position of the bit. The forward kinematic equations for x, y, and z in the rig's coordinate system is found by using Denavit Hartenberg method, which gives the following equations:

$$x = a_3 \cdot Cos(\theta_2)Cos(\theta_3) \tag{2.2}$$

$$y = a_3 \cdot Sin(\theta_2)Cos(\theta_3) \tag{2.3}$$

$$z = a_3 \cdot Sin(\theta_3) + d2 + d1 \tag{2.4}$$

Where a_3 is the distance from drill bit to the bent sub, d_2 is the distance from the bend to the top of the pilot hole, d_1 is distance from the stone to top drive, θ_2 is the top drive angle and θ_3 is the angle of the bent sub.

2.5   Universal Data Acquisition Module

The HBM QuantumX MX840B was implemented for the 2017-2018 and allows for detailed post-analysis of our experiments. It has 8 high precision channels for reading analog and digital inputs. The internal analog-to-digital converter samples rates of 40 kS/s per channel, and is rated for an accuracy of 0.05% and 24-bit resolution. [17] Readings can be filtered in real-time using a low-pass filter to remove outliers. The HBM Catman Easy software enables the system to calculate and return pre-calculated values instead of raw 24-bit measurements.

As a stand-alone device, the HBM is capable of sampling with a 9600Hz frequency.

From previous analysis of data sampled at 9600Hz the rig requires a sampling frequency at around 50Hz for real-time application to be able to monitor trends while drilling.

The HBM Common API is used to operate the output PLCs from a C# program. The continuous sampling frequency is limited by communication overhead for requests to 90Hz, still within the requirements for monitoring trends. By reverse-engineering the HBM API demo the data acquisition module provides real-time data streams to the control system.
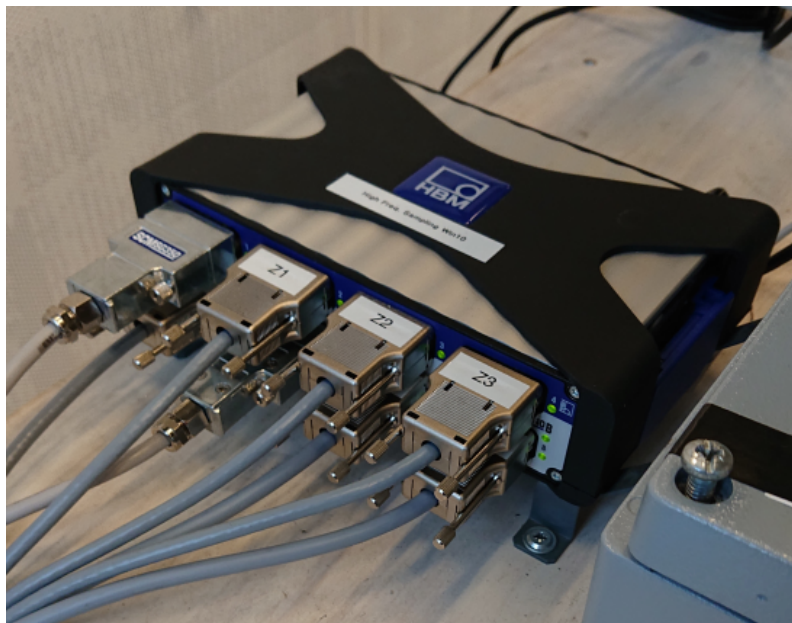
Figure 2.22: HBM QuantumX MX840B with all 8 channels connected to the analog outputs of the rig.

2.6   Measurement Computing PLCs

Inexpensive PLCs generally have either a high number of analog outputs or inputs. Because outputs and inputs happen asynchronously, two PLCs were ordered instead of one. A class of PLCs from Measurement Computing met all the requirements for our system, with additional Python support.

2.6.1 USB-1608GX

The analog and digital input reader USB-1608GX has 16 analog inputs for Single-Ended (SE) usage and 8 channels for Differential Inputs (DIFF) usage with a 16-bit resolution. [10] The difference between SE and DIFF measurements is the baseline voltage. SE measurements compare the voltage to the common ground, whereas DIFF compares the voltage to a ground cable running in parallel to the voltage being measured. With DIFF there will be an equal amount of electromagnetic noise affecting both wires, giving more precise and consistent measurements. Measurements can be in the range of ±10V. There are also 8 digital I/O channels on the device. Each channel does not have its own dedicated ADC, meaning the PLC does not support synchronized measurements of all channels. Instead, all channels are sampled in bursts with a 500.000Hz sampling rate. Sampling across all channels only takes 0.032ms and should not be an issue in our use case. The PLC is connected to the control system computer using an USB interface. [16]

Figure 2.23: Input PLC for the system, USB-1608GX.

2.6.2 USB-3114

The output device USB-3114 is meant to replace all the Arduinos. There are 16 analog output channels with a 16-bit resolution capable of providing ±10V with an adjustable current of up to 40mA per channel[8]. Outputs can be altered at a maximum frequency of 100.000Hz. There are also 8 digital I/O channels on the device. Controlling the outputs directly from the control system computer instead of through serial commands passed to an Arduino will improve reliability and simplify integration of new equipment. The Arduinos have software and hardware limitations making some rig operations difficult to integrate. For further detail regarding the Measurement Computing PLCs and why the Arduinos should be replaced, please refer to the computer science thesis from 2019. [16]

Figure 2.24: Output PLC for the system, USB-3114.

2.6.3 PLC Issue

During testing of the new PLCs and trying to control a stepper motor through the stepper motor driver using the USB-3114 the team was unable to switch between 3.3

V and 0 V fast enough. To control the stepper motors the PLC needs to send pulses each 66 µs and during testing only 2 milliseconds was achieved. The issue was not related to software, nor was it operating system specific. The hardware design of the USB-3114 is such that it can only accept one value per channel at one time (per write). The hardware was not designed to buffer an array of data and pace it out based on an internal clock. The USB-3114's specs are 100 Hz, which is not enough to control the stepper motors. Due to limited access to the rig setup, it was decided to revert back to the Arduinos until new PLCs were ordered or a workaround was found.

The team invited Beckhoff Automation Technology to the University to investigate if their PLCs would suit our needs. Early dialog indicates that their system would remove a lot of the unnecessary wiring in the electrical cabinet and fit our needs in terms of performance. In addidition, they are able to provide the team with servo motors that can be used to replace the current hoisting system.

2.7 Control System

A control system is a system of devices or set of devices, that manages, commands, directs or regulates the behavior of other devices or systems to achieve desired results. [35] Our system is written in Python programming language, as it is one of the most popular languages with access to an extensive library. The gRPC framework was used as it is suited for making distributed systems such as ours. The control system is split into individual modules that run microservices. Each module represents a gRPC server and a gRPC client, this makes it capable of both sending and receiving data. In addition, the modules are divided into layers that reflect their functionality, this gives the system a clear structure. Layers may contain a core element that all modules within the layer is dependent on. Modules subscribe to lower layer modules to receive all or some of the processed data. The control system architecture was designed with future implementations in mind by allowing additional modules to be easily added.
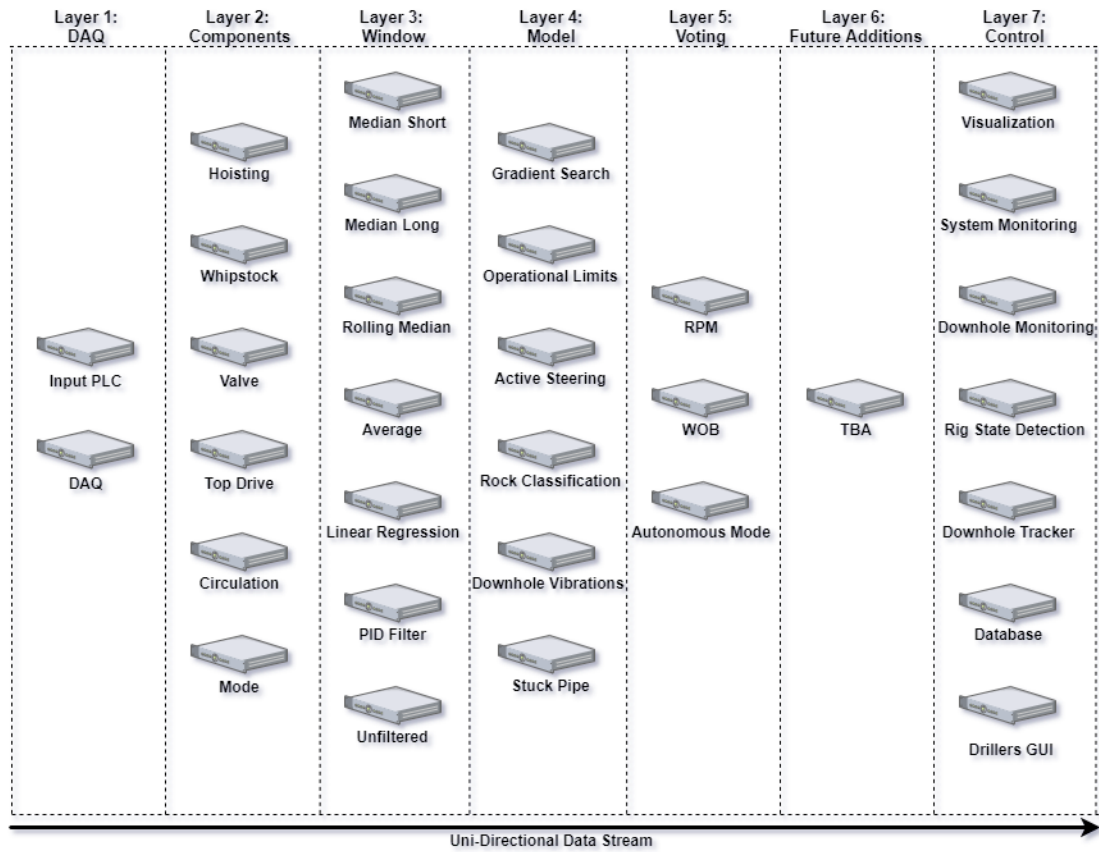
Figure 2.25: Illustration of the control system architecture. The data stream is uni-directional from left to right. Modules are represented as servers. The dotted lines separate each layer.

2.8 Calibration

All sensors on the rig must be calibrated when installed. If a factory calibration has been done and the calibration data is documented with the sensor, this can be used to quickly prepare the device to query data in the correct physical unit. This section describes the installation and calibration of the HBM load cells, WOB measurements and pneumatic motor speed.

2.8.1   U9C Miniature Load Cell

One of the upgrades to the rig this year was the addition of new HBM load cells to increase the maximum WOB from 30kg to 60kg. The U9C is suited for very fast measurements and its welded design from stainless steel makes the force sensor extremely robust in comparison to our previous load cells. The three load cells are mounted below the top plate, and each load cell is able to measure up to 200N. As the loads from drilling are divided close to equally between the three measuring points, we achieve the new maximum WOB of approximately 60kg.

$$\frac{200N \cdot 3}{9.80665} = 61,183Kg \tag{2.5}$$

The measuring body is a steel loaded member on which strain gauges are installed. The influence of a force deforms the measuring body, so there is deformation in places where the strain gauges are installed. The strain gauges are attached so that two are stretched and two are compressed when a force is applied.
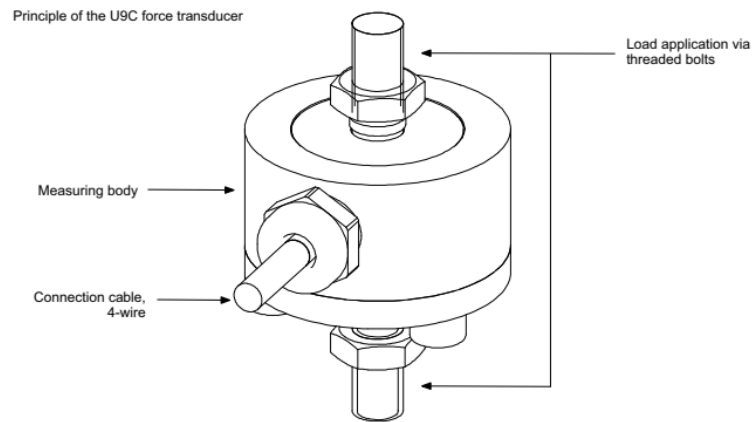
Figure 2.26: U9C Miniature Load Cell: for measurement of tensile and compressive forces. [18]

Installation

The forces to be measured must act on the transducer as accurately as possible in the direction of measurement. Torques, bending moments resulting from lateral force, eccentric loading and lateral forces themselves, may produce measurement errors and destroy the transducer if limit values are exceeded.[18] To minimize any errors, the U9C load cell was mounted with initial stress on the tension and compression bars as it was the recommended installation method for dynamic loading.

For this mounting variant, the transducer is mounted with tension/compression bars on a construction element and can measure tensile and compressive forces. Alternating loads are also correctly recorded if the transducer is mounted without axial play. For dynamic alternating loads, the upper and lower threaded connectors must be pre-stressed to above the maximum force to be measured and then locked in place. To ensure this the procedure was the following;

- Unscrew the locknut and screw on the threaded connector

- Pre-stress transducer to 110% operating load in tensile direction. The transducer itself can be used to measure this force if calibration is complete.

- Hand-tighten the locknut

- Relieve load on transducer

Calibration

As explained above, the load cells use strain gauges. The strain gauges are wired to form a Wheatstone bridge circuit. This mean that they change their ohmic resistance in proportion to their change in length and so unbalance the Wheatstone bridge. As the rig uses an excitation voltage, the circuit produces an output signal proportional to the change in resistance and thus also proportional to the applied force. Hence, the measured property from the sensor is the change in millivolt per volt of excitation voltage [mV/V] powering the bridge.

To calibrate the three load cells to correctly record tension and compression known weights are used. By using the Catman Easy software's "Adaption" function, we are able to measure the generated output in mV/V as a response to the applied weight.

The Root Mean Square (RMS) of 3 seconds of recording with the associated weight is presented in table 2.2.

Weight [g]	Z_1 [mV/V]	Z_2 [mV/V]	Z_3 [mV/V]
0	0.014456	-0.024777	0.048212
22260	1.086023	1.059558	1.129378

Table 2.2: Data measured with the HBM DAQ System using 2.5V DC Excitation - 500Hz Carrier Frequency.

2.8.2   Weight On Bit Calibration

Due to a flexible hose and wires mounted in drag chains, the measured load changes with respect to the position of the top plate. A correction must be implemented to correct for this effect to increase the accuracy of the WOB measurements. It is important that the measured load must be defined as the zero reference, such that the load cells measure the external weight applied to the bit only.

WOB is measured as the sum of the three load cells output in grams, divided by 1000 and multiplied by negative one to receive a positive number. The load cells measure a negative weight as the top plate is pushed upwards during drilling which causes the load cells to be in tension.

$$WOB = -\frac{Z_1 + Z_2 + Z_3}{1000} \tag{2.6}$$

To correct for the varying load experienced by the load cells during tripping, a polynomial function was generated using the polyfit function in matlab. Polyfit returns the coefficients for a polynomial function P(x) of degree n that is a best fit (in a least-squares sense) for the data. The polynomial function P(x) where P equals the weight calculated using Equation 2.6 and x equals the measured height of the top plate is found below in equation 2.7.

$$
\begin{aligned}
P(x) = &- 0.00000957341160996571x^3 + 0.00110493606784309x^2 \\
&- 0.0321241782842823x + 15.7694641736062
\end{aligned}
\tag{2.7}
$$
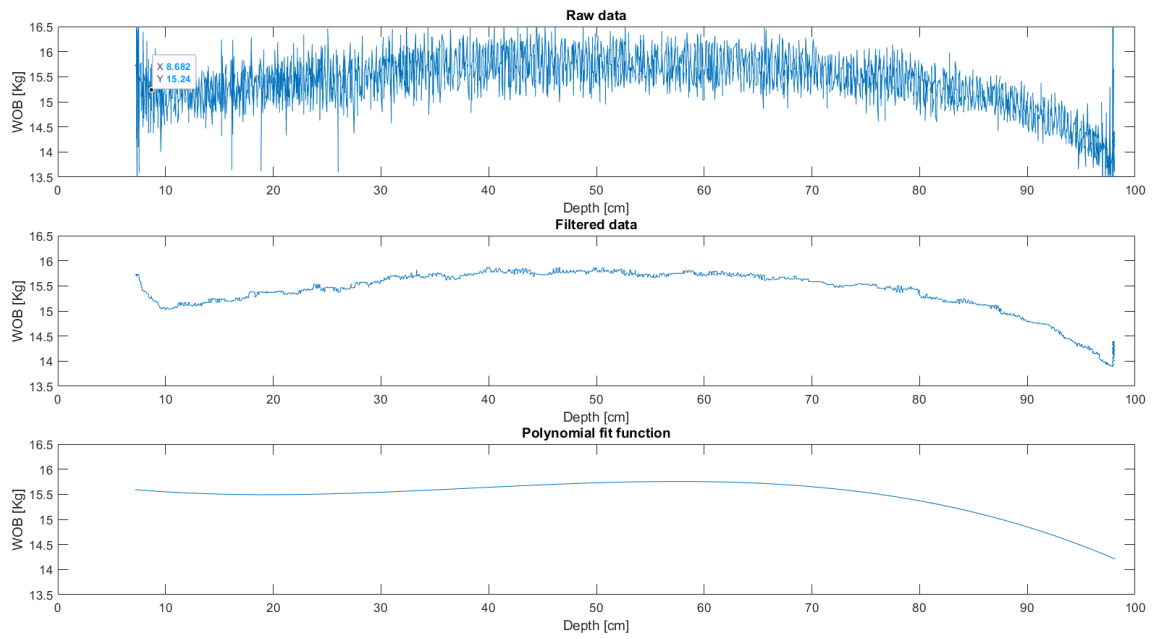
Figure 2.27: The change in load from lowering the top plate from its top position to its bottom.

By creating the polynomial function in matlab, one can subtract this function from the WOB data gathered by the load cells to achieve corrected WOB measurements that are used during drilling, as seen in Figure 2.28.
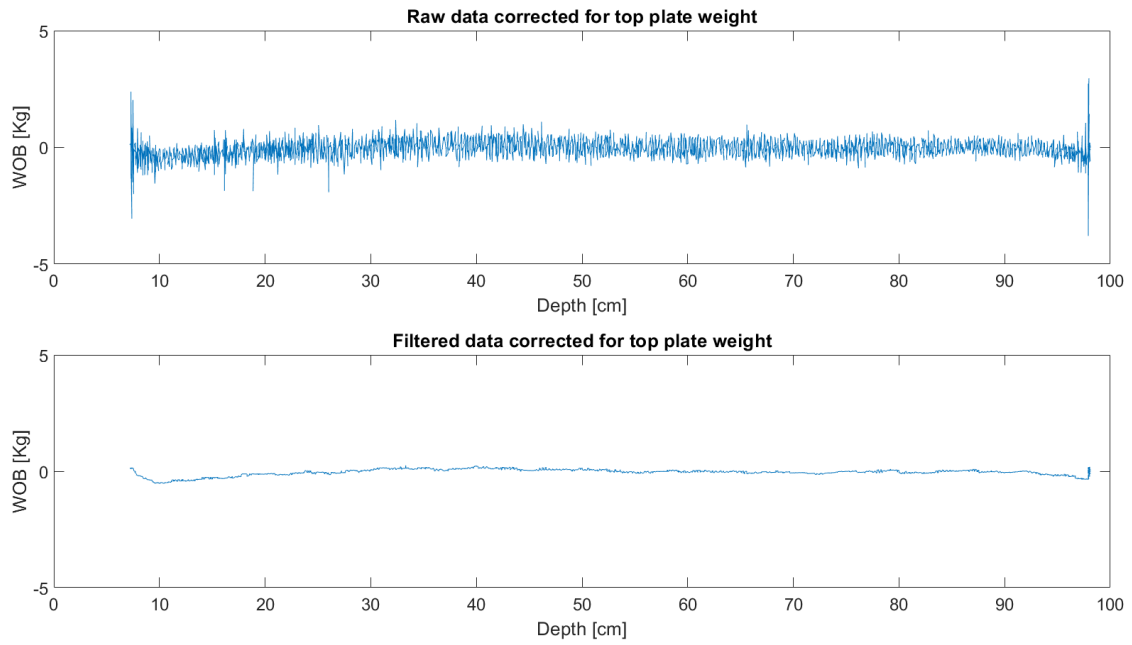
Figure 2.28: Lowering the top plate from its top position to its bottom after correcting for the varying load.

Chapter 3

Theory

3.1 Directional Drilling

Directional drilling is defined as the practice of controlling the direction and deviation of a wellbore to a predetermined underground target or location. [26] This requires tools, sensors and procedures to determine the location of the borehole and the path while drilling. The following list shows the main steps required to create a directional well for the laboratory-scale drilling rig.

- Calculation of the desired well trajectory

- Calculating northing, easting, TVD, vertical section and dogleg severity.

- Monitoring of the actual well path while drilling

- Correction of the drilling path during drilling by various algorithms

3.1.1 Directional Well Profiles

The shape of the well will depend on the penetration requirements. In practice, these generic shapes will be modified by local conditions.
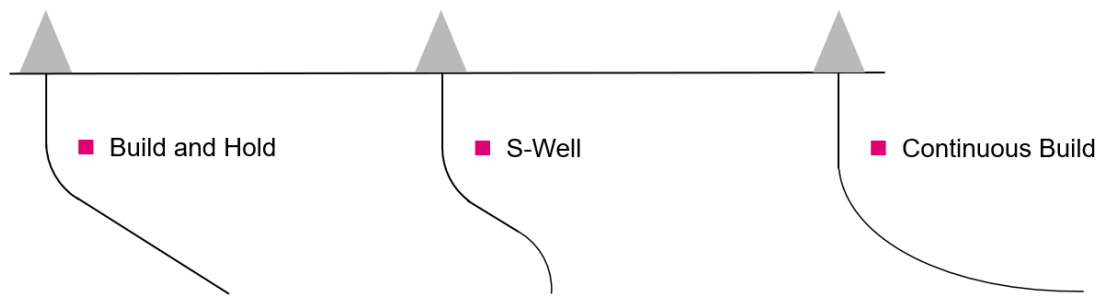
Figure 3.1: The three main 2-D shapes of a well; Build and hold, S-shaped and Continuous build.

According to the guidelines, the proposed wellpath for the Drillbotics competition may be any variant of a directional well profile. Figure 3.1 represents these profiles.

Build and hold

A build and hold profile is planned so that the initial angle is obtained at a shallow depth and then is maintained as a straight line to the target zone. Often, this profile is used as the building block of the extended-reach wells that require large horizontal displacement.

S-shaped

The S-shaped wells are often drilled due to their completion requirements. The well sets the initial deflection angle near the surface, similar to the build and hold profile. After attaining the appropriate lateral displacement, the hole is returned to near vertical and drilled to target.

Continuous build

A well profile with constant build to the target point can be applied to explore a stratigraphic trap or to obtain additional geological data.

3.1.2   Steerable Motors

A steerable motor can be used to steer the wellbore without drillstring rotation in directional drilling operations, or to drill ahead in rotary drilling mode. To enable steering of the bit, there are two operating modes; orienting and rotating. In orienting mode a downhole motor, Positive Displacement Motor (PDM) or turbine, rotates the bit whilst the drillstring is static. The BHA is designed to impart a sideload on the bit through either offset stabilizers or bend(s) in the BHA. This sideload causes the bit to build angle. In rotary mode the drillstring is rotated in addition to the bit rotation from the motor. The sideloading rotates with the drillstring and negates its deviating effect which causes a straight wellpath to be drilled. [19]
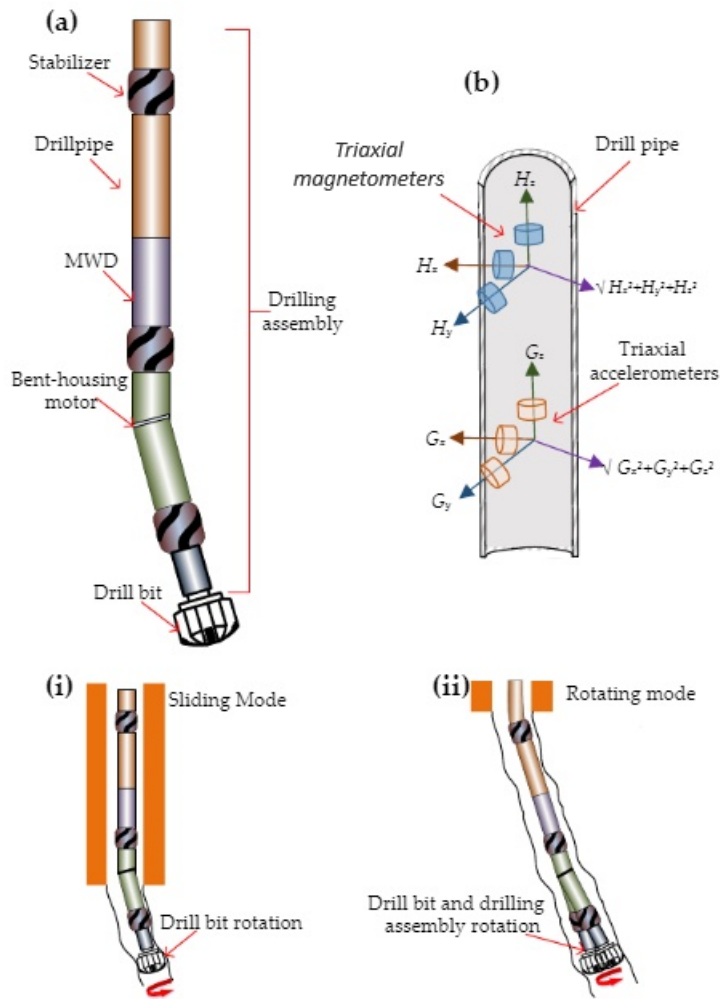
Figure 3.2: (a) Drilling assembly for directional drilling. (b) Triaxial magnetometers and accelerometers to obtain azimuth and inclination measurements of the well. (i) Orienting mode to build angle. (ii) Rotating mode initiated when the desired angle is obtained. [9]

3.1.3   Rotary Steerable System

Rotary Steerable Systems (RSS) entered the spotlight due to the oil industry requiring higher degrees of accuracy and improved rates of penetration, whilst also reducing overall drilling costs. RSS are able to drill faster, farther and more accurately than conventional steerable systems. [32] RSSs are much more complex

mechanically and electronically and are as a result more expensive to run compared to conventional steerable motor systems. These steerable systems have two different modes of operation, point-the-bit and push-the-bit.

Point the Bit

Point-the-bit systems are operated by placing a bend in the system, similar to conventional steerable motors. However, in the RSS, the bent housing is contained by means of an electric motor which rotates opposite to the direction and at the same speed as the drill string. This effect allows the bent housing to remain non-rotating while the collar is rotating. The bent housing orients the bit in the desired direction, whilst the drillstring is rotating. Point-the-bit systems claim to allow the use of a long-gauge bit to reduce hole spiraling and drill a straighter wellbore.
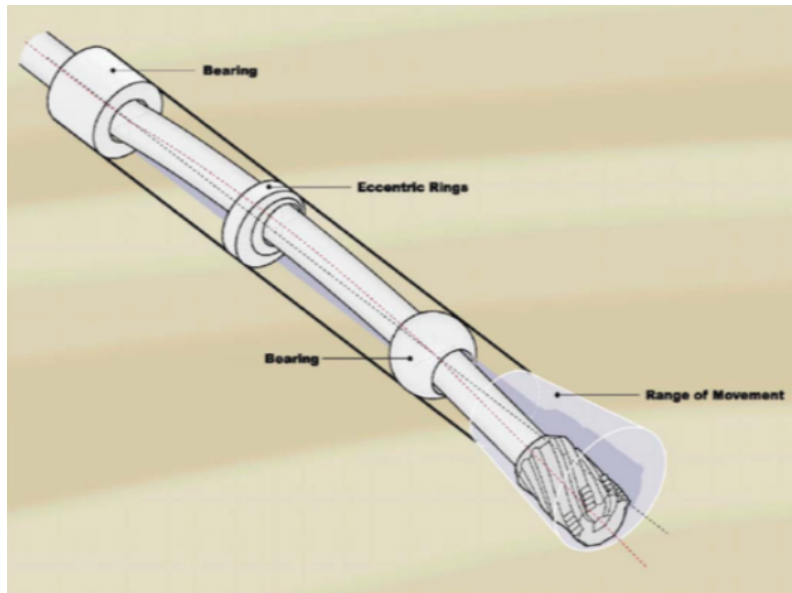
Figure 3.3: Rotary Steerable System - Point the bit. [3]

Push the Bit

Push-the-bit tools apply a side force against the formation in the bore-hole by using hydraulic pressure, or in the form of mechanical forces. A popular design has been to use pads near the bit which can be controlled and pushed against the wellbore to steer in any direction. Figure 3.4 shows a typical push-the-bit design.
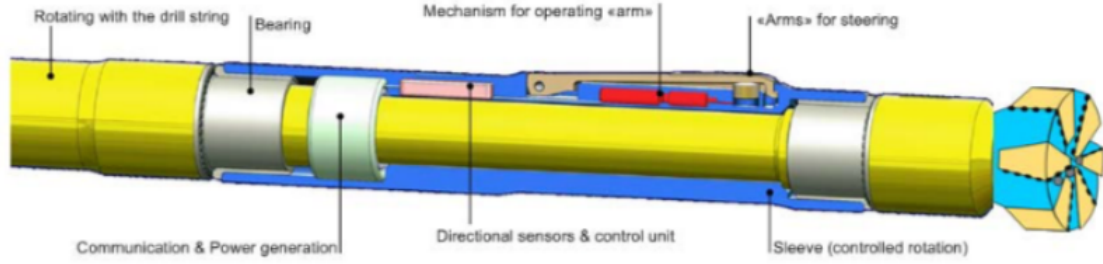
Figure 3.4: Rotary Steerable System - Push the bit.[3]

3.1.4 Concepts & Definitions

As downhole sensors are a key aspect in any directional drilling operation, it is important to understand what measurements are required to reach the specified target.

Measured Depth

Measured Depth (MD) is measured along the wellpath, and is the actual length of the well. MD is easily found by measuring the length of the tools and pipe lowered into the hole.

Azimuth

The angle between the geographic north and the projection of the wellbore onto the horizontal plane (directional angle).

To calculate the azimuth by use of an Inertial Measurement Unit (IMU) one can use formula 3.1. Where G_x, G_y and G_z, the gravity field strength, are measurements from the accelerometer and B_x, B_y and B_z, th magnetic field strength, are the measurements from the magnetometers. G is the gravity field

$$A = tan^{-1}\left(\frac{(G_xB_y - G_yB_x)\sqrt{G_x^2 + G_y^2 + G_z^2}}{B_z(G_x^2 + G_y^2) - G_z(G_xB_x + G_yB_y)}\right) \tag{3.1}$$

Inclination

The inclination is the angle between the tangent to the wellbore and the wellbore.

$$I = cos^{-1} \left(\frac{G_z}{\sqrt{G_x^2 + G_y^2 + G_z^2}} \right) \quad (3.2)$$

Toolface Orientation

The toolface can be described as the orientation of the motor bend which is aligned in a particular direction to make a desired deflection within the wellbore.[20] There are two ways to express the toolface orientation.

Magnetic or Gyro Toolface is the toolface orientation on the horizontal plane. It is measured in this way at low inclinations of less than 5°.

High Side Toolface is the toolface orientation measured from the high side of the borehole in a plane perpendicular to the axis of the hole. [20] To convert the magnetic or gyro toolface readings to high side toolface orientation one can use the following equation:

$$Highsidetoolface = Mag/Gyrotoolface - holeazimuth \quad (3.3)$$
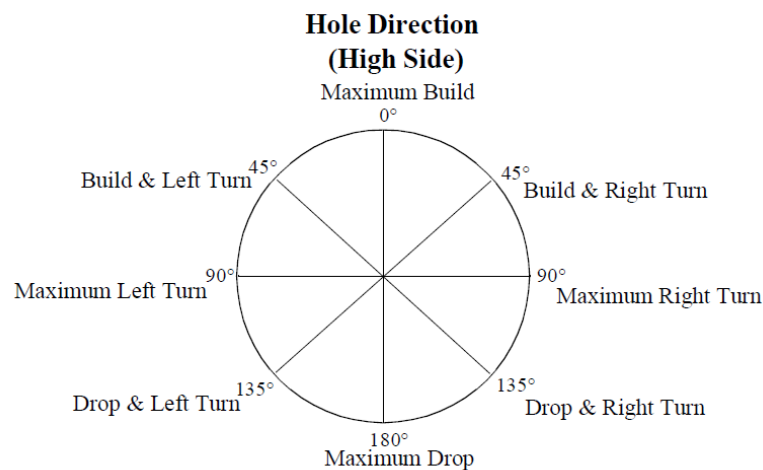
Figure 3.5: Rule of thumb chart when orienting steerable motors.[20]

Dogleg Severity

Dogleg Severity (DLS) is the combination of build and turn rate, where build rate is the change in inclination and turn rate is the change in azimuth between two survey points. The theoretical geometric dogleg severity is defined by three points of contact on a drilling assembly.

- The bit

- The motor stabilizer or upper bearing housing stabilizer (UBHS)

- The first string stabilizer above the motor

To calculate the theoretical geometric dogleg severity on can use equation 3.4, where L_1 and L_2 are the lengths between the bit and string stabilizers and ϕ is the tilt angle.[20]

$$TGDS(°/30m) = \frac{\phi \cdot 60}{L_1 + L_2} \qquad (3.4)$$

3.1.5 Survey Calculations

This section will present the method used for survey calculations for the small-scale drilling rig. There are five commonly used methods used for performing survey calculations in the industry.

- Tangential Method

- Average Angle Method

- Balanced Tangential Method

- Radius of Curvature Method

- Minimum Curvature Method

Whilst there are advantages and disadvantages for all of the methods. The balanced tangential method was chosen for the experiments as the uncertainty calculations used are based upon this method. The methods and how they are used is explained more thoroughly in [22]. Once the desired trajectory has been determined, survey

stations are defined at discrete intervals along the trajectory. At each survey point drilling is stopped to measure inclination and azimuth as a function of the measured depth.

Balanced Tangential Method

The method is applied by taking the direction of the previous survey point for the first half of the course length, then the direction of the lower survey point for the second half of the course length. Both the upper and lower portions of the assumed wellbore course are in error, but the errors are opposite and will nearly cancel each other. This method is simple to program in spreadsheets and gives accuracy comparable to the minimum-curvature method, which is regarded as the most accurate method. [26] The outputs from this method are ΔV, ΔN and ΔE. The 3D well path is derived from MD, inclination and azimuth.

$$\Delta V = \frac{1}{2} \cdot \Delta MD \cdot (cos(I_1) + cos(I_2)) \tag{3.5}$$

$$\Delta N = \frac{1}{2} \cdot \Delta MD \cdot (sin(I_1)cos(A_1) + sin(I_2)cos(A_2)) \tag{3.6}$$

$$\Delta E = \frac{1}{2} \cdot \Delta MD \cdot (sin(I_1)sin(A_1) + sin(I_2)sin(A_2)) \tag{3.7}$$

3.1.6 Ellipsoid of Uncertainty

Every survey measurement has an associated uncertainty. The source of the error associated with the measurement may be attributed to the equipment error for the measurements of inclination and azimuth. The equipment error can be accuracy limitations, instrument alignment errors in the tool, tool misalignment and magnetic interference from other components on the rig. [28]

The uncertainty may also be caused by the assumptions made while calculating the trajectory, for example the balanced tangential method assumes that the tangent to the angle determines the wellbore course which may not always be practically true.

The deeper in the well, these errors will accumulate with increasing depth and is expressed by the uncertainty ellipses.

For further information regarding bit position uncertainty one should read the findings from the master thesis written by Khadisov, Magomed in affiliation with the Drillbotics team. [22]
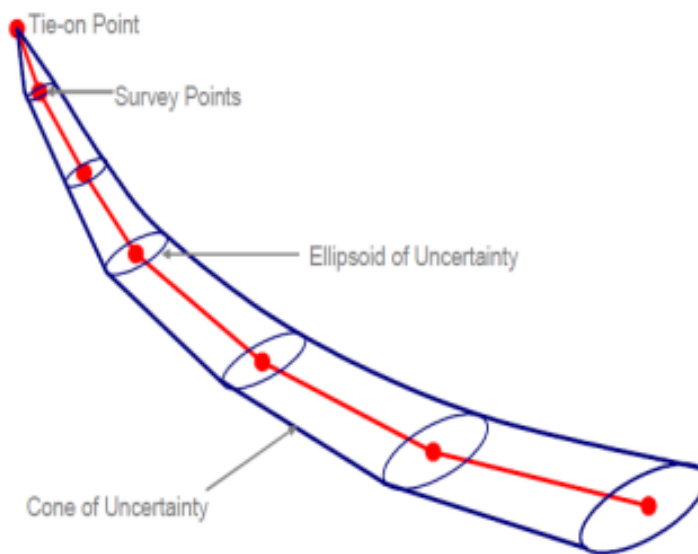
Figure 3.6: Ellipsoid of Uncertainty. [28]

3.2 Drill String Mechanics

In this section, the fundamental physics of material mechanics will be covered with a particular focus drill pipe. In the case for this thesis, the drill pipe is a limiting component so it is natural to have the drill pipe in focus. Mechanics of materials gives an insight of internal effects of bodies being subjected to external loads. Understanding mechanics of materials gives the ability to predict how bodies respond to experiencing different loads under different conditions. Mechanics of materials are usually used to analyse:

- Stress

- Strain

- Stiffness

- Burst

- Collapse

- Buckling

All theoretical material presented in this section is based on the material taught by Mesfin Belayneh Agonafir's in the course Advanced Well and Drilling Engineering (PET 580) at the University of Stavanger [2], unless else is stated.

3.2.1 Stress & Strain

Stress

The definition of stress is force per unit area. The force can either be exerted perpendicular or parallel to the unit area. Perpendicular force acting on a unit area is generally known as normal stress, σ, while parallel force is known as shear stress, τ. The equation expressing stress is shown in equation 3.8, where σ is stress, F is force and A is unit area.

$$\sigma = \frac{F}{A} \tag{3.8}$$

3D Stress State   Plane Stress
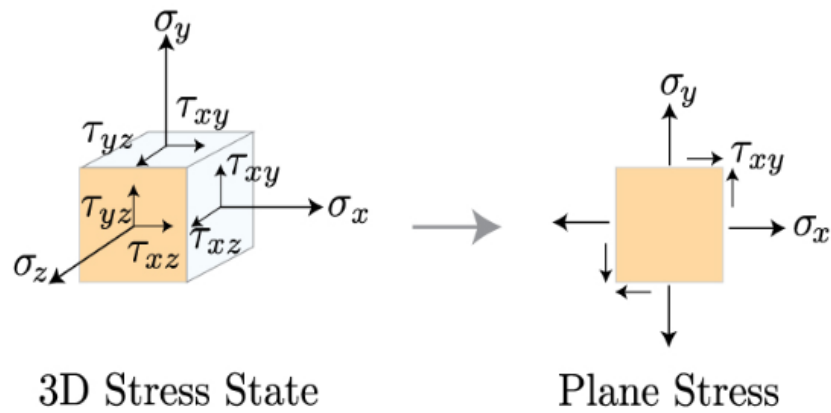
Figure 3.7: Normal and shear stress of a cube. [36]

Strain

The definition of strain is deformation of an object relative to its original dimensions. For a specimen, strain is calculated by dividing the change in length (δ) on the original length (L_0), as equation 3.9 describes.

$$\epsilon = \frac{\delta}{L_0} \tag{3.9}$$
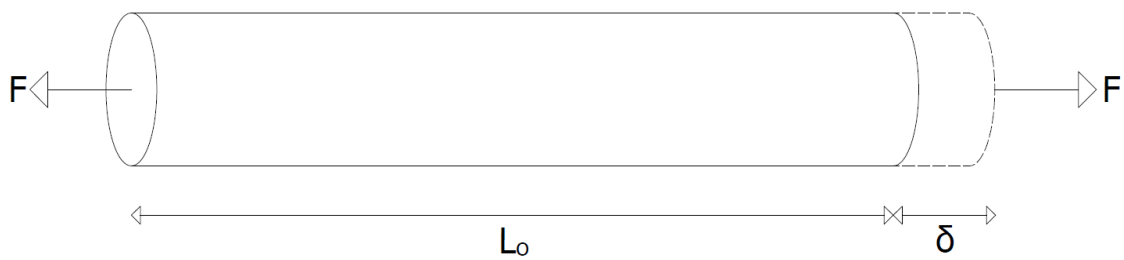
Figure 3.8: Strain of a cylinder.

3.2.2 Axial Loading

In regard to load-bearing structures, axially loaded bodies are highly common and have an important role in such structures. Axially loaded bodies are arguably the simplest load-regime to analyse and are either in a compressive or tensile state. For stress calculations, normal sign convention is negative for compression (-) and positive for tension (+).
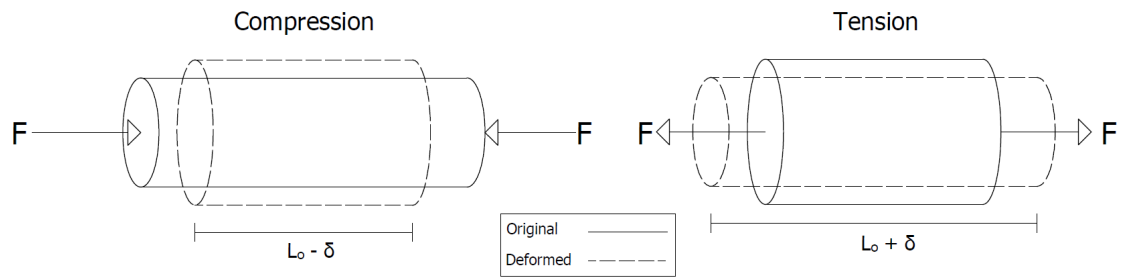
Figure 3.9: Compressive and tensile stess of cylinder.

Stress-Strain Diagram.

From a stress-strain diagram, a lot of material properties can be obtained. The material properties obtained from the diagram provides information about the strength of the material. The diagram created by performing a tension test. A tension test is conducted by gradually increasing a load on a piece of material while measuring elongation. By using equation 3.8 and 3.9, the stress and strain values can be found and plotted.
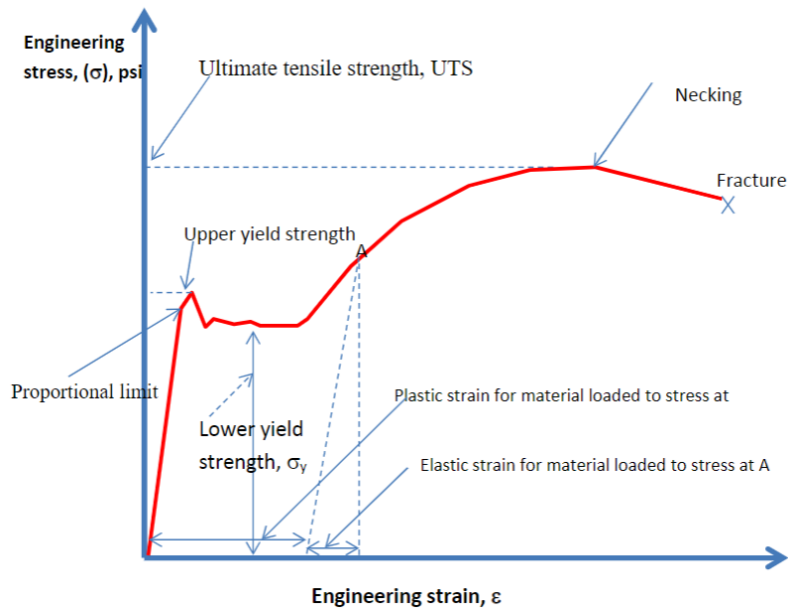
Figure 3.10: A stress-strain diagram of steel. [2]

Elastic region is where stress is proportional to strain. If a piece of material is kept within the elastic region, the strain will return to zero as the stress is removed. No permanent deformation will happen within this region. From the elastic region, the **modulus of elasticity** E can be obtained by using equation 3.10. Equation 3.10 is only valid for the elastic region with proportionality limit as the upper boundary. Modulus of elasticity is an important material property which relates stress and strain in the elastic region.

$$E = \frac{\Delta\sigma}{\Delta\epsilon} \tag{3.10}$$

Yield strength σ_y is the maximum stress a material can endure before starting to plastically deform. It is a measure of material strength and is usually expressed in MPa. In materials like aluminum and steel alloys, there is no clear boundary between the elastic and plastic region. In that case, a parallel line to the elastic region with a 0.2% offset on the strain axis is constructed. The yield strength can

then be found at the point where this constructed line crosses the stress-strain curve.

Plastic region is the region subsequent of surpassing the yield strength. Exceeding the yield strength will cause the material to be permanently deformed, i.e. when stress is released, the strain does not go to zero.

Ultimate tensile strength, σ_{TS} is defined as the maximum stress observed in the stress-strain diagram. When a material is loaded beyond the yield strength, the material experiences a strain-hardening effect causing an increase in strain to increase the stress. As stress surpasses the ultimate tensile strength, a reduction in cross-sectional area, called necking, will occur.

Rupture will happen as the necking proceeds and the cross-sectional area is reduced to a level where the material fails.

Modulus of Resilience is the area under the stress-strain curve in the elastic region up until yield. It is a measure of absorbed energy per unit volume up to the yield point. For materials with a clear transition from elastic to plastic equation 3.11 can be used. Otherwise, the area must be divided into sections and calculated using regular geometry calculations.

$$R = \frac{\sigma_y \epsilon}{2} = \frac{\sigma_y^2}{2E} \tag{3.11}$$

Modulus of toughness is the area under the entire stress-strain diagram. It provides a measure of the material's ability to absorb energy until rupture.

Poisson's ratio, ν is the relation between lateral and longitudinal strain. When a piece of material is being elongated (longitudinal), the specimen experiences a lateral contraction as shown in Figure 3.9. The Poisson's ratio is defined according to equation 3.12, where Δw is change in width (lateral direction), w_o is original width, ΔL is change in length (longitudinal direction) and L_o is the original length.

$$\nu = -\frac{\frac{\Delta w}{w_0}}{\frac{\Delta L}{L_0}} \tag{3.12}$$

True vs Engineering Stress and Strain.

True vs Engineering Stress

Engineering stress considers the cross-sectional area to be constant. From equation 3.13, the force is divided on the original cross-sectional area A_0.

$$\sigma_e = \frac{F}{A_0} \tag{3.13}$$

True stress considers an instantaneous cross-sectional area. From equation 3.14, the force is divided on the instantaneous cross-sectional area A_t.

$$\sigma_t = \frac{F}{A_t} \tag{3.14}$$

The relation between engineering and true stress is shown in equation 3.15.

$$\sigma_t = \frac{F}{A_t} = \frac{F}{A_0}\frac{L_f}{L_0} = \sigma_e(\epsilon_e + 1) \tag{3.15}$$

When the deformation is small, change in cross-sectional area is insignificant and can be neglected. The deformation is small in the elastic region and when the material is very brittle. In these particular cases, it makes sense to use engineering stress.

However, when the deformation is large, the change in cross-sectional area is significant and is not necessarily neglected. In the plastic region and for very ductile materials, deformation can be large and true stress can be used in calculations.

True vs engineering strain

Engineering strain follows the same definition as the strain presented earlier.

$$\epsilon_e = \epsilon = \frac{\Delta L}{L_0} = \frac{L_f - L_0}{L_0} \tag{3.16}$$

True strain, on the other hand, is defined by the continuity equation expressed in equation 3.17.

$$\epsilon_t = \int_{L_0}^{L_f} \frac{dl}{l} = ln\left(\frac{L_f}{L_0}\right) \tag{3.17}$$

For small strain, the true and engineering strain can be related according to equation 3.18 by using the definition of each type.

$$\epsilon_t = ln(\epsilon_e + 1) \tag{3.18}$$

When the strain is large, equation 3.18 does not hold true and equation 3.17 has to be used.

For calculations in the plastic region, assuming that the material is incompressible, i.e. density does not change and that the volume is constant, equation 3.19 can be obtained.

$$\epsilon_t = ln\left(\frac{A_0}{A_t}\right) = 2ln\left(\frac{D_0}{D_t}\right) \tag{3.19}$$
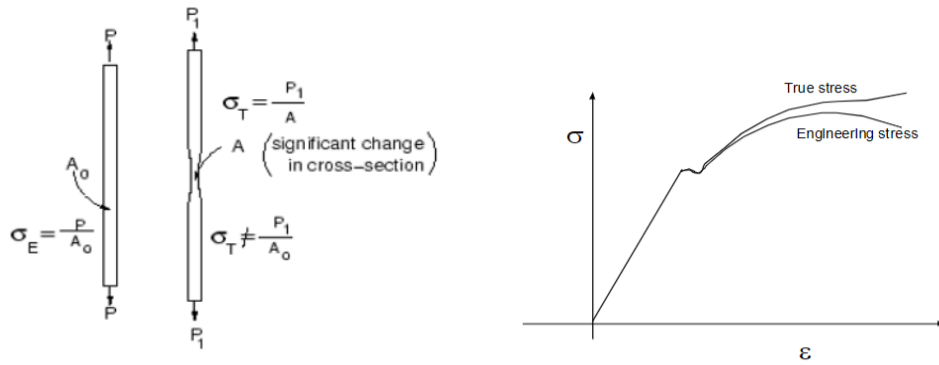
(a) Visualization of true vs engineering stress and strain.

(b) Stress strain diagram comparing true vs engineering.

Figure 3.11: True vs engineering stress and strain. [2]

3.2.3 Buckling

Buckling of a pipe is defined as lateral deflection during compressive loading. A pipe will deflect laterally if the compressive loading exceeds the critical buckling load. On this project, the weight of the pipe and BHA is not sufficient to be able to penetrate the formation. To accommodate this, the pipe and BHA are continuously being pushed by actuators effectively giving sufficient WOB. Due to being continuously pushed against the formation, the pipe is always in compression and is highly prone to deflection. In addition to being always in compression, the pipe is mostly in an unconstrained state due to having a long and large BHA compared to the pipe.

Slenderness

A pipe's tendency to buckle can be indicated by assessing its slenderness ratio. If the pipe has a high slenderness ratio, it is more susceptible to buckle and can be categorized as long. For long pipes, i.e. high slenderness, Euler's critical load formula

is applicable. A high slenderness ratio is defined as slenderness ratio larger than the critical slenderness ratio, $R_s > R_{crit}$. However, if the slenderness ratio is less than the critical slenderness ratio, $R_s < R_{crit}$ it can be categorized as intermediate or short and Johnson's formula has to be used.

The slenderness ratio is defined as,

$$R_s = \frac{L}{r_g} \tag{3.20}$$

Where L is unsupported length and r_g is radius of gyration. Radius of gyration is defined as,

$$r_g = \sqrt{\frac{I}{A}} \tag{3.21}$$

Where I is second moment of area and A is cross-sectional area. The second moment of area can be calculated by using formula 3.22.

$$I = \frac{\pi}{64} \left(D_o^4 - D_i^4 \right) \tag{3.22}$$

The critical slenderness ratio is determined by using formula 3.23.

$$R_{Crit} = \sqrt{\frac{2\pi^2 E}{K^2 \sigma_y}} \tag{3.23}$$

All parameters in this formula have previously been addressed except effective length factor, K. K represents the length between the inflections on the buckled pipe.

Euler Buckling

There are several models for assessing buckling of drill pipe. Due to the pipe not being constrained and having a large slenderness ratio, Euler's critical column buckling load model is the best suited for this project. Euler's critical load is given as follows,

$$F_{Cr,E} = \frac{\pi^2 EI}{(L_{eff})^2} \tag{3.24}$$

Where E is the modulus of elasticity, I is second moment of area, L_{eff} effective length. The effective length, L_{eff} is calculated by,

$$L_{eff} = KL \tag{3.25}$$

where K is effective column length factor and L unsupported length. The effective length factor relates columns with different end conditions as depicted in Figure 3.12.

End Condition:	Pinned-Pinned	Fixed-Fixed	Fixed-Pinned	Fixed-Free
Illustration:				
Theoretical Effective Length Factor, K:	1	0.5	0.699	2
Recommended Effective Length Factor, K:	1	0.9	0.9	2.1

Figure 3.12: Effective length factor selection based on end condition. [25]

Johnson Buckling

Even though the Euler' model is better suited for this project, it is worth to mention Johnson's critical buckling load. Johnson's formula is applicable for intermediate slenderness pipes. If it is decided to drill with a shorter pipe than the usual length - one must assess buckling in regard to Johnson's formula. Johnson's formula is expressed as,

$$\sigma_{Cr,J} = \sigma_y - \left(\frac{\sigma_y}{2\pi} \frac{KL}{r}\right)^2 \left(\frac{1}{E}\right) \tag{3.26}$$

3.2.4 Torsional Loading

To understand torsion one can consider a cylindrical rod that is fixed on one end and twisted on the other as shown in Figure 3.13. Shear stress τ resists the twisting moment across the rod. At the center of the rod, the shear stress is zero and is linearly increased as radial distance from center increases with maximum at full radius.
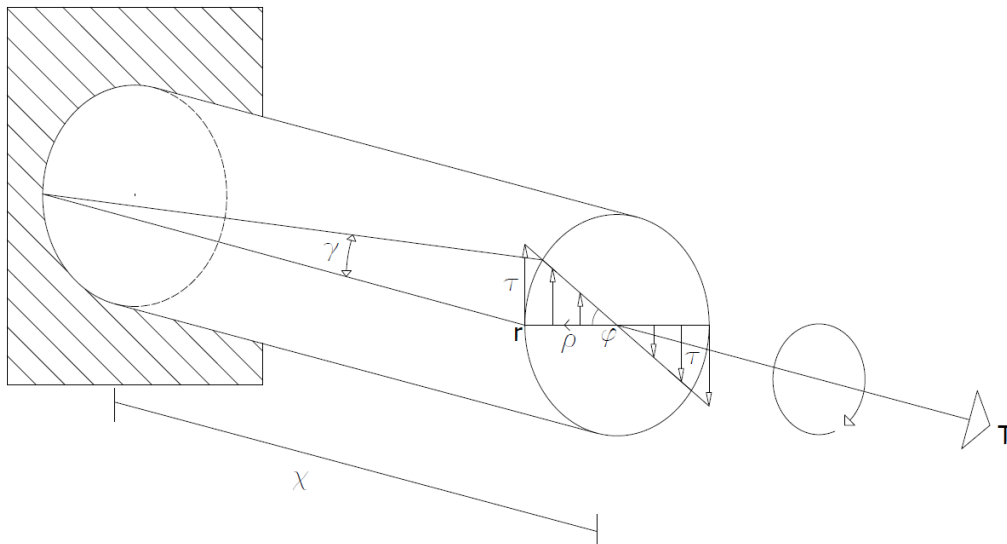
Figure 3.13: Torsion of a cylinder including symbols.

In this Figure (3.13), A is cross-sectional area, x is distance along the cylinder, T is torque, r is radius of cylinder, ρ is radial distance, φ is twist angle, γ is shear strain and τ is shear stress.

Some assumptions are made in order to calculate and analyze torsional strength:

- Torque applied axially at one end
- Uniform cross-section
- Uniform material

- Shear strain γ is maximum at the surface and zero at the center with a linear proportionality.

- Small angle of twist φ

- Hooke's law applies due to being linearly elastic.

Shear Stress

As mentioned and shown at the end cross-sectional area in of Figure 3.13, **shear stress, τ,** increases from zero at center to maximum,τ_{max}, at surface. Due to the proportionality of shear stress, equation 3.27 can be used to calculate shear stress at other radial positions than at full radius.

$$\tau = \frac{\rho}{r}\tau_{max} \tag{3.27}$$

By applying the theory of moment equilibrium, $\sum M = 0$, torque must be shear stress, τ, multiplied by area, A.

$$T = \int \rho\tau dA = \int \rho \left(\frac{\rho}{r}\tau_{max}\right) dA \tag{3.28}$$

As stated in the assumptions, $\frac{\tau_{max}}{r}$ is constant , which leads to equation 3.29,

$$T = \frac{\tau_{max}}{r} \int \rho^2 dA \tag{3.29}$$

The integral is now reduced to only depend on the geometry, i.e. radial distance ρ from center, of the cylinder. In fact, the remaining integral is called polar moment of inertia, J. The polar moment of inertia can be determined by using an area element of differential rings. For a cylinder, the rings have a thickness dp and circumference of $2\pi\rho$. Thus, dA can be expressed as $2\pi\rho d\rho$.

$$J = \int \rho^2 dA = \int_0^r \rho^2 (2\pi\rho d\rho) = \frac{\pi}{2}r^4 \tag{3.30}$$

For a pipe, one simply subtracts the hollow area with radius r_i from the total area with radius r_o as expressed in equation 3.31.

$$J = \frac{\pi}{2} \left(r_o^4 - r_i^4 \right) \tag{3.31}$$

By substituting the integral in equation 3.29 with polar moment of inertia, J, one is left with

$$T = \frac{\tau_{max} J}{r} \tag{3.32} \qquad\qquad \tau_{max} = \frac{Tr}{J} \tag{3.33}$$

Shear Strain

If Figure 3.13 is revisited, **shear strain, γ,** can be explained. Shear strain can be determined by the angle of twist φ, radial distance ρ, and the length of the specimen x according to equation 3.34.

$$\gamma = \frac{\rho \varphi}{x} \tag{3.34}$$

As stated in the assumptions, the maximum strain γ_{max} is located at the surface of the specimen, namely at radius r. Hence, equation 3.35 is obtained.

$$\gamma_{max} = \frac{r \varphi}{x} \tag{3.35}$$

Since neither the twist angle φ or length x changes of a cross-sectional area, $\frac{\varphi}{x}$ remains constant throughout the specimen. Thus, combining equation 3.34 and 3.35 gives the following equation.

$$\gamma = \frac{\gamma_{max}}{r} \rho \tag{3.36}$$

Shear Stress vs Strain Diagram

The shear stress - strain diagram will have a similar shape and characteristic as for normal stress - strain diagram. In Figure 3.14, a simplified diagram is displayed with important properties. Subscript y represents at yield, u at ultimate and r at rupture of the shear stress and strain. G is the shear modulus.
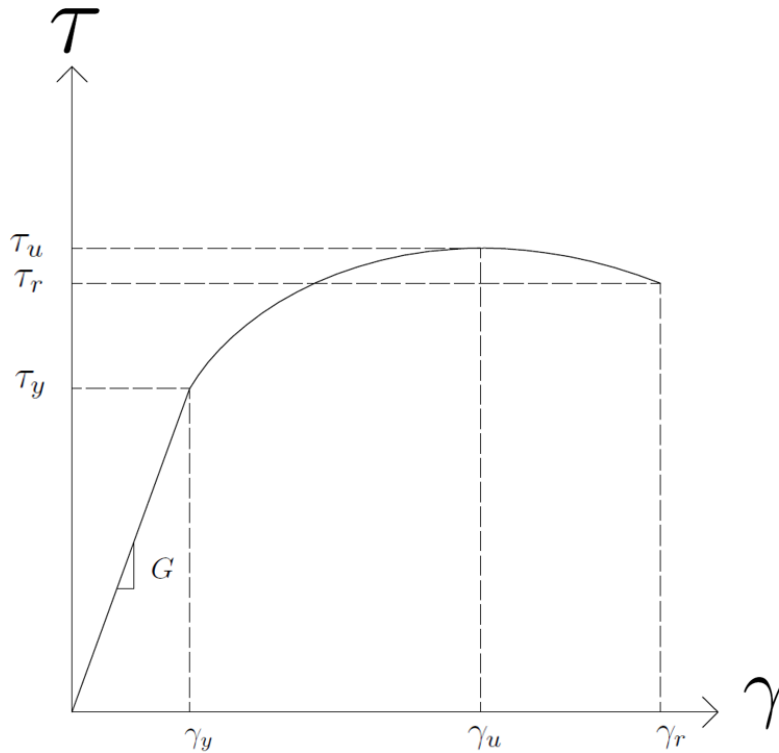
Figure 3.14: Shear stress-strain diagram

Shear modulus, G, is the shear equivalent of modulus of elasticity, E, for normal stress-strain diagram. It describes the relation between shear stress and strain in the elastic region of a specimen being subjected to torque.

$$G = \frac{\Delta \tau}{\Delta \gamma} \tag{3.37}$$

Since both modulus of elasticity, E, and shear modulus, G, are derived from Hooke's law, the moduli is related by equation 3.38 for an isotropic material.

69

$$G = \frac{E}{2(1 + \nu)} \tag{3.38}$$

3.2.5 Tubing Stresses

Tubing stress calculations are differentiated based on whether the tubing is thick-walled and thin-walled. A tubing is defined as thick-walled if the thickness is larger than 10 % of the inner radius. For this project, all tubings used are thick-walled. Thus, thick-walled tubing stress theory is considered in this thesis. For thick-walled tubing stress theory, Lamé's equations have been used to derive the tubing stress equations. In Figure 3.15, the tubing stresses are visualized.
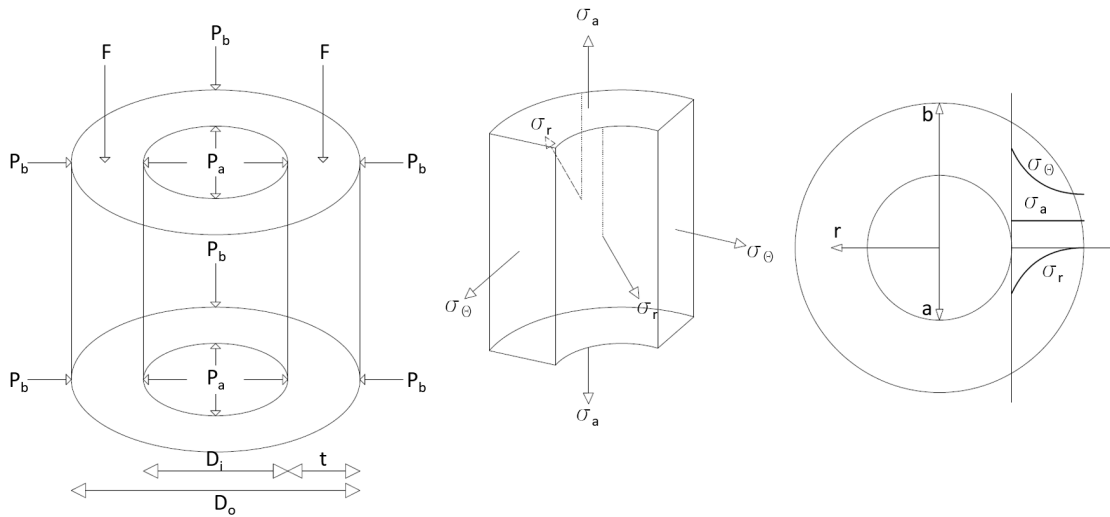
Figure 3.15: Tubing stress.

Axial Stress

Axial stress comes from the contribution of axial force in either tension or compression distributed across the cross-sectional area.

$$\sigma_a = \frac{F_a}{A} + \frac{p_a a^2 - p_b b^2}{b^2 - a^2} \tag{3.39}$$

Bending Stress

When drilling deviated wells, bending stress occurs in the tubing. The bending stress is a result of inclination of well and buckling. The bending stress caused in deviated wells can be calculated using formula 3.40.

$$\sigma_B = \pm \frac{ED_o}{2R_c} \tag{3.40}$$

Where σ_B is the bending stress, D_o is outer diameter, E modulus of elasticity and R_c is radius of curvature.

To get a more conservative axial stress, the bending stress has to be added to find maximum axial stress.

$$\sigma_a^{max} = \sigma_a + \sigma_B \tag{3.41}$$

Hoop Stress

Hoop stress is stress in the circumferential direction generated due to pressures.

$$\sigma_\theta = \frac{p_a a^2 - p_b b^2}{b^2 - a^2} + \frac{a^2 b^2}{(b^2 - a^2) r^2}(p_a - p_b) \tag{3.42}$$

Radial Stress

Radial stress is stress in the radial direction generated due to pressures.

$$\sigma_r = \frac{p_a a^2 - p_b b^2}{b^2 - a^2} - \frac{a^2 b^2}{(b^2 - a^2) r^2}(p_a - p_b) \tag{3.43}$$

3.2.6   Von Mises Yield Criterion

The von Mises yield criterion or maximum distortion criterion describes the yielding of materials under combined states of stress. Von Mises yield, σ_ν, is calculated based on the principal stresses (axial, radial and hoop stress) in addition to the shear stress caused by torque. In equation 3.44, the von Mises yield stress equation is displayed.

$$\sigma_\nu = \sqrt{\frac{1}{2}\left((\sigma_\theta - \sigma_r)^2 + (\sigma_r - \sigma_a)^2 + (\sigma_a - \sigma_\theta)^2\right) + 3\tau^2} \qquad (3.44)$$

3.3 Bit design Theory

[] Naturally, drill bits are essential in every drilling operation due to being one of the strongest contributors to drilling performance. Drill bits have a great influence on ROP, borehole quality and time consumption which effectively are measures of drilling performance. In the oil & gas industry today, three types of drill bits dominate the marked:

- Roller cone

- PDC

- Hybrid

When selecting or designing a drill bit, several key aspects must be understood in order to make the right bit considerations for your need. These aspects for Polycrystalline Diamond Compact bits will be covered in this section.

3.3.1 Bit Bodies

Polycrystalline Diamond Compact bits are the most common in the fixed-cutter bit family. They are usually considered as quite durable since they are comprised of a single rotating steel or matrix body where the synthetically made diamonds are brazed into the blades of the body. In Figure 3.16 basic nomenclature for PDC bits are presented.
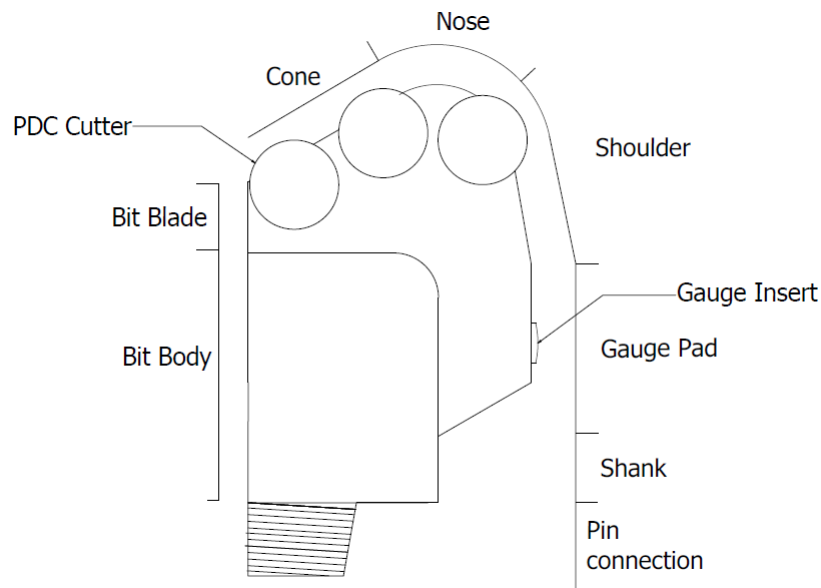
Figure 3.16: Basic bit nomenclature

The steel and matrix body are structurally dissimilar and have different capabilities and advantages. The matrix body is considered as a very hard composite material comprising of tungsten carbide and a metallic binder. The process of manufacturing a matrix body bit is done by using a mold and furnace. In the furnace, the tungsten carbide grains are metallurgically bonded to the softer, tougher binding material. The steel body on the other hand, is manufactured by machining a piece of steel according to the design.

The different manufacturing processes give quite different metallurgical properties. The very hard matrix body gives great strength in tensile direction, making it capable of withstanding high compressive loads i.e. WOB. In addition, the hardness makes it resistant to erosion and abrasion, but less capable of absorbing impact energy. Due to steel having a higher ductility than the composite of tungsten carbide, steel body bits are less likely to fail of impact loads. The steel body being softer makes it more prone to failure by erosion and abrasion. One can say the matrix body and steel body are metallurgically opposite. [31]

3.3.2 Bit Profile

The bit profile represents the shape of the PDC bit. The bit profile is an important design parameter that governs hydraulic efficiency, cutter loading and wear characteristics across the bit face. The principle influence of the bit profile is hydraulic flow efficiency. Optimal ROP will be impeded if the bit is not capable of removing cuttings at the same rate as it is generated, i.e poor hydraulic efficiency. In that case, the generated cuttings restrict the penetration, leading to a sub-optimal ROP. The hydraulic flow across the bit also prevents thermal damage to cutter elements as it cools the bit with fluid. [30]

The bit profile also directly influences:

- Stability

- Steerability

- Cutter density

- Durability

Generally, bit profiles are divided into four categories.

- Long parabolic profile

- Medium parabolic profile

- Short parabolic profile

- Flat profile

The different profiles are presented in Figure 3.17 below.
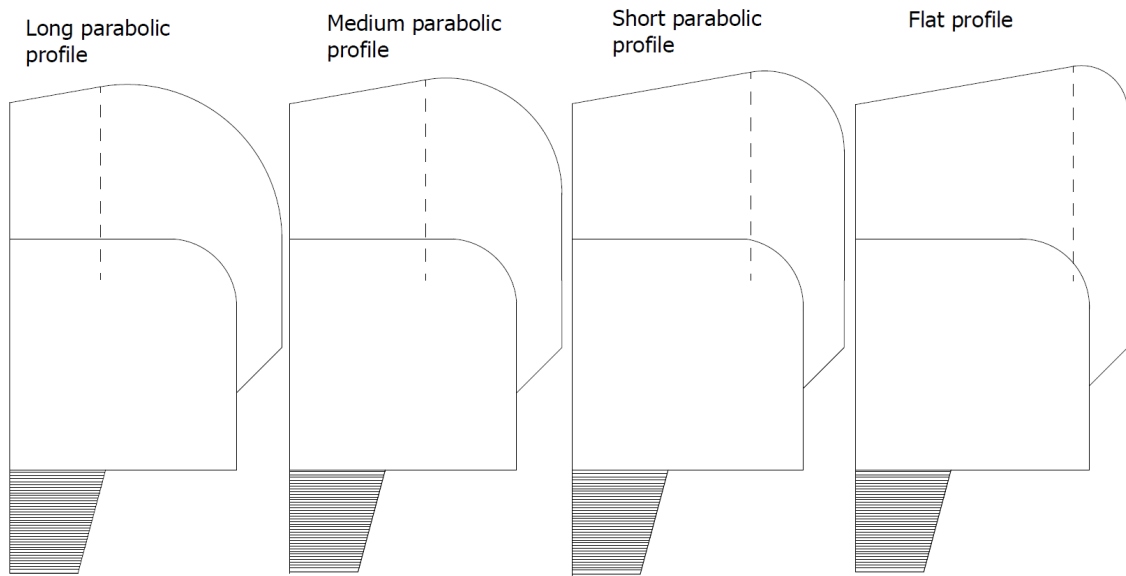
Figure 3.17: Simple representation of bit profiles

Flat bit profiles are considerably less aggressive than parabolic profiles. Flatter profiles distribute axial loading more uniformly on the individual cutters, making the bit more suitable for drilling in harder formations as it allows for a higher WOB. As the nose radius increases, the profiles becomes more parabolic leading to higher aggressiveness. More aggressive bits produce high ROP at the expense of accelerated abrasive wear on the nose of the bit. Short to medium parabolic profiles are preferred over flat and long parabolic profiles due to the balance of performance and longevity. [30]

Another important aspect of the bit profile is the cone angle. Cone angles are usually categorized as shallow, medium and deep as shown in Figure 3.18. Deeper cone angles result in a more stable bit with increased diamond volume in the center. The deep cone angle naturally creates a cone in the formation while drilling, keeping the bit stable in the center of the well. The increased diamond volume in the center reduces the aggressiveness of the bit. However, good stability comes at the expense of steerability. Shallower cone angles are significantly more steerable and aggressive than deeper angles. Another benefit of a shallower cone angle is the increased cleaning efficiency across the bit face. [15]

75
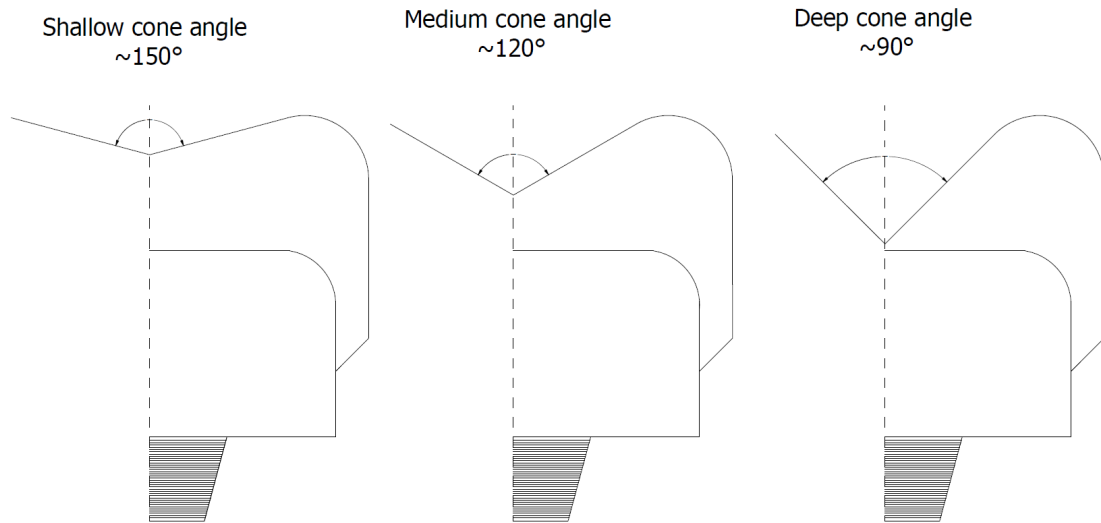
Figure 3.18: Simple representation of cone angles

3.3.3 PDC Cutter Considerations

PDC bits mainly drill by shearing the formation using the PDC cutters. The formation failure modes experienced are brittle and plastic failure. Under plastic failure mode, the formation is elastically deformed until it yields, then plastically deformed until rupture of the formation. Brittle failure has no or very little elastic deformation before failure is experienced. These effects can more easily be understood using a stress-strain curve.
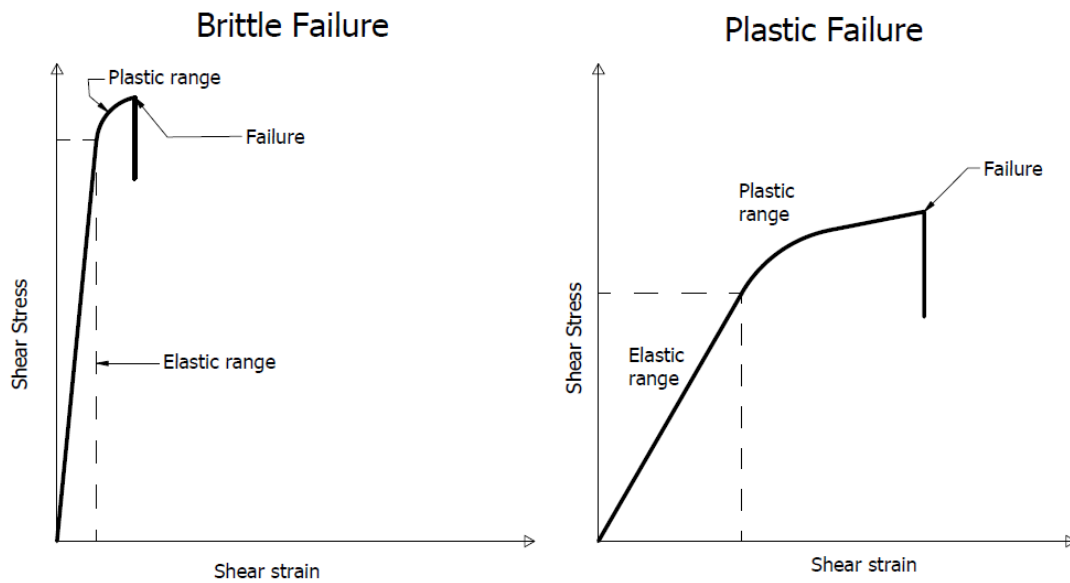
Figure 3.19: Formation failure from shear stress and strain

The shear stress is generated by applying vertical penetrating force, i.e. WOB, and horizontal force are transmitted into the cutters from either a top drive or downhole motor. The resultant force from the vertical and horizontal forces defines a thrust plane for the cutter as shown in Figure 3.20. While rotating, cuttings are sheared off at a formation strength dependent angle relative to the thrust plane, also shown in Figure 3.20.
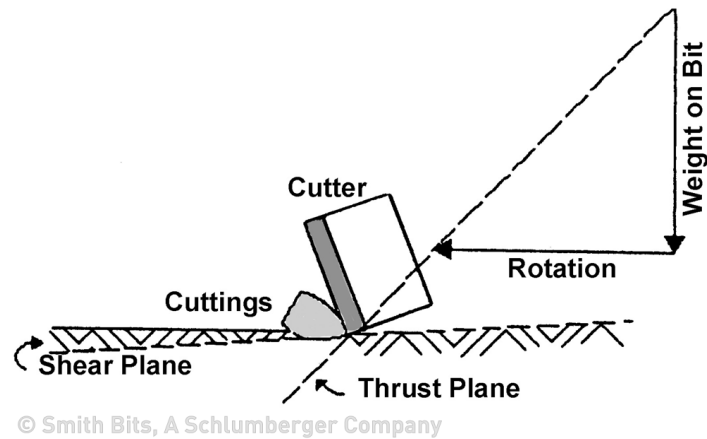
Figure 3.20: Shear and thrust on a cutter. [29]

Following these basics of how PDC bit drill, considerations like cutter placement, layout and orientation will be addressed more thoroughly, in addition to how these considerations affect drilling performance.

Cutter Placement

The cutters must be placed in such a way that they ensure complete coverage from the apex of cone to gauge of the bit. If complete coverage is not achieved, the drilling performance and longevity of the bit will be significantly reduced as some formation has to be crushed or ground away by the body itself rather than the extremely hard PDCs. Complete coverage of cutters is not necessarily enough to make a long-lasting bit. Since the PDC cutters are placed in different radial positions, they will experience different linear velocity. As radial distance from the center of the bit increases, the relative linear velocity increases in the same manner. This relationship is described in equation 3.45, where v is linear velocity, ω is angular velocity and r is radial distance from center. [29]

$$v = \omega \times r \tag{3.45}$$

Since cutters more closely to the gauge of the bit has a higher linear velocity and a longer travel path to complete one revolution, wear on these cutters are more apparent. To accommodate this, one usually sees a higher concentration of cutters

around the nose and shoulder towards the gauge. To visualize cutter density one can rotate all cutter placements from the different blades onto a single radial plane. [29]
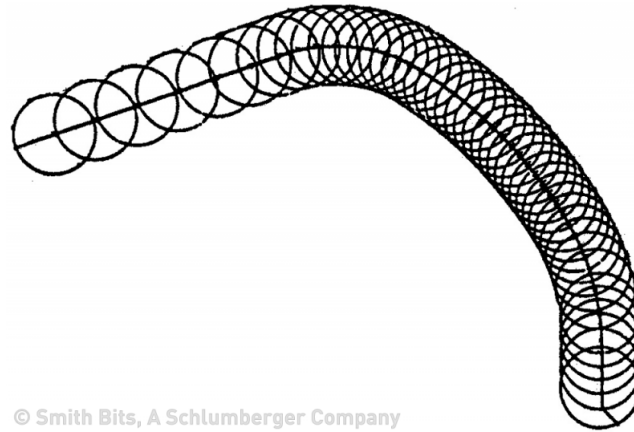
Figure 3.21: Representation of cutter density increasing with radial distance.[29]

Increasing cutter density does not come without an expense. As the more cutters are placed on the bit face the depth of cut is decreased, effectively reducing the ROP. In addition, the cleaning efficiency across the bit is impeded by fewer paths of flow. However, increasing cutter densities has some preferable benefits. More cutters on the bit mean more contact points on the formation distributing forces more equally. The reduced depth of cut in combination with better force distribution extends the longevity of the bit. The longevity of bits has a direct influence on cost and overall drilling performance due to prolonged drilling without bit-changing-trips or maintenance due to dull, chipped or broken cutter elements. [29]

Cutter Layout

Cutters are usually laid out following a spiral from center to gauge of the bit. They are laid out such that each increment in radial position from center is placed onto the next blade creating the spiral of the layout. For simplicity, this concept is shown in Figure 3.22 for a symmetrically spiraled four-blade bit. By looking at Figure 3.22, one can notice that there is a 90°angle between cutter one (1) & two (2), two (2) & three (3) and three (3) & four (4) and so on. [4]

Relatively recently, the traditional concept has been challenged by a new way of laying out cutters. The new alternative concept is obtained by rearranging cutters angularly without changing the radial position from center. As shown in Figure 3.23, the angle between cutter one (1) & two (2) and three (3) & four (4) is now 180°rather than 90°as in the traditional concept. [4]
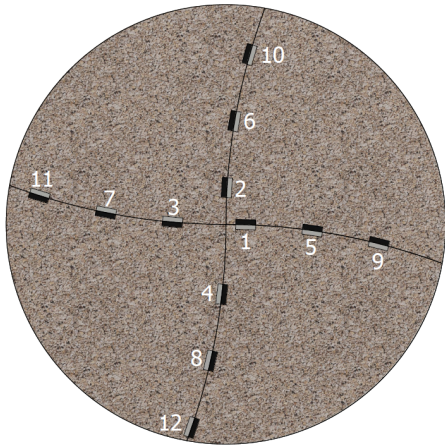
Figure 3.22: Traditional cutter layout.
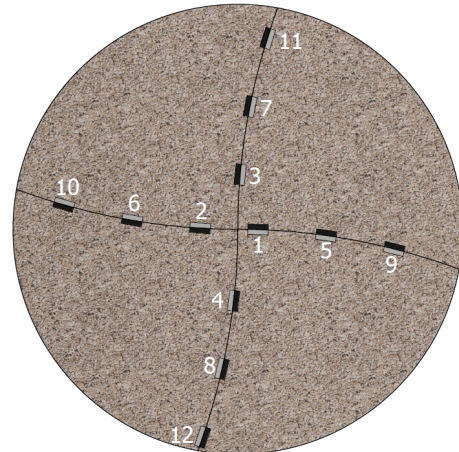
Figure 3.23: New alternative cutter layout.

The reasoning behind developing the new concept is to minimize imbalanced forces. If a four-blade bit with one cutter on each blade is considered, one can group cutter one (1) & two (2) and cutter three (3) & four (4) into an inner and outer formation removal ring respectively. Since there is only 90°angle between the cutters in each respective group in the traditional layout, cutter two (2) and four (4) removes more formation than cutter one (1) and three (3). For one revolution (360 °), cutter two (2) and four (4) will rotate 270°before entering the same angular position as their neighbor in the pair, while cutter one (1) and three (3) will only rotate 90°. Since they remove a dissimilar amount of formation, the imbalance forces is increased and drilling efficiency is reduced. Figure 3.24 shows a representation of the traditional cutter layout segmented into an inner and outer ring, visualizing what was just described.

The new cutter layout on the other hand is more balanced as the cutters remove the same amount of formation. Placing the cutters in each group 180 °of each other

makes the length before entering their neighbor's initial angular position the same. In other words, one revolution means all cutters will rotate 180°before entering their respective group-neighbor's initial angular position. In Figure 3.25 a representation of the concept is shown. The imbalance forces are minimized which results in more efficient drilling is achieved by laying out cutter this way. [4]
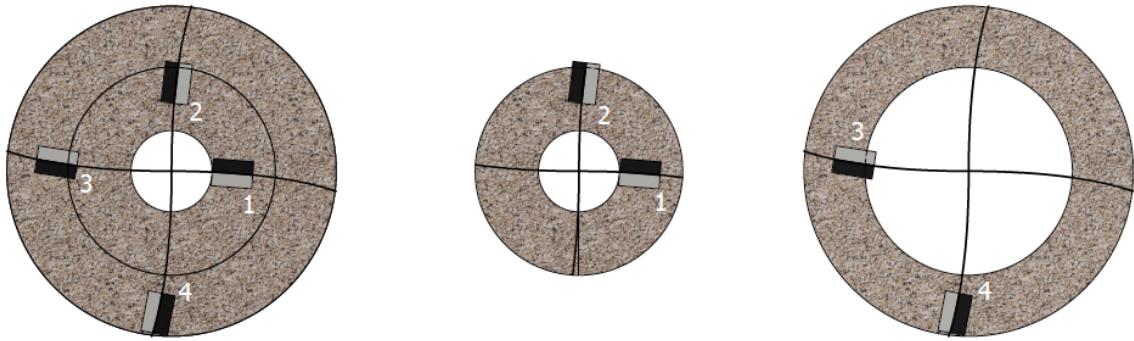
Figure 3.24: Traditional cutter layout segmented it into an inner and outer ring.
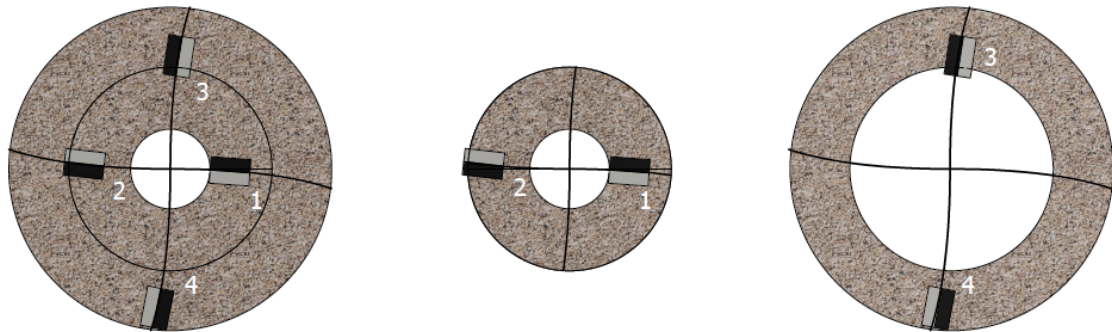
Figure 3.25: New alternative cutter layout segmented it into an inner and outer ring.

Cutter Orientation

Cutters are oriented in such a way that they attack the formation at a specific angle. This attack angle is called back-rake angle. Back-rake angle is defined as the angle between a cutter's face and a perpendicular line to the formation being drilled. Looking at Figure 3.26, back-rake angle can be obtained by rotating the cutter around the red axis.
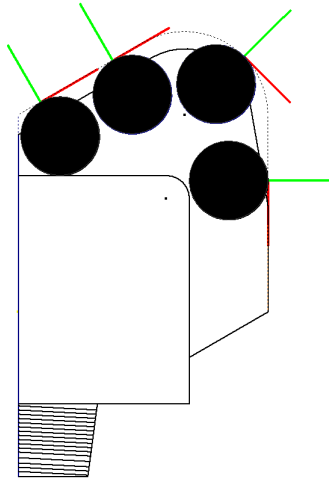
Figure 3.26: Back-rake side-rake

Back-rake angle is one of the key factors defining the depth of cut, i.e. aggressiveness, of a cutter. As back-rake angle increases, depth of cut decreases resulting in a less aggressive bit with reduced potential maximum ROP. However, by increasing the back-rake angle cutters will be more durable and bit vibrations will be reduced as the depth of cut is shallower. When hard formation is expected to be drilled, larger back-rake angles are required to avoid cutter breakage from impact loading and accelerated wear. The back-rake angle on the individual cutters is usually set to be variable or increasing as radial distance from center increases due to the difference in linear velocity. In Figure 3.27, typical back-rake angles are presented as they interact with the formation. [26]

Side-rake angle is also an important aspect when determining cutter orientation. Side-rake angle is defined as the angle between the cutter's face and a line passing through the center of the bit as shown in Figure 3.28. This angle can be obtained by rotating the cutter around the green axis in Figure 3.26. Mainly side-rake angle influences the cleaning efficiency as it causes the cuttings to curl away from the cutting element and the tendency for cuttings to adhere to the bit face is reduced. [26]
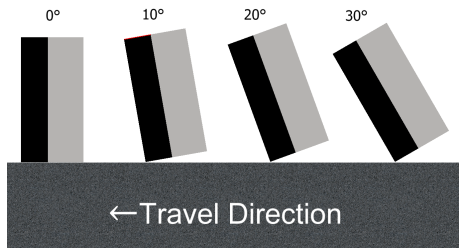
Figure 3.27: Back-rake angles.
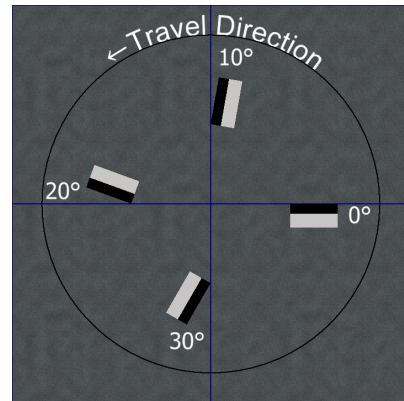
Figure 3.28: Side-rake angles.

Chapter 4

PDC Bit Design

Each year, DSATS will provide a bit to use in the annual competition. The committee provides a directional poly-crystalline diamond compact (PDC) bit which is designed and manufactured by Baker Hughes. It is a well functioning bit, which team UiS Drillbotics achieved good results within the 2019 competition.

It is stated in the Drillbotics guidelines that the students may use the bit provided by the committee, or create their own bit design. Creating your own bit opens up the opportunity for a fit for purpose drill bit, optimizing it for your needs. In the Drillbotics competition, each well is drilled under very controlled circumstances and uncertainties like formation strength, pressures and fluids are already known. Knowing these types of uncertainties allows for customization of the bit such that it will have an enhanced performance, reduced bit wear and ensure good borehole quality. These arguments were quite compelling, so it was decided to create a completely new and proprietary bit design in collaboration with Lyng Drilling, a Schlumberger Company, to use in the 2020 competition.

In this chapter, the theory from Section 3.3 will be put into practice and will cover the constructional steps of creating a proprietary designed PDC bit. For this project, Autodesk Inventor has been used to make the 3D design of the bit. The main reason for deciding to use Autodesk Inventor was due to it having a free student license and that it is made for professional use.

4.1 Design: Bit Profile

The design processes started by creating a complete 2D model of the bit profile. A medium cone angle of 120°followed by a short parabolic profile was chosen to achieve good stability as well as sufficient steerability. Together with the bit profile, two additional parallel profiles were included to act as the center of cutter profile and the bit body profile. To ensure long-lasting cutters the maximum depth of cut was set to be 1.3 mm of the 6 mm PDC cutter. In Figure4.1, the designed profile is represented. The solid line profile is the bit profile, dashed line profile is the bit body profile and the dotted line is the centerline of the cutters following the bit profile.
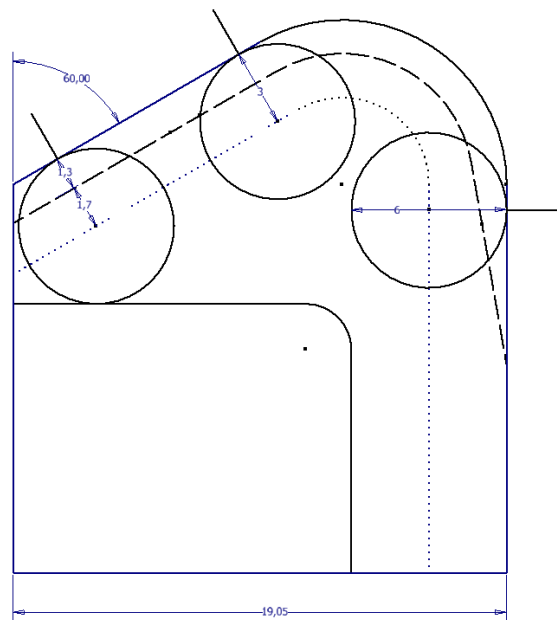
Figure 4.1: 2D model of bit profile including cutters on the first blade. Dimension 1 mm

4.2 Design: Cutter layout and placement

The next step in the design process was to space out cutters. The desired profile allowed a total of 12 cutters to be placed on the bit, ensuring complete coverage and sufficient cutter density along the bit profile. By having three cutters on each

blade and applying the new alternative cutter layout, the forces will be balanced as effective as possible - reducing vibrations and increasing drilling efficiency. In Figure4.2, all the cutters are projected onto a single blade, where each color represents a blade on the bit. Red represents blade 1, yellow blade 2, blue blade 3 and green blade 4. This is to demonstrate the coverage of the profile and how they are positioned according to the blades. The radial position of each cutter placement is also presented in Figure4.2.
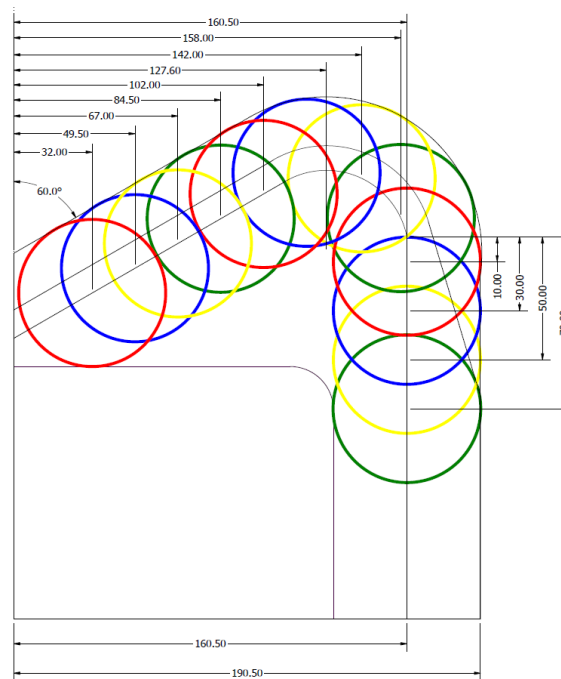
Figure 4.2: 2D-model of bit profile including all cutters projected onto the same plane. Dimension 10:1 mm.

4.3 Design: Cutter orientation

When all cutters were placed at their respective radial distance from center, the cutter could then be oriented according to desired back-rake and side-rake angles. Currently, all modeling has been done in a two-dimensional space, but orienting the cutters triggers the need for a third dimension. Thus, from now on 3D-modelling starts. The orientation is done by extruding cylinders which represents cutters. The cylinders are then rotated around a tangential axis along the common point

between the cutter edge and bit profile to create back-rake angle. Side-rake angle is created by rotation around a perpendicular axis from the same common point between cutter edge and bit profile.
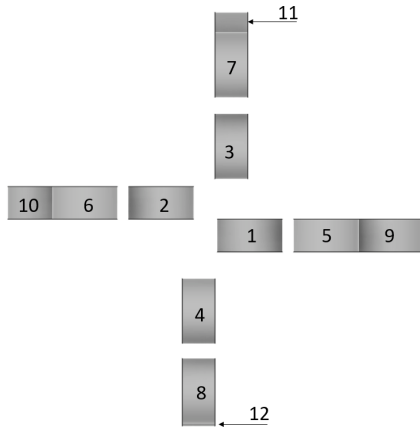
Figure 4.3: Placed out cutters.
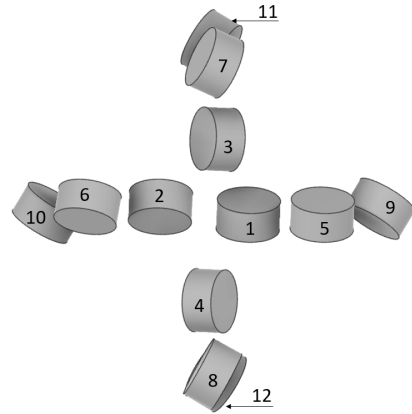
Figure 4.4: Placed out cutters with orientation.

For this project, the pneumatic motor (down-hole motor) rotates at around 800-1500 RPM, which is approximately 10 times faster than a typical industry parameter. Due to these high rotational velocities, the bit wear is naturally accelerated and much more apparent. As discussed in the theory section, back-rake and side-rake angles are key factors to prolong the lifetime of a bit. Based on this fact, all cutters on this bit has been given a large back-rake angle, varying from 20° to 30°. Having such large back-rake angles reduces the aggressiveness, however the longevity of the bit is substantially increased which is preferred for this project. All cutters have been given a constant 15° side-rake angle for increased cleaning efficiency. In Table4.1 the back- and side-rake angles are presented for each individual cutter.

	Cutter	Back-rake	Side-rake
	1	20°	15°
Blade 1	5	20°	15°
	9	30°	15°
	3	20°	15°
Blade 2	7	25°	15°
	11	30°	15°
	2	20°	15°
Blade 3	6	20°	15°
	10	30°	15°
	4	20°	15°
Blade 4	8	25°	15°
	12	30°	15°

Table 4.1: Table of back-rake and side-rake for each specific cutter.

4.4 Design: Bit Body and Bit Blades

A body is needed to act as a foundation for the cutters. To create the spiral of bit blade, each individual blade was revolved 90° (figure 4.5a). The blade- and bit body had to be revolved separately in order to make extrusions on each individual solid. The spiral profile was created by dividing the gauge length into four sections. Each section was set at a positive 5° angle relative to the previous section. When all sections had correctly been angled, a circle which passed through all end-points of each section was created to smooth out the curve. The circle was duplicated and diameter reduced to set the desired blade thickness of 6 mm. (figure 4.5b). Figure 4.5c shows the result when all spiral blades were extruded out.

(a) Revolve blade.   (b) Cut spiral shape.   (c) All spiral blades.
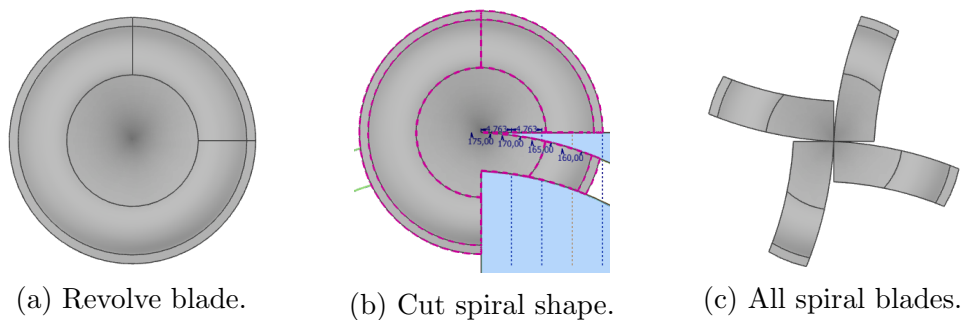
Figure 4.5: Creating the spiraling of the blades.

In order to achieve good stability, it is beneficial to have a robust gauge pad that covers sufficient area of the borehole wall. By inspecting Figure4.6a, the gauge pad appears to be somewhat frail. Therefore, it was decided to place the gauge pad at a 20° angle to make it more robust and increase possible contact area to the formation as shown in Figure4.6b. In addition to making the gauge pad more robust, it also makes more room for gauge inserts.
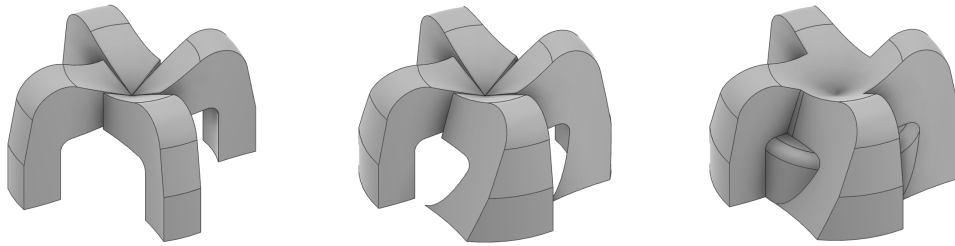
(a) Initial gauge pad thickness.   (b) Gauge pad 20° angle.   (c) Revolve bit body 360°.

Figure 4.6: Increasing gauge pad thickness and revolving bit body.

While creating the bit body, cylinders representing cutters were temporarily suppressed as a feature. However, when the bit body and blades were completed, the cylinders could be unsuppressed, bringing them back to the model. At this point, the cylinders were only spaced out and oriented, not placed in the blades (figure 4.7a). Thus, the cylinders must be rotated around the center-axis and into the blades (figure 4.7b). The cylinders could then be extruded away to create the cutter pocket which will hold the cutter in the correct position. The cutter pockets are 0.2 mm larger in diameter than the cutter to make sure they will fit inside the blade. By looking at Figure4.7b one can observe that the cutters closer to the apex are fully surrounded by the bit body. In order to place cutters at these positions, an extended semicircle had to be extruded such that the PDC cutter could be slid down and brazed in place. Figure 4.7c shows the cutter pockets and gauge insert pockets after they had been extruded. To avoid stress concentrations in the sharp edges on the bit, fillets have been used diligently.
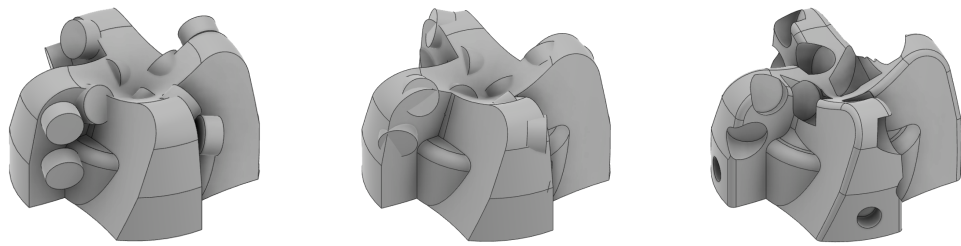
(a) Bring back cutters. (b) Rotate the cutters into their respective blade. (c) Extrude cutter pockets and gauge insert.

Figure 4.7: Making the cutter pockets, gauge insert pocket and fillets.

4.5   Design: Pin Connection and Nozzles

The only part remaining of the design is the make the base for the pin connector and the nozzles for cuttings transport. It was decided to use the same threads as the bit provided by DSATS, namely 1/4" NPT thread. This meant that a cylinder with a diameter of 13.62 mm had to be extruded 10 mm to make the base for the threading. Later a 1/4" NPT screw die will be used to make threads on the cylinder.

The nozzles were made by constructing two cross-sectional planes along the length of the bit as shown in Figure4.8a. On these planes, the flow channels inside the bit were created using the sweep-function in Inventor. The main channel has a diameter of 3 mm and is branched out to four 1 mm nozzle paths - one for each blade - as shown in Figure4.8b. One might think 1 mm nozzles is too small, but in this project air is used as cuttings transportation fluid. Therefore, 1 mm is enough to create sufficient hole cleaning.
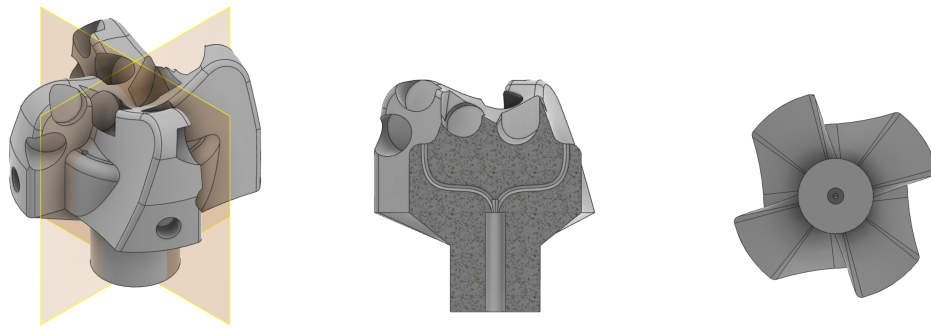
(a) Cross-sectional planes. (b) Main channel and nozzle paths. (c) Main fluid channel from bottom.

Figure 4.8: Nozzles.

Once the nozzles are completed, the drill bit design is ready for 3D-printing in 17-4 PH stainless steel. To visualize how the miniature PDC drill bit will look when it is 3D printed and when all cutters and inserts are brazed in place, rendered pictures of the model are displayed below.

(a)   (b)   (c)
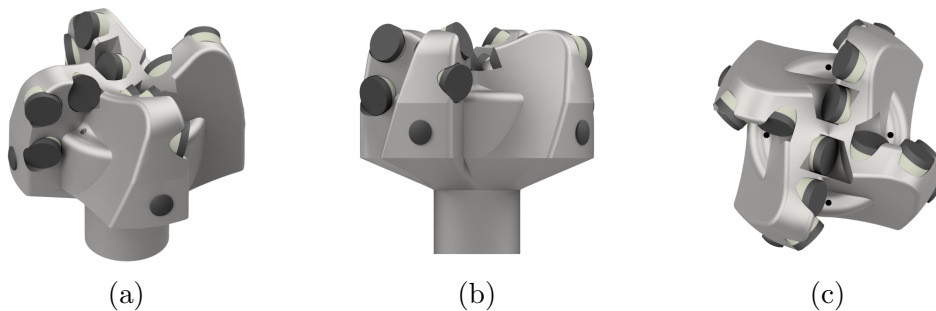
Figure 4.9: Final bit design including PDC cutters and TSP inserts.

4.6 Miniature Bit Overview

When the proprietary bit design is finished in manufacturing, team UiS Drillbotics will have - and plan to test - four (4) different bits from different suppliers. The team has two (2) advanced bit designs - the proprietary one and the one provided by DSATS, manufactured by Baker Hughes. The two drill bits which were found on Alibaba, are much simpler. They have poor coverage as they only comprise of two and three large PDCs placed at the same radial position at full gauge. That

means there is a large gap between the cutters which will create a huge cone in the formation. There are no cutters present at the cone of the bit to shear away this formation-cone, so it is reasonable to believe that these bits will struggle to penetrate the formation. It is noteworthy that both the Alibaba bits lack side-rake angle on the cutters which does not improve the hydraulic efficiency. Despite both bits having 15° back-rake, they appear to be very aggressive and prone to high torque on bit values. Given that the pneumatic motor on the system only provides 2.1 Nm of torque, it is a chance that they will stall the motor even at very low rotational velocity and shallow depth of cut.

(a) Isometric view. (b) Orthographic view.
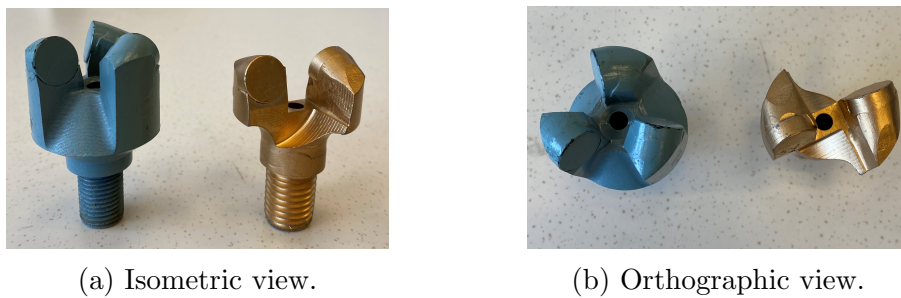
Figure 4.10: Alibaba bit 1 being blue and Alibaba bit 2 being gold.

As mentioned, the UiS bit and the one provided by DSATS is more advanced. Both of them have good coverage of the bit face. The DSATS bit has one PDC on each of the four blades, but they are larger than on the proprietary design which has 12. Since the proprietary design has three times as many PDC cutters, it is significantly less aggressive. However, bit torque is also significantly reduced, making the chance of stalling the downhole motor less likely. One particularly clever feature about the DSATS bit is that the depth of cut is configurable. By using a special adhesive or brazing a Tungsten Carbide (TC) insert at the face of the bit one can set the desired depth of cut. The same technique is used to configure gauge pad clearance. One can have a gauge pad clearance of 0" if the TC insert is used. Otherwise, the gauge pad clearance will be 0.150" (3.175 mm). The UiS bit does not have a configurable depth of cut, but is fixed at a maximum of 1.3 mm, depending on the drilling parameters. By having the rather shallow depth of cut, approximately 16% of the cutter face will be exposed. Even though the depth of cut is not configurable, the gauge pad clearance is. The same technique as for the DSATS bit is used to control the gauge

pad clearance. However, instead of using Tungsten Carbide (TC) inserts, the UiS bit is designed for a specific Thermally Stable Polycrystalline (TSP) insert provided by the partner, Lyng Drilling - a Schlumberger company.

(a) Isometric view.   (b) Orthographic view.
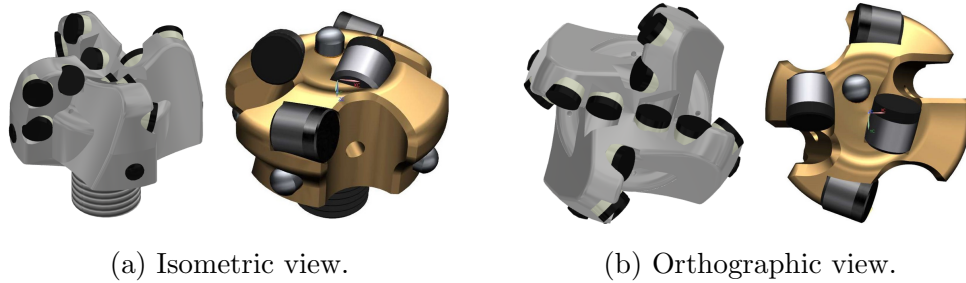
Figure 4.11: UiS bit being grey and DSATS bit being gold.

In regard to the cutter layout, similar methods have been used. Both the DSATS bit and UiS bit have chosen to use the new alternative method of laying out cutters. This results in both bits having less imbalance forces. Cutter orientation has been done in a dissimilar way. While the proprietary design increases back-rake angle as radial distance from center increases, DSATS have decided to do the opposite. However, both designs have been given quite large back-rake angles as shown in Table 4.2.

	Location	Cutter number	Back-Rake Angle
	Cone	1, 2, 3 and 4	20°
UiS Bit	Nose/Shoulder	5, 6, 7 and 8	20/25° *
	Gauge	9,10,11 and 12	30°
	Cone	1 and 2	25°
DSATS bit	Nose/Shoulder	3 and 4	20°
	Gauge	-	-

* Cutter 5 and 6 have 20° while cutter 7 and 8 have 25° back-rake.

Table 4.2: Back-rake comparison of DSATS bit and UiS bit.

Below there is a table that summarizes specifications for the drill bits to be used in testing and evaluate their performance.

Specification	UiS		DSATS		Alibaba 1		Alibaba 2	
	US	SI	US	SI	US	SI	US	SI
Diameter	1.5	38.1	1.5	38.1	1.5	38.1	1.5	38.1
Length	1.437	36.5	1.35	34.3	2.4	61	2	51
No. Blades	4		4		3		2	
No. PDC Cutters	12		4		3		2	
PDC Diameter	0.236	6	0.323	8.2	0.511	13	0.511	13
No. TSP Inserts	4		0		0		0	
No. TC Inserts	0		5		0		0	
No. Nozzles	4		4		1		1	
Nozzle diameter	0.039	1	0.125	3.175	0.197	5	0.197	5
Connection	1/4" NPT		1/4 NPT		M14/M16		M16	

Table 4.3: Basic bit specifications. [US:inch] [SI:mm].

Chapter 5

Material Testing

The Drillbotics committee introduced the option of using a stainless steel tubing for the competition. An analysis of the Aluminum 6061 T6 pipe and the Stainless Steel 316 A269 pipe was conducted to determine the proper selection of material. Buckling limits, plastic deformation and twist-off tests were carried out using both theoretical calculations and experimental testing. The objective was to test the drill pipes with respect to tensile, compression, fatigue and torsional limitations. The following results in conjunction with the experimental tests will determine which material is the most suitable for this year's drill string. For further details regarding the drillpipe testing, please see (Byman, 2020) [8].

5.1   Drill Pipe Dimensions

The drill pipe specification are determined by the guidelines and are subject to change each year. The dimensions used for testing of the drill pipes and during drilling operations are listed in table 5.1. 5.2 describes the mechanical properties of the drill pipes.

| | Aluminum 6061 T6 | | Stainless Steel 316 A269 | |
Properties	SI-units	US-units	SI-units	US-units
Outer Diameter (D_o)	9.525 mm	3/8"	10 mm	0.394"
Inner Diameter (D_i)	7.035 mm	0.277"	7 mm	0.276"
Wall Thickness (W_t)	1.245 mm	0.049"	1.5 mm	0.059"

Table 5.1: Drill pipe dimensions as per Drillbotics 2019-2020 guidelines. [12]

Properties	Aluminum 6061 T6	Stainless Steel 316 A269
Ultimate Tensile Strength [MPa]	310	515
Tensile Yield Strength [MPa]	276	205
Modulus of Elasticity [GPa]	69.9	193
Ultimate Shear Strength [MPa]	207	-

Table 5.2: The mechanical properties of Aluminum 6061 T6 and Stainless Steel 316 A269.

In the followings subsections the tests conducted on the drill pipes in the UiS mechanical workshop will be described in detail. The tests are performed as components test, meaning a full length drill pipe was used to replicate a drilling operation.

5.2 Tensile Test

The tensile tests were performed on two pipe samples of each material. Figure 5.1 and Figure 5.2 represent the results from the tensile tests for stainless steel and aluminum material, respectively. Despite slight variations in values between the specimen, it can be assumed that the repeatability of the tests is satisfied.
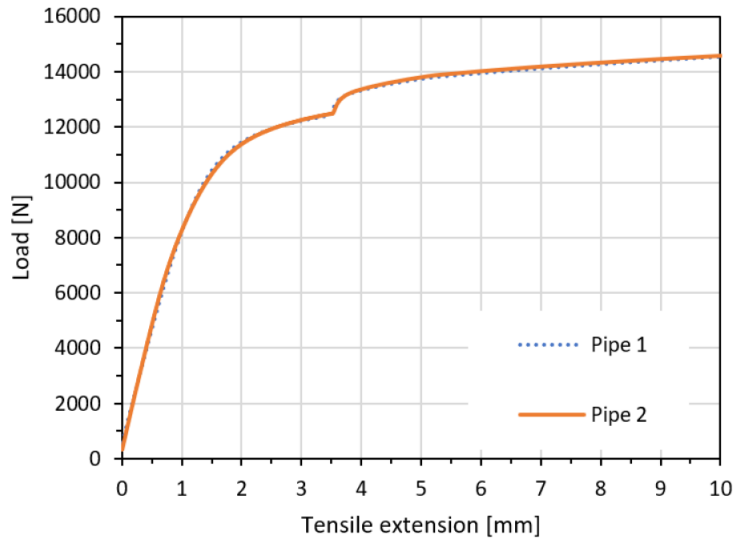
Figure 5.1: Stainless Steel 316 A269 Tensile test.
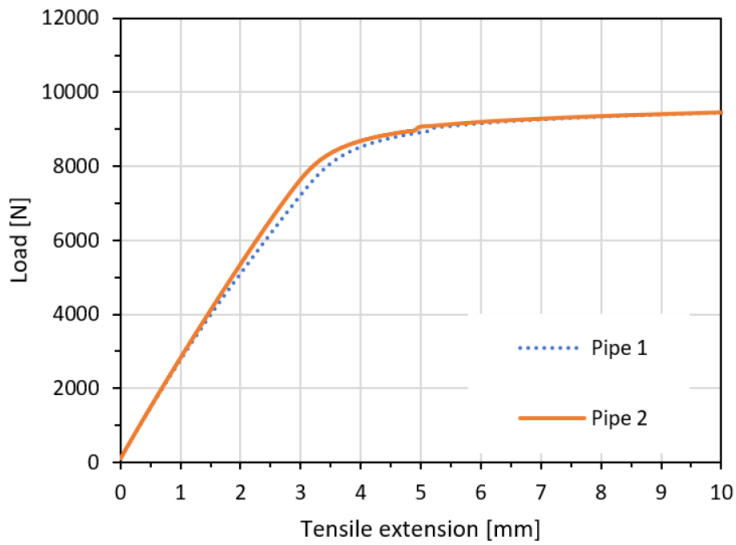
Figure 5.2: Aluminum 6061 Tensile test.

The tensile load for the stainless steel and aluminum pipe was around 10500 N and 8000 N, respectively. As the maximum pulling force that the rig is capable of is 600N, there would be no danger of breaking the pipes during tripping out of the wellbore. The results from the tensile tests can be seen in Figure 5.3 below.

97

	Aluminum 6061 T6		Stainless Steel 316 A269	
Properties	Pipe 1	Pipe 2	Pipe 1	Pipe 2
Modulus of Elasticity [GPa]	42.8	46.8	156.7	150.2
Yield tensile strength [MPa]	231.6	232	309.7	311.3
Ultimate tensile strength [MPa]	265.5	266.2	362.7	363.6

Table 5.3: The results from the tensile tests.

5.3 Compression Test

The compression tests were performed on three pipe samples of each material to establish a comparative result. The results are represented below for both the stainless steel (Figure 5.3) and aluminum (Figure 5.4) pipe. The compression load for the stainless steel and aluminum was 4443.86 N and 1325.98 N on average. The results of the different pipes are shown below in Figure 5.4.

	Aluminum 6061 T6			Stainless Steel 316 A269		
Properties	Pipe 1	Pipe 2	Pipe 3	Pipe 1	Pipe 2	Pipe 3
Compression Stress [MPa]	41.6	40.3	40.9	101.3	112.0	119.5
Load [N]	1347.4	1306.4	1324.2	4056.2	4486.6	4788.8

Table 5.4: The results from the compression tests.

There would be no danger of buckling the pipe under these circumstances and both the aluminum and stainless steel pipe is applicable for the setup.
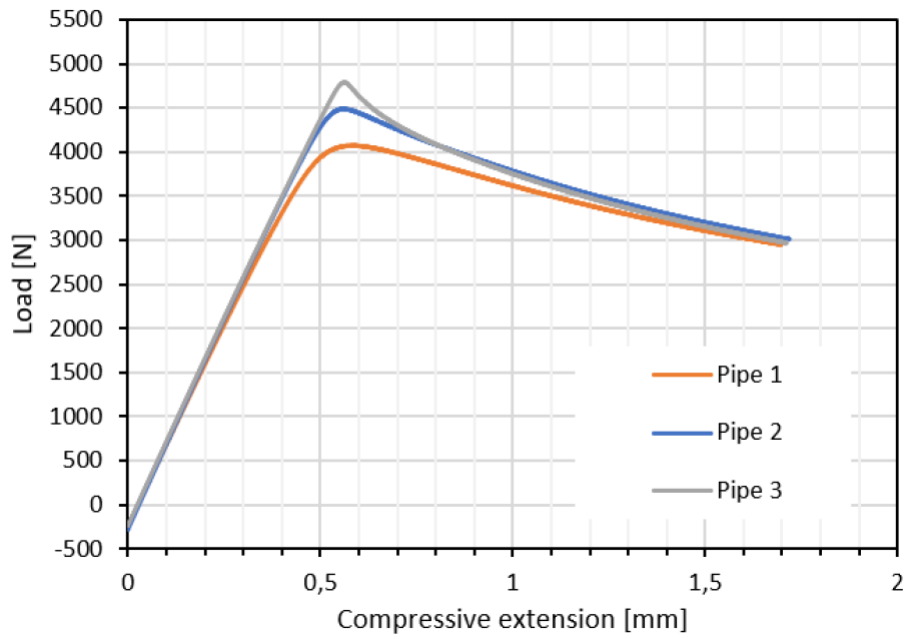
Figure 5.3: Stainless Steel 316 A269 Compression test.
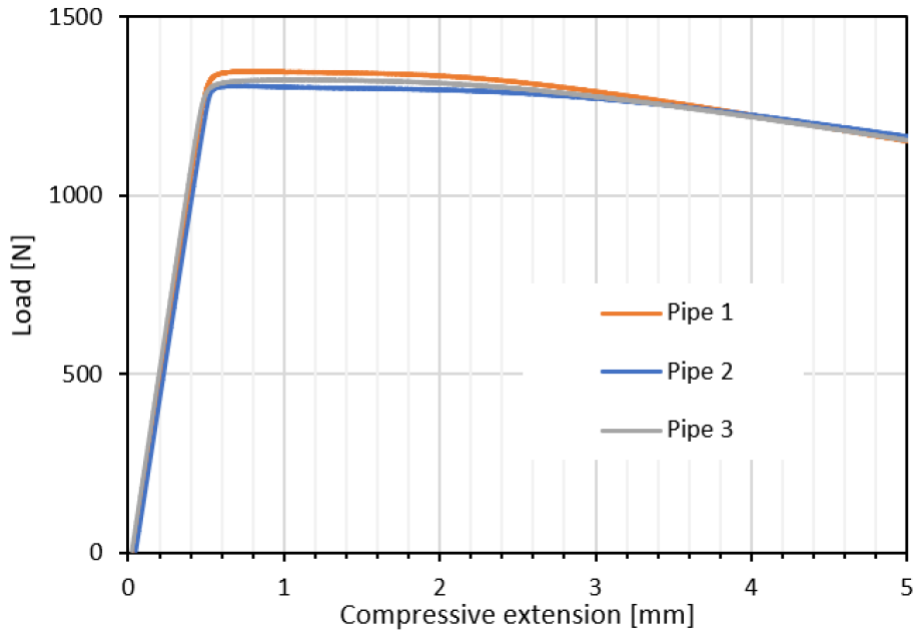
Figure 5.4: Aluminum 6061 Compression test.

99

5.4 Torsional Test

As the previous tests showed that it was unlikely for the drill pipe to buckle or break during compression and tension, a torsion test was conducted. A torsion testing can be done by twisting the pipe along an axis until twist off occurs. This can then be used to acquire information about the torsional shear stress, maximum torque, and shear modulus for example. In this work, only information about the maximum torque was collected. The drill pipes were torsion tested by attaching one end of the pipe to the chuck in a lathe, whilst the other side of the pipe was supported by the lathe support rollers, as shown in Figure 5.5
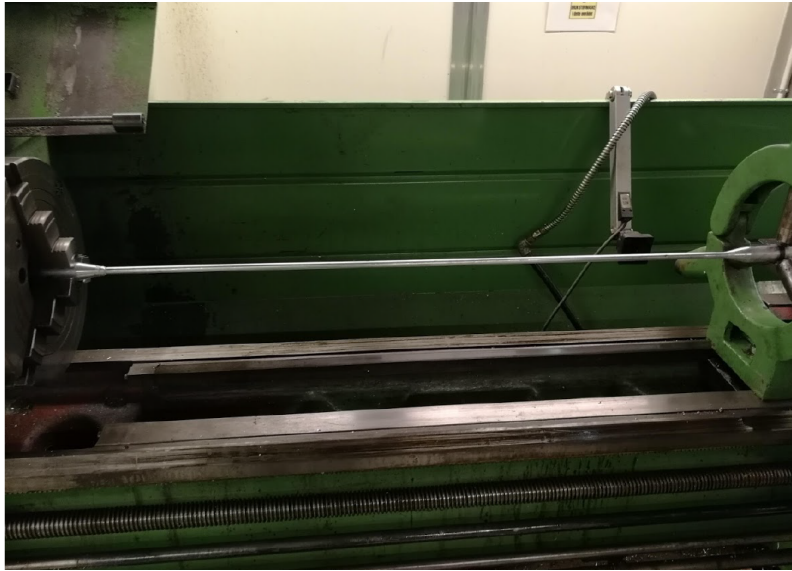
Figure 5.5: Pipe attached to the lathe.

To perform the test, one end of the adapters was drilled and threaded before mounting a bolt of 12.9 quality. Then a torque wrench was attached to the bolt. The torque readings were done manually. Before starting to apply torque, a straight line was drawn across the pipe, making it easier to spot when the pipe plastically deformed. The torque wrench moment was increased by 2 Nm each time when torque was applied. The accuracy of the reading is $+-3\%$ (the minimum increment of applied torque was 0.5 Nm). [8]

100

Figure 5.6: Stainless Steel 316 A269 Torsional test.
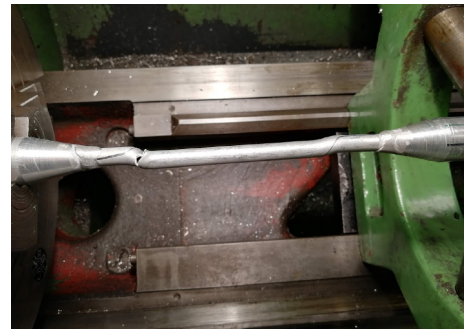
Figure 5.7: Aluminum 6061 Torsional test.

Properties	Aluminum 6061 T6		Stainless Steel 316 A269	
	Pipe 1	Pipe 2	Pipe 1	Pipe 2
Yield torque (T_y)	14 Nm	12 Nm	32 Nm	32 Nm
Max torque (T_{max})	19.5 Nm	18 Nm	86 Nm	90 Nm

When comparing these results to the theoretical values from before, the stainless steel material performed better and the aluminum worse than expected. The maximum instantaneous torque from the top drive is 8.59 Nm, meaning that both materials have the required torsional strength. However, as the cyclic forces experienced by the drill pipe during a rotary drilling operation is quite severe, twist off of the pipe at the connector has been an issue and fatigue testing to determine which pipe would be the most suited was necessary.

5.5 Fatigue Testing

During a drilling operation the drill pipe is exposed to cyclic forces over a long period. The team has experienced pipe failure in the past at much lower forces than expected from calculations and tests. Extensive fatigue testing was performed in the MTS 809 Bi-Axial testing system to evaluate the effect of fatigue on the drill pipe. In the MTS-machine, the drill pipe is under compression and torsional forces simultaneously. The test duration was set to 90 minutes at a compression force of 600 N (max load cell compression) and 9 Nm torsional force (max top drive torque). During testing of the aluminum pipes the maximum angle of rotation was reached for

101

the MTS-machine and a re-calibration of the system would be necessary to perform the test. Unfortunately, no resources at the University was able to perform the re-calibration at this point and the tests were only conducted for the stainless steel sample.

Fatigue testing was performed in the MTS-machine for the stainless steel pipe, one sample was tested for 138000 cycles of torsional forces applied whilst being under constant compression load of 600 N. Following the fatigue testing, a Nondestructive testing (NDT) was performed to detect any cracks in the material. The NDT was done using Bycotest C10, RP20 and D30 plus. No signs of cracks were visible for the stainless steel pipe as shown in Figure 5.8.

Figure 5.8: Stainless Steel 316 A269 after 138000 cycles in the MTS system, fatigue test.

5.6   Summary - Pipe testing

The theoretical values for Euler's critical load, maximum torque ETC ETC are calculated for the aluminum and stainless steel pipe by Jonatan Byman [8] and presented in Table 5.5 to compare the theoretical and experimental values.

| | Aluminum 6061 | | Stainless Steel 316 | |
Properties	Exp.	Theo.	Exp.	Theo.
Euler's critical load [N]	4443.86	476.2	1325.98	1724.4
Yield torque [Nm]	13	19.74	32	18.35
Maximum torque [Nm]	19	24.07	88	46.10

Table 5.5: Theoretical values compared to the experimental data recorded in this chapter.

The stainless steel drill pipe had a marginally lower yield torque than the aluminum pipe, however the maximum torque before shearing was almost twice as high for the aluminum pipe. Having a higher yield and maximum torque limit is advantageous when selecting the material of the drill pipe. The drill pipes were also tested for their tensile, compression and torsion limits, in addition to a fatigue test. The tensile test results for both materials of the drill pipe exceeded the theoretical values. As for the compression test, the drill pipes were able to withstand compression load much higher than the theoretical values and should not be in danger of buckling during a drilling operation. However, the test conditions for the compression test are not equal to the conditions whilst drilling as the pipe is not fixed-fixed, but rather fixed-pinned. The fatigue test performed on the stainless steel pipe showed no signs of cracks or mechanical weakness after the non-destructive testing of the pipe. The torsional test results showed a large discrepancy between the theoretical values and the values from testing. The stainless steel pipe was able to withstand 50% more than the expected yield and 100% more than the maximum theoretical torque. In contrast, the aluminum pipe performed worse than the theoretical values for both yield and maximum torque. Some discrepancy is to be expected between the experimental and theoretical values as the test specimen used for the experiments have handles welded onto them in each end. In addition, the experimental setup for the torsional testing was not optimal and some deviation is expected.

Operational Limits – Drill Pipes

	Overpull ↑	WOB ↓	Torque ↶
Aluminum 6061 T6	**Overpull** 815,5 kg	**WOB** 135,17 kg	**Torque** 19,0 Nm
Stainless Steel 316 A269	**Overpull** 1070,34 kg	**WOB** 452,99 kg	**Torque** 88,0 Nm
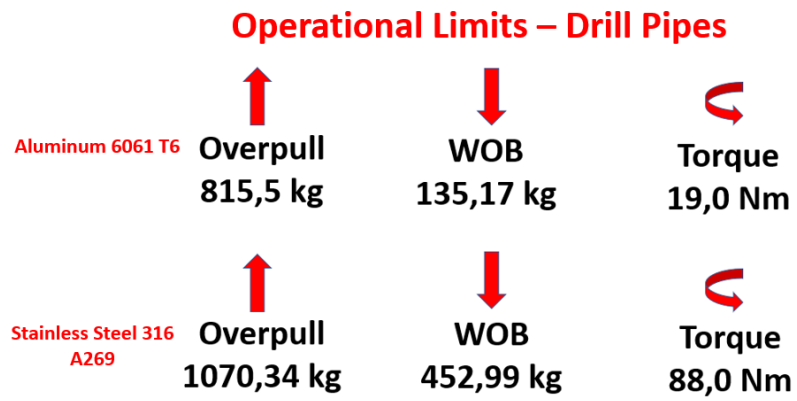
Figure 5.9: The operational limits for the Aluminum and Stainless Steel drill pipes.

Chapter 6

Results and Discussions

In this chapter the performance of four (4) different PDC drill bits are tested to compare their performance. The performance criterion for the test drilling are ROP values, vibrations severity, inclination built and hole quality. Prior to the test drilling, several drill bit simulations have been performed for the UiS Drillbotics bit. These simulations were important during the bit design phase to compare the performances of different versions of the cutter profile.

6.1 Drill Bit Simulations

Prior to 3D-printing of the proprietary designed drill bit, some simulations were performed by Are Funderud from Lyng Drilling, a Schlumberger company. The simulations were performed to analyze torque and WOB response of the bit in addition to relative contribution from the individual cutters.

6.1.1 WOB and TOB response from various DOCs

The first simulation was done to investigate how Depth of Cut (DOC) in mm per revolution affected the torque experienced by the bit. Two different strength sandstones were used as formations in the simulation. The weakest formation had a Uniaxial Compressive Strength (UCS) of 8 ksi while the stronger sandstone had a UCS of 18 ksi. Both of them have a higher UCS value than the competition

rock, which has a UCS of approximately 5.4 ksi. That means, even for the weaker formation, the results from the simulation will be conservative.

The torque on bit is dependent on how much area of the cutter's face interacts with the formation. As the DOC gets deeper, the more area will interact with the formation essentially increasing torque on bit. The DOC is dependent on how much weight one applies to the bit. By increasing the WOB, the DOC will increase in the same manner until it reaches a point where the bit body interacts with the formation. If one continues to increase the WOB beyond this point, there will be no changes to the DOC and the torque will be wasted to friction between bit body and formation rather than drilling. Therefore, this simulation will give valuable information for determining well suited drilling parameters in addition to give the basis for calculating the theoretical maximum achievable ROP.

In Figure 6.1, the results from the simulation are shown.
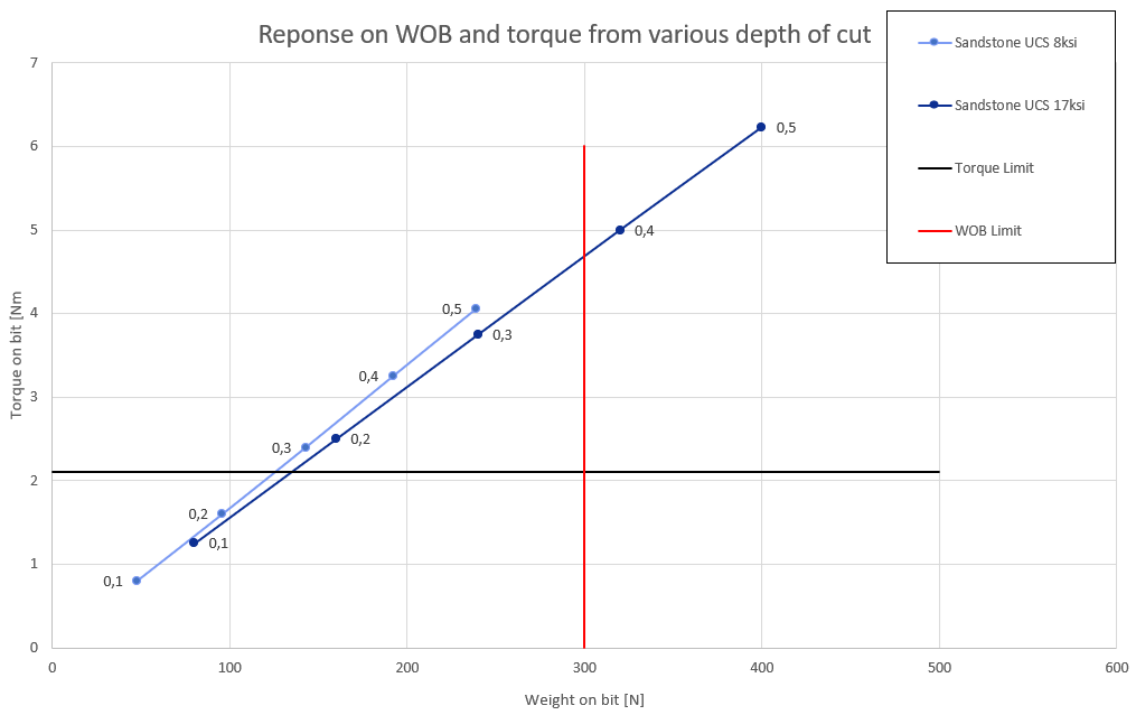
Figure 6.1: Response on WOB and torque from various Depth of Cuts.

From the figure, one can immediately observe that the torque is the strongest lim-

106

iting factor setting the strictest restriction for DOC. As expected, the torque limit is exceeded much earlier than the WOB limit. Since the pneumatic motor has to be small in order to fit inside the BHA, the torque rating for a such motor is relatively low. For the WOB, the limit is set based on the buckling limit of the aluminum pipe.

For the 17 ksi UCS sandstone, the bit is expected to stall at a DOC of 0.168 mm/rev. At this DOC, the WOB is simulated to be at 134.1 N which is well below the limit. Under ideal conditions, i.e. perfectly gauged hole, little to no vibrations, homogeneous formation, no loss of rotational velocity from the motor and no WOB loss to friction against the borehole wall, the maximum theoretical ROP will be,

$$ROP_{max} = DOC \times RPM = 0.168mm/rev \times 1071rev/min = 180mm/min. \quad (6.1)$$

For the more comparable sandstone with an UCS of 8 ksi, the bit is expected to stall if the DOC exceeds 0.262 mm/rev. A DOC of 0.262 mm/rev is acheived when 125.4 N is applied. Under ideal conditions the maximum theoretical ROP will be,

$$ROP_{max} = DOC \times RPM = 0.262mm/rev \times 1071rev/min = 280.6mm/min. \quad (6.2)$$

Since the simulation included two different rock strengths, it is also possible to predict the trend for other rock samples. Rock samples with lower UCS will have a deeper DOC and drill with a lower WOB before the bit experiences more torque than the motor can provide and eventually stall out. Stronger rock samples will have the opposite response and a shallower DOC and higher WOB is needed to achieve the same torque response.

The exact values from the simulation are shown in Table 6.1. However, each data point is given for a specific DOC. Thus, at torque limit the values are interpolated.

Sandstone UCS 8ksi			Sandstone UCS 17ksi		
DOC[mm/rev]	WOB[N]	TOB[Nm]	DOC[mm/rev]	WOB[N]	TOB[Nm]
0,10	48	0,80	0,10	80	1,25
0,20	96	1,60	0,20	160	2,50
0,30	143	2,40	0,30	240	3,75
0,40	192	3,25	0,40	320	5,00
0,50	239	4,06	0,50	400	6,23
Interpolation			Interpolation		
0,262	125,40	2,10	0,168	134,10	2,10

Table 6.1: Results from WOB, TOB and DOC simulation. Interpolated values at torque limit.

6.1.2 Cutter Contribution

[] In addition to investigating torque and WOB responses for the entirety of bit, one can dig even deeper and simulate contribution for each individual cutter placed on the bit. By inspecting axial and torsional loads on individual cutters, one can determine if cutter placement and/or orientation needs to be adjusted to avoid accelerated wear or broken cutters.

For this simulation, the 8 ksi UCS sandstone was used and the DOC was set to be 0.3 mm/rev. The numbering of the cutters are done such that number 1 represents the cutter with the smallest radial distance from center while cutter 12 has the largest.
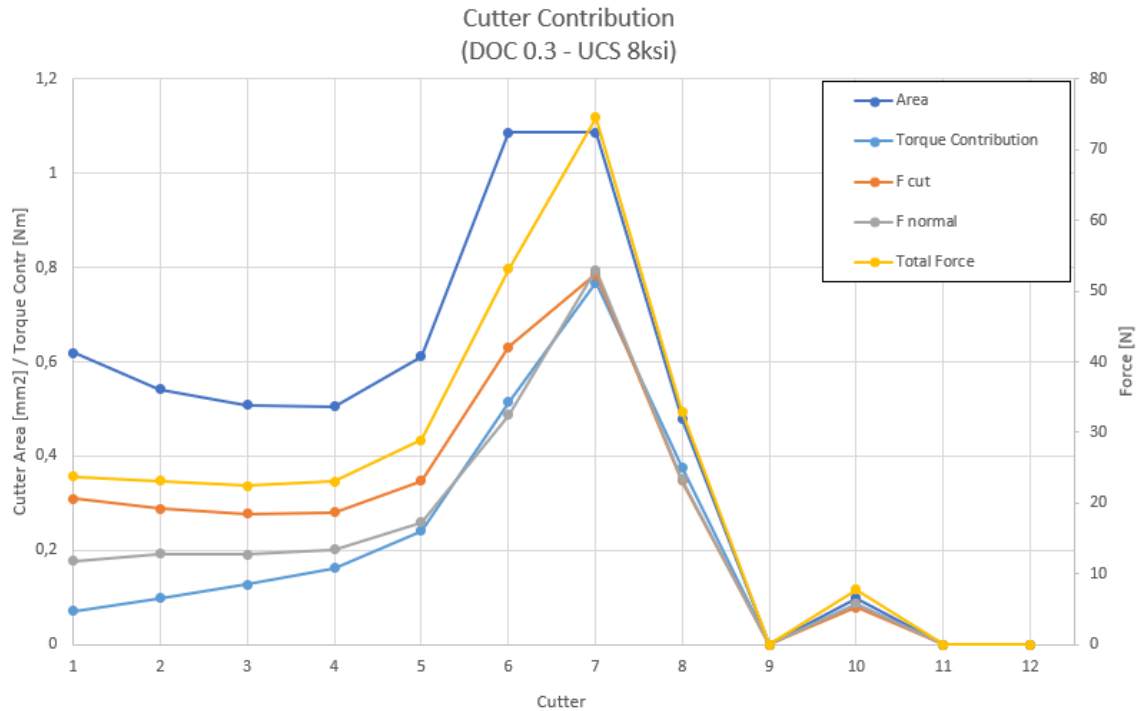
Figure 6.2: Cutter area, torque contribution and force distribution from the different cutters.

If Figure 6.2 is assessed, one can say it fairly well-balanced. There is a noticeable spike at cutter number 7, but it is not drastic compared to neighboring cutters. Cutter number 5,6,7 and 8 are located at the nose of the bit, so it is natural that they will experience somewhat higher values in terms of force, torque and cutter-rock interaction area. This effect is visualized in Figure 6.3. From the figure, one can clearly see that the cutter at the nose has a larger exposed area (in green) than the others.
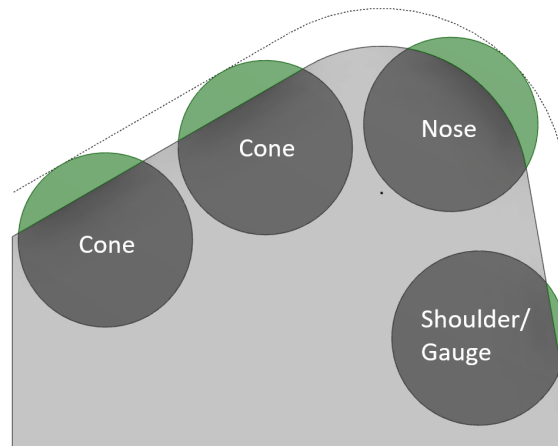
Figure 6.3: Representation of exposed cutter area.

As mentioned in the bit theory section, the cutter density is usually higher at the nose of the bit in order to accommodate for this. In this design there was no more room to increase the cutter density. The cutters at the nose are therefore more exposed than the cone and gauge cutters. If a longer parabolic profile was used, the cutter density at the nose would be able to increase. However, a longer parabolic profile is less desirable for the particular usage of the bit due to it being significantly less stable.

It is also worth to mention the small spike at cutter number 10. Intuitively one might expect cutter 9 to have a spike rather than cutter 10 due to the number representing radial position. It is important to remember that cutter 9, 10, 11 and 12 are all placed at the same radial distance from center, namely at full gauge. Hence, only one of them will have any contribution to drilling. Due to applying the new alternative method of laying out cutters, cutter number 10 is located on the blade 90° behind cutter 8 (if direction of rotation is followed). Therefore, cutter 10 will be the first cutter at full gauge which interacts with the remaining area of the formation.

Even though 9 cutters in total are enough to ensure complete coverage of the bit, the design still has 12 cutters where 4 of them are placed at full gauge. The reason for placing several cutters at the same radial position is to ensure that the gauge diameter is never less than what it is designed for. If the well is slightly under

gauge, the BHA might get stuck on ledges or struggle passing through the inclined sections of well. Under those circumstances, the drilling operation will not be able to progress and has to be discontinued. To avoid this, several cutters at gauge are placed to create redundancy if a cutter gets worn or broken. As explained in the theory section, the cutter at full gauge experiences a higher linear velocity than cutters closer to the bit center and is therefore more prone to wear.

In Table 6.2, the values from the simulation are tabulated.

Cutter	Blade	A [mm^2]	F_{cut} [N]	F_{nor}[N]	F_{tot} [N]	T [Nm]
1	1	0,619	20,614	11,848	23,777	0,072
2	3	0,542	19,275	12,808	23,142	0,099
3	2	0,509	18,488	12,8	22,486	0,127
4	4	0,505	18,74	13,481	23,085	0,162
5	1	0,612	23,215	17,307	28,956	0,241
6	3	1,087	42,076	32,436	53,127	0,514
7	2	1,086	52,431	52,972	74,532	0,768
8	4	0,48	23,178	23,417	32,948	0,376
9	1	0	0	0	0	0
10	3	0,099	5,259	5,795	7,825	0,087
11	2	0	0	0	0	0
12	4	0	0	0	0	0

Table 6.2: Cutter contribution on force, torque and cutter-rock interaction area.

6.1.3   Summary - Bit Simulation

The parameter response simulation presented in Section 6.1.1, shows promising results for drilling. For the weaker sandstone (USC=8 ksi), the bit will stall if the DOC exceeds 0.262 mm/rev. Having a DOC of the maximum value, will the torque on bit be 2.1 Nm and WOB be 125.4 N. Drilling with these parameters under ideal conditions will give a ROP of 280.6 mm/min. If this ROP is observed during drilling, it will exceed all previous ROP records by tenfold. In order to hit the maximum ROP, drilling must be performed just below the torque limit. Experiments have shown that at 2.1 Nm of nominal torque, the bit will rotate at 537.3 RPM. Therefore, a maximum achievable ROP of 140.7 mm/min is more realistic.

For the stronger sandstone (UCS=17 ksi), the maximum DOC will be 0.168 mm/rev. At maximum DOC, the torque on bit will be 2.1 Nm, while the WOB will be 134.1 N. Assuming ideal conditions, these drilling parameters will give a ROP of 180 mm/min. However, the realistic maximum ROP will be 90.2 mm/min.

The cutter contribution simulation presented in Section 6.1.2 shows a quite well balanced bit. Some cutters will do more work and experience more axial and torsional loading than others, but should not have any substantial effect of the drilling performance. On this design it is impossible to achieve perfect balance on contribution from each cutter due the geometry of the bit profile not having more room to increase cutter density at the nose of the bit.

When analysing the results from these simulations, it is important to keep in mind what the primary application of the simulation software really is for. These simulations were done by Arne Funderud at Lyng Drilling, a Schlumberger Company. Lyng Drilling, specializes in producing drill bit technology for full-scale offshore drilling. Thus, the simulation software used for these simulations may not be as suitable and accurate as desired for a miniature drill bit. However, the results still can give sufficient information to draw some conclusions and predict some trends.

6.2 Test Drilling

Due to damage during transport the top drive was non-operational at the time of these drilling operations. Due to this the experiments described in this section only evaluates inclination and no azimuth as toolface orientation could not be achieved by the experimental setup.

6.2.1 Experimental Procedure

In this section, the performance of four PDC bits will be analyzed. The bits to be tested were acquired from different sources; two bits were purchased from Alibaba and have two and three PDC cutters, one bit is provided by Baker Hughes and DSATS and the fourth bit is a customized bit designed by UiS in cooperation with Lyng Drilling as described in Chapter 4. As mentioned above; ROP values, vibration

severity, inclination and hole quality are the performance criterion when comparing the drill bits. To evaluate the criterion, the experiments are conducted in the same manner for each bit. An overview of the activities executed from starting the system to completing the drilling operation is given in Figure 6.4.
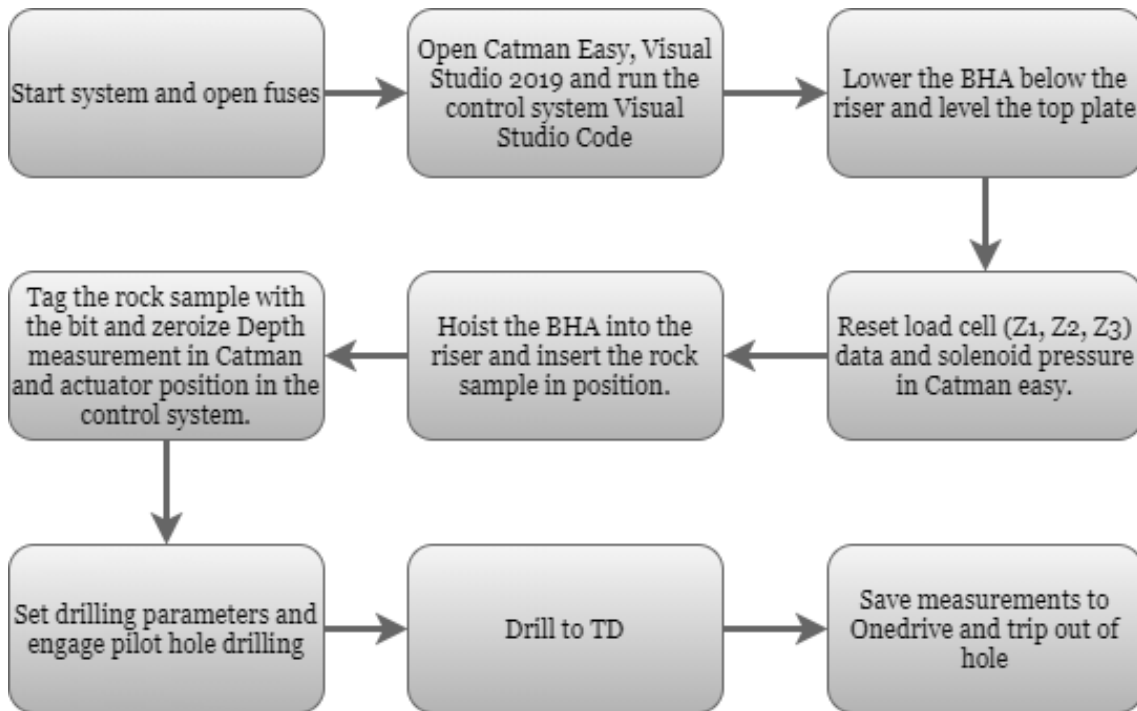
Figure 6.4: Flowchart describing the experimental procedure for test drilling.

The experiment is divided into two main phases; pilot hole drilling and drill to target depth (TD).

Pilot Hole During drilling of the pilot hole the drilling parameters remain constant at 1074.6 RPM (100% valve opening), 6 kg WOB setpoint and 0.2 mm/s actuator velocity. The reduced actuator velocity is to diminish vibrations and bit walking on the surface of the rock. The rotational speed was set to 1074.7 RPM, the maximum for the system, to achieve more consistent results when comparing the WOB setpoints as the experiment emphasis is to increase the WOB in increments to observe its result on the ROP. For the following experiments the pilot hole phase ends at 50

mm into the rock, at this point the bit body is fully emerged and vibrations lessen due the gauge pad being in contact with the wellbore walls.

Drill to TD Following the pilot hole, the system drills to the target depth by increasing the drilling parameters systematically. At 50 mm MD the drilling parameters are immediately increased to 10 kg WOB and 0.7 mm/s actuator velocity, whilst the rotational speed remains at 1074.6 RPM. Throughout this phase the WOB is increased by 1 kg every 2 minutes as shown in Table 6.3, the actuator velocity remains constant at 0.7 mm/s. During this period it is expected that the ROP will increase as the parameters used for the pilot hole are quite conservative. The ROP plotted in the performance charts is defined as the distance drilled in 2 minutes divided by 2 to attain the average ROP for the WOB setpoint in mm/min. TD is at 600mm to replicate the length of the rock sample provided by DSATS and used in the Drillbotics competition.

During testing of the "lego" cutout bent sub it was discovered that severe vibrations cause the bend to straighten, even at lower WOB setpoints that should not be able to deform the bend. The bending and straightening of the component intensifies the vibrations and causes the bit to move laterally. Due to this observation the no-cutout bent sub is used for the experiments in this chapter, consequently the drilling assembly is only able to continuously build inclination as the bent sub cannot straighten.

WOB	Rotational Speed	Actuator Velocity	Duration
[kg]	[RPM]	[mm/s]	[min]
6	1074.6	0.2	Until 50mm drilled
10	1074.6	0.7	2min
11	1074.6	0.7	2min
12	1074.6	0.7	2min
13	1074.6	0.7	2min
14	1074.6	0.7	2min
15	1074.6	0.7	2min
16	1074.6	0.7	2min
17	1074.6	0.7	2min
18	1074.6	0.7	2min
19	1074.6	0.7	2min
20	1074.6	0.7	2min

Table 6.3: Test drilling parameter overview

6.2.2   Experiment 1: Alibaba 3-Cutter PDC Bit

The 3-Cutter PDC Bit ordered from Alibaba was the first one to be tested following the standardized procedure to evaluate bit performance. The bit features 3 large PDC cutters, a long gauge pad and a massive bit body as seen in Figure 4.10. Ahead of testing it was assumed that the drill bit will perform well for the pilot hole phase due to the stability from the gauge pad, however the absence of a cone-cutter was a cause of concern for further drilling. The drilling operation was initiated by following the flowchart in Figure 6.4 and the rock was tagged with the pilot phase drilling parameters of 6 kg WOB and 0.2 mm/s actuator velocity. The bit was able to drill the first 40 mm at a ROP of approximately 10 mm/min, during this time one of the team members observed a large piece of the rock being ejected from the hole, it is assumed that this was the cone created by the bit breaking off. At 340 s the 50 mm pilot hole was completed at a ROP of 8.82 mm/s, the team was impressed at the bit performance as the pilot hole was drilled with minimal vibrations and the WOB measurement was always chasing the setpoint and hardly overshooting. The drilling parameters were changed to 10 kg WOB and 0.7 mm/s actuator velocity as per Table 6.3. At 56 mm the bit stalled and was unable to continue drilling, in an attempt to further test the bit performance the drilling parameters were reduced back to the pilot hole parameters. This had a positive effect on the drill bit as it was able to drill ahead at a low ROP of 2-3 mm/min. The WOB setpoint was steadily increased by 1 kg each minute, and the actuator velocity remained constant at 0.2 mm/s. At 9 kg WOB no axial movement of the drilling assembly was observed, albeit the drill bit seemed to rotate at full speed no formation was being drilled. The decision was made to trip out of hole to investigate the abnormal behaviour. As the drill bit reached the surface it was clear that the lack of a cone-cutter was the issue and a piece of rock stuck (cone) between the blades of the bit was present, as seen in Figure 6.5a. The possible explanation of the abnormal behaviour is that even though the bit was still rotating, the cutters were unable to reach the rock as the two cones (One inside the bit and one present on the rock) were pushing against each other and hindering the bit. At this depth the cone is no longer able to escape the wellbore as it was in the beginning of the pilot hole. In addition, due to the great stability of the Alibaba 3-Cutter PDC Bit the vibrations were so negligible

116

that the bit would not be able to crush the cone. In Figure 6.5b it can be observed on the walls of the wellbore that vibrations have been minimal as the hole quality is good, however not much inclination was built as this bit was designed for vertical drilling and lacks steerability.

(a) The cone stuck in the bit.

(b) The cone in the wellbore.

Figure 6.5: Alibaba 3-Cutter PDC Bit - Test Drilling

Figure 6.6 plots the relation between the ROP and the WOB, and the relation between depth and WOB. As the experiment was designed to evaluate bit performance for increasing WOB setpoints, the data recorded after reducing the WOB setpoint back down to 6 kg are removed. However, as the bit stalled twice at 10 kg WOB at different depth in the wellbore one can assume that the depth of cut was too deep, causing the motor to stall.
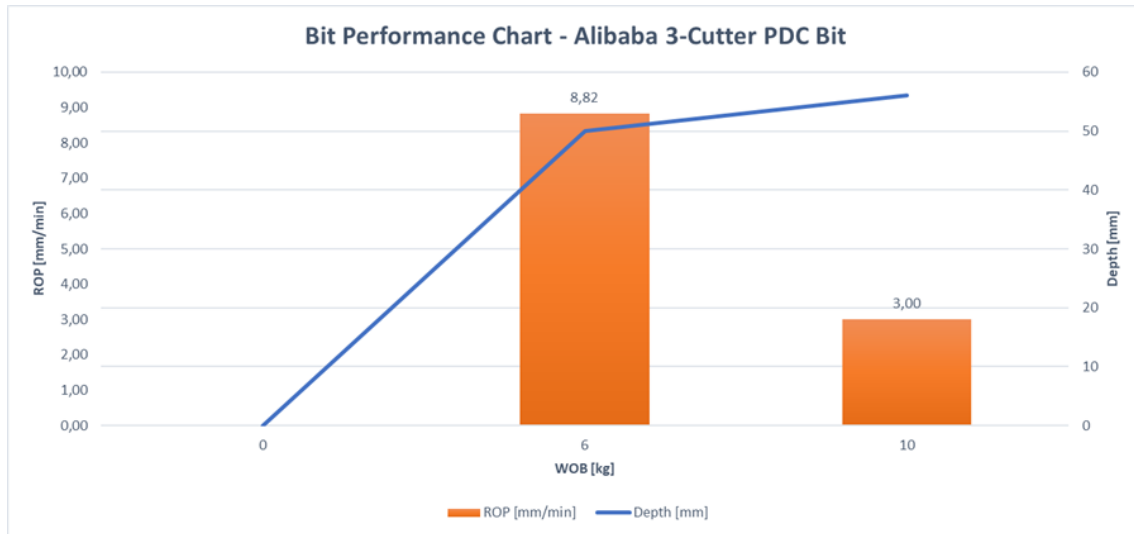
Figure 6.6: WOB in relation to ROP and Depth for Alibaba 3-Cutter PDC Bit.

6.2.3   Experiment 2: Alibaba 2-Cutter PDC Bit

The second well to be drilled was with the Alibaba 2-Cutter PDC Bit as seen in Figure 4.10. Prior to testing, the team expected the 2-Cutter PDC Bit ordered from Alibaba to perform poorly due to poor rock coverage, a large gap between the cutters leaving a cone of uncut material and too deep of a depth of cut for the pneumatic motor to sustain. On the flip side, the long gauge pad will keep the bit stable and improve the hole quality and reduce lateral vibrations.
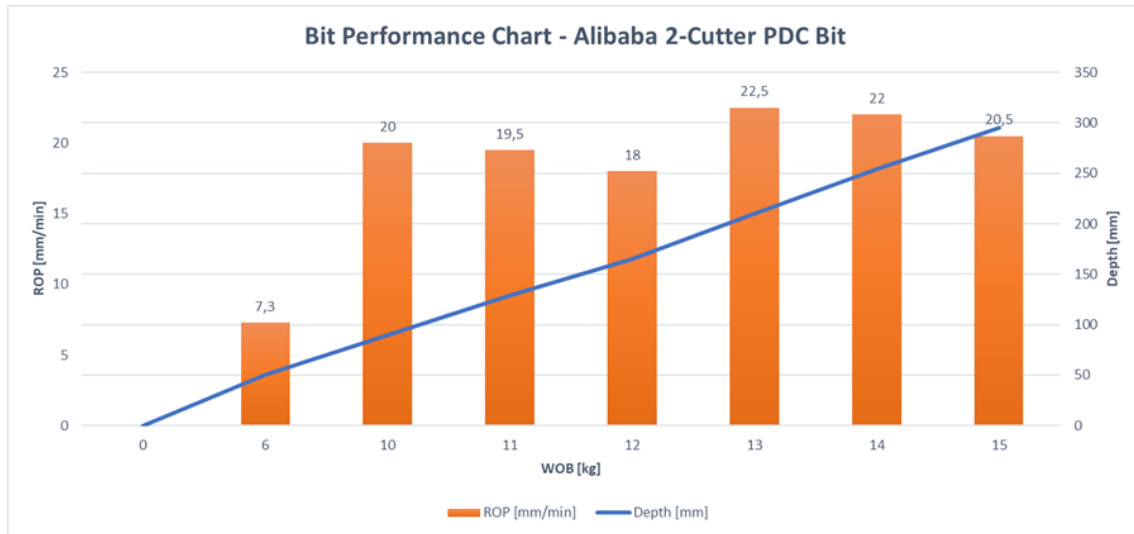
Figure 6.7: WOB in relation to ROP and Depth for Alibaba 2-Cutter PDC Bit.

The rock sample was tagged with 6 kg WOB and 0.2 mm/s actuator velocity and drilling was commenced. Initial bit reaction was as expected quite stable and the first 30 mm were drilled at a ROP of 10 mm/min with minimal vibrations. The WOB measurements for this section was near the setpoint meaning that the speed of 0.2 mm/s was appropriate to control overshooting the WOB setpoint, as have been the case previously. At 39 mm drilled the drilling assembly starts vibrating and the ROP decreases, after a few seconds of no axial movement besides axial vibrations the drilling assembly continues to drill into the rock. The increased vibrations were likely due to the cone between the cutters touching the bit body and causing the bit to walk in the hole. At 43 mm drilled the vibrations come to a stop and ROP decreases drastically, and it was observed that the gap between the motor shaft and gauge pad was a problem. This lead to heavy vibrations as the motor shaft was about to enter the wellbore and was stuck onto the surface of the rock. The lateral vibrations and enlarged hole is shown in Figure 6.14. External lateral forces had to be applied to the motor sleeve in order for the motor shaft to enter the wellbore. As the motor shaft entered the wellbore, the vibrations were eliminated. The additional vibrations caused by the stuck motor shaft likely crushed the cone in between the cutters. The 50 mm pilot hole was drilled in 410 s, resulting in a

119

ROP of 7.30 mm/s. At 410 s the drilling parameters were changed to 10 kg WOB and 0.7 mm/s actuator velocity as described above in Section 6.2.1. The observed vibrations are minimal and the ROP increases drastically as seen in Figure 6.7 to 20 mm/s and drilling continues. At 219 mm at 14 kg WOB the bit stalls and no rotation is observed. In this scenario, the procedure is to raise the drill bit 2 mm of bottom in an attempt to re-establish rotation. The remedial action was successful and drilling continued at a high ROP, the sudden decrease in ROP can be observed below and relates to the bit stalling. At a ROP of 22 mm/min at 290 mm into the rock, the bit stalls at 15 kg WOB setpoint. The same remedial action is repeated in an attempt to re-establish rotation, unfortunately the bit was unable to resume and the drilling operation was discontinued. The drill bit was able to reach a record total average ROP of 18.54 mm/min over the course of 290 mm. Due to the absence of vibrations at the acquired depth, the on-site conclusion was that the bit was unable to rotate as the cone between the cutters was not being destroyed by vibrations any more. Another explanation could be that the motor shaft, which rotates at the same rotational speed as the bit, was stuck on a ledge in the wellbore. This was further supported by the visual inspection of the wellbore subsequent to tripping out the drilling assembly. The wellbore created by the Alibaba 2-Cutter PDC Bit is shown below in Figure 6.8a. The ledges in the wellbore are only present when drilling with this bit, it is reasonable to think that this is caused by the long gap between the motor shaft and PDC cutters as seen in Figure 6.8b in gold. This would not be an issue when drilling a vertical well, but as the well is drilled with a constant bend in the BHA the motor shaft is likely to be in contact with the inclined wellbore. In addition, the bits ordered from Alibaba are 38 mm OD instead of 38.1 mm (1.5 in) making it slightly harder to fit the drilling assembly in the hole.
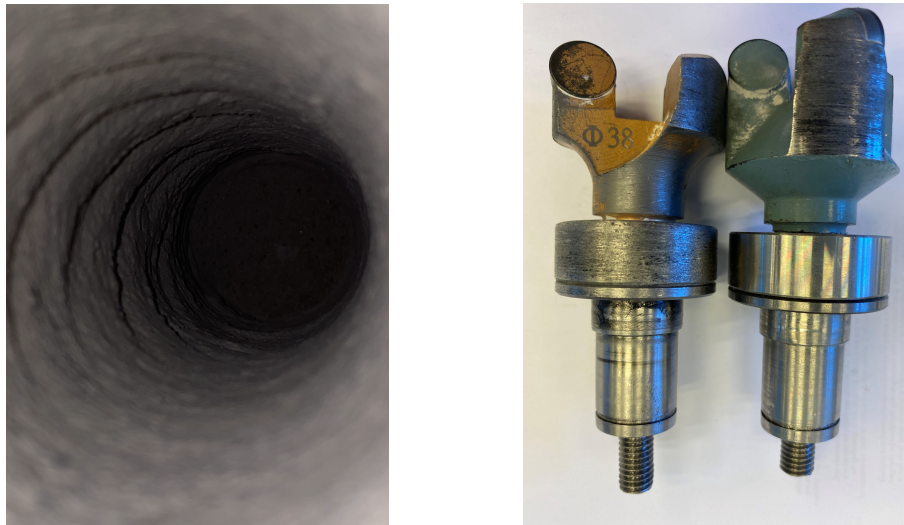
(a) The 290mm deep well drilled.   (b) The bit connected to the motor shaft.

Figure 6.8: Alibaba 2-Cutter PDC Bit

6.2.4 Experiment 3: Baker Hughes 4-Cutter PDC Bit

The third well was drilled using the Baker Hughes 4-Cutter PDC Bit without the supplied tungsten carbide inserts provided by DSATS. The inserts would help stabilize the drill bit by reducing the gauge pad clearance and depth of cut, however due to time limitation test drilling was only performed without the inserts. Consequently, bit walking and lateral vibrations were expected for this test. The bit was used for several tests prior to the test drilling presented in this chapter, and the observed vibrations were severe in the top section of the pilot hole. As the bit progresses into the formation and the first stabilizer enters the wellbore, the vibrations lessen and ROP increases. If the vibrations in the top section had been too severe, the hole would be too large for the stabilizers to be able to have its full effect. The vibrations would often lead to damage to the BHA components and one bent sub was broken during previous testing. Even at low WOB setpoints the WOB measurements were unstable and the PID controller would struggle to remain at the desired setpoint. These observations were the main incentives to investigate the effect of the actuator velocity as the depth of cut appeared to be too aggressive. For the initial tests, a maximum measured depth of 150 mm and 10 mm/min ROP was

achieved at 1 mm/s actuator velocity. The section below will describe the experience of drilling with the Baker Hughes 4-Cutter PDC Bit after making the adjustments to the actuator velocity.
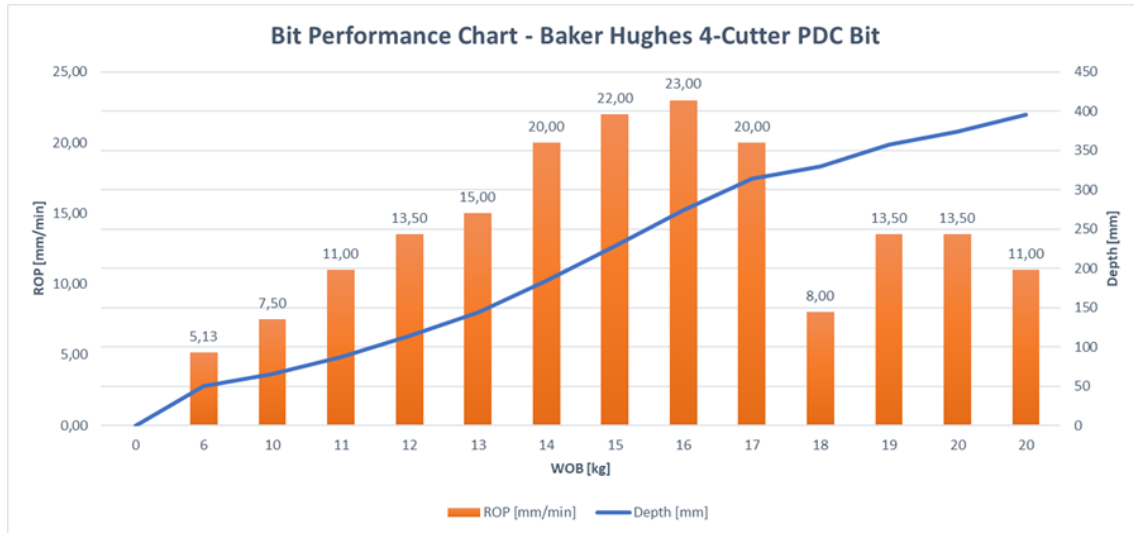
Figure 6.9: WOB in relation to ROP and Depth for Baker Hughes 4-Cutter PDC Bit.

The rock sample was tagged with 6 kg WOB at a actuator velocity of 0.2 mm/s. The bit performed well in comparison to previous tests at 1.0 mm/s and the vibrations were not as severe. At 30 mm into the formation the ROP was 4.74 mm/min, half of the ROP of the Alibaba 2-Cutter PDC Bit at the same depth. The reason for the slow drilling speed is due to the poor bit stability and the bit walking in the hole. A considerable amount of energy is wasted through lateral movement of the bit, causing a larger hole and little axial movement, the ovality caused by the lateral movement can be seen in Figure 6.10a. Even then the observed vibrations are less intense than they were in previous tests using the same drill bit and the WOB measurements correspond with the setpoint. The 50mm pilot hole phase is completed at 585 s at an average ROP of 5.13 mm/min. Immediately as the pilot hole phase ends, the Drill to TD phase begins and the drilling parameters are changed to 10 kg WOB and 0.7 mm/s. It is immediately observed that the actuator velocity is too aggressive for the drill bit at this depth as the vibrations aggravate

and energy is lost to lateral movement. From Figure 6.9 one can observe the ROP increasing from the previous 5.13 mm/min to 7.5 mm/min, a minor increase from the pilot hole phase. As the bit continues to drill ahead and the WOB setpoint is increased every 2 min the vibrations lessen as the stabilizers begins to enter the wellbore. At 12 kg WOB and 120 mm into the rock, the majority of lateral vibrations dissipate and ROP increases. As observed in the bit performance chart this trend continues until 16 kg WOB and a maximum of 23 mm/min ROP is achieved. From this point onward the drilling speed slows down significantly and large quantity of cuttings had to be manually removed from the hole by the use of an external air supply. However, it seemed to have little effect on the drilling operation as the ROP continued to drop. Based of previous experience it is clear that as the bit travels deeper into the rock, the friction between the wellbore and BHA increases. The inclination causes the drilling assembly to rest on the low side of the wellbore and the drill pipe further complicates the situation by applying weight directly onto the low side of the wellbore for an inclined well as shown in Figure 6.10b. Thus, the measured WOB at the surface is not corresponding to the actual WOB applied to the bit. In shallow parts of the well this situation is avoided due to lower dogleg severity and lateral vibrations enlarging the hole, this allows the drilling assembly to comfortably fit in the hole. Despite the fact that the ROP drop due to the described phenomena, the drilling operation is still making progress and the ROP increases for the 19 kg and 20 kg WOB setpoints. To spare components for excessive wear and damage the test drilling was initially planned to end after 2 minutes at 20 kg WOB. An additional 2 minutes were added to the drilling operation at the same drilling parameters to reach approximately 400 mm and a slight drop in ROP was observed. It is probable that the drilling speed would continue to drop as the wellbore seems to taper. However, further testing would have to be conducted to solidify this theory. The drilling operation is stopped at 400 mm into the rock at a total average ROP of 14.1 mm/min. As the bit was yet to stall, it would be interesting to increase the WOB further to reach the point where the depth of cut would be too large and the pneumatic motor would be unable to provide enough torque to maintain rotation.

(a) Hole drilled to 400 mm.
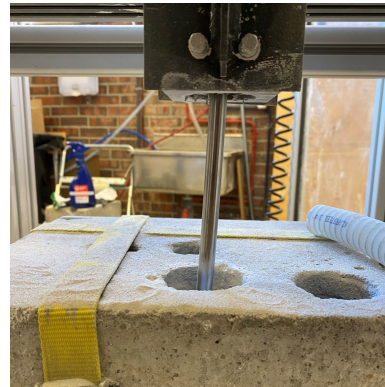
(b) Deflection of the steel pipe.

Figure 6.10: Baker Hughes 4-Cutter PDC Bit

6.2.5 Experiment 4: UiS 12-Cutter PDC Bit

For the fourth and final well the UiS 12-Cutter PDC Bit was used for the first time. The team was eager to see the results from many hours of bit design and optimization of design iterations based on the simulations discussed above. The design concepts described in Chapter 4 lay the foundation of a fully customized bit made for the purpose of directional drilling with the aim of remaining stable, reducing vibrations and increasing ROP.

Identically to the previous experiments the rock sample was tagged with a WOB setpoint of 6 kg and an actuator velocity of 0.2 mm/s. During the first minute of the drilling operation the bit achieved a ROP of 10 mm/min and further increased this to 11 mm/min by 40 mm. The WOB measurement is steady at approximately 6 kg and continuously chasing the setpoint to maintain it. The pilot hole was drilled without any issues, and lateral vibrations and the occurrence of bit walking was absent. At 50 mm drilled the pilot hole finishes with a new best time of 290 s, resulting in an average ROP of 10.35 mm/s. The drilling parameters were increased to 10 kg WOB and 0.7 mm/s actuator velocity and ROP started to increase. At both 10 and 11 kg WOB setpoints the WOB measurements exceeded the setpoint, similar to Baker Hughes, indicating that the actuator velocity may have been too aggressive this shallow in the well. However, no lateral movement was observed as it was for the Baker Hughes bit. Interestingly the ROP started to decrease from 18

mm/s to 9 mm/s, this observation was not expected and the trend continued for the following WOB increments. By analyzing the data during the drilling operation the team noticed that the WOB measurements were at the setpoint, or close to it, even when the actuators had not moved for a while. This was also the case when the BHA was fully emerged in the hole whilst drilling with the Baker Hughes PDC Bit. However, this response was not expected at such an early stage of the wellbore, but it was clear that not enough WOB was being applied to the bit, instead it was being wasted to friction against the walls of the wellbore. The presumed reasoning was that the absence of lateral vibrations had caused a perfectly on-gauge hole with the drill bit at 1.5". As the BHA components are only a little bit smaller than the bit (to be able to fit the sensor in the sleeve), issues arise and very little WOB can be utilized to drill the formation. Immediately as the WOB setpoint is raised to 18 kg, the ROP increases as there is enough force to overcome the friction and to push the bit into the rock. Unfortunately, this trend does not continue as it seems more friction is generated the further the bit travels and ROP decreases yet again. As there it little room between the wellbore and motor sleeve, a possible issue is the removal of the cuttings. However, for this experiments the cuttings were easily removed when the air flow conduit from the motor exhaust entered the wellbore. The cuttings generated are very fine and act similarly to dust, therefore the high rotational speed and air flow are able to remove the cuttings even if the clearance between wellbore and motor sleeve is low. The experiment ends as the last WOB setpoint at 20 kg is completed at 233 mm MD with a total ROP average of 8.57 mm/min. The hoisiting system was unable to trip out of hole as the BHA was stuck due to friction, the rock had to be manually wobbled whilst rotating the drill bit at 1074 RPM and running the actuators to be able to trip out of hole. The contingency plan if no movement was observed using this method was to cut the pipe and manually pull the BHA out of hole, and if there was still no movement the rock would have to be cut.
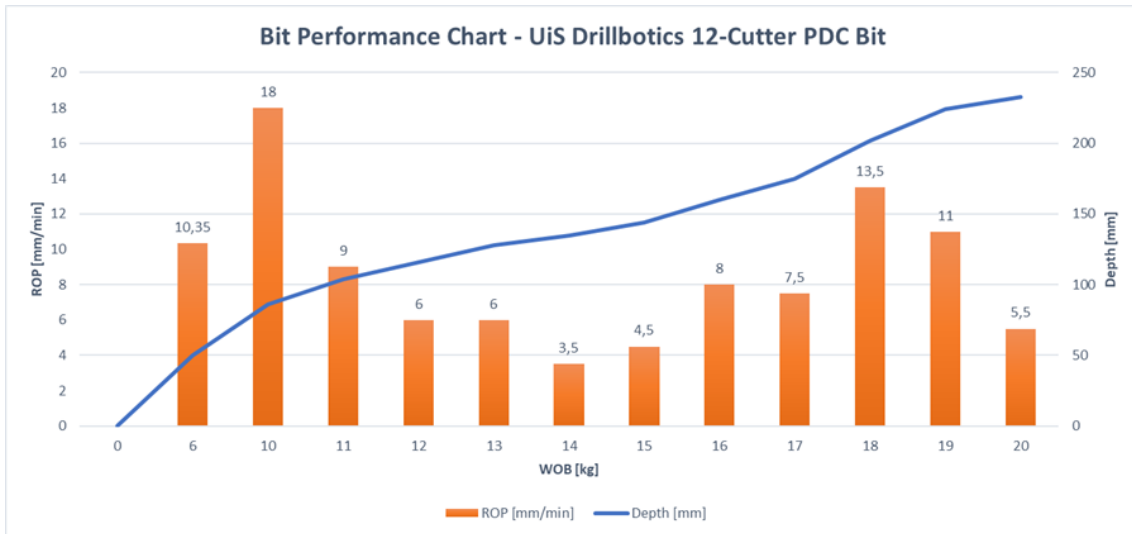
Figure 6.11: WOB in relation to ROP and Depth for UiS 12-Cutter PDC Bit.

(a) Hole drilled to 243 mm.

(b) Zoom in off the wellbore to inspect hole quality.

Figure 6.12: UiS 12-Cutter PDC Bit

6.2.6 Summary - Test Drilling

To evaluate the performance criterion introduced in the experimental procedure, upper and lower limits are set to determine each criterion's result for the drill bits tested and compare them relative to each other. The highest total average ROP was

calculated to be 18.54 mm/min and the lowest average ROP to 3.05 mm/min. With these values in mind, the ROP performance is split into low ROP (0 - 5 mm/min), moderate ROP (5 - 10 mm/min) and high ROP (10 - 20 mm/min). In Figure 6.14 the well profiles of three drill bits are shown and the horizontal displacement is calculated and compared at 243 mm measured depth to estimate which bit has the potential of building the greatest inclination with the current setup. The UiS bit accomplished a horizontal displacement of 33.48 mm and the Baker Hughes and Alibaba 2-Cutter bit accomplished 16.4 mm and 20.86 mm, respectively. In the scenario that the UiS bit would continue with the same build rate it would accomplish a horizontal displacement of approximately 69 mm in 500 mm MD drilled. The previous year's setup was able to achieve a horizontal displacement of 55 mm in the same distance, indicating that the improvements made to this year's BHA and bit benefit directional drilling. The well drilled by the 3-Cutter bit from Alibaba was not cut and the horizontal displacement could not be calculated to evaluate the inclination criteria. To determine vibration severity for the drill bits, each experiment was observed carefully by the team members and drilling anomalies were recorded. Both axial and lateral vibrations are evaluated for this criteria. The UiS bit experienced little to no vibrations in any direction, this is further supported by the fact that the measured hole diameter is approximately 1.5 inches, the same as the bit diameter. This also applies for the 3-cutter bit from Alibaba where the vibrations severity was observed to be low. Heavy lateral vibrations and excessive bit walking were observed during drilling with the Baker Hughes bit and early testing lead to damage of components due to the severity of vibrations. The 2-cutter bit from Alibaba experienced very little vibrations during the first minutes of drilling, unfortunately the large gap between the bit and motor shaft caused large vibrations when the motor shaft was stuck, this is further described in Section 6.2.3. Due to the infrequent heavy vibrations, the overall vibration severity was determined to be moderate for the 2-cutter bit. Upon cutting the homogeneous cement, the team was able to further investigate the hole quality of the wells drilled. The hole drilled by the UiS bit was on gauge and no anomalies were observed, similarly the hole drilled by the Baker Hughes bit was smooth, but the lateral vibrations caused ovality. The 2-cutter bit from Alibaba created ledges all through the wellbore and the hole quality was poor. The short distance drilled by the 3-cutter bit from Alibaba was stable and the

127

hole is of good quality, the biggest flaw being the cone created between the cutters. A summary of the performance criterion is shown below in Table 6.4.

	ROP	Inclination	Vibration Severity	Hole Quality
UiS	Moderate	High	Low	Excellent
Baker Hughes	High	Low	High	Moderate
Alibaba 2-Cutter	High	Moderate	Moderate	Poor
Alibaba 3-Cutter	Low	n/a	Low	Moderate

Table 6.4: The evaluation of the performance criterion.

In an attempt to have a stable top section of the wellbore, a pilot hole is drilled at conservative parameters to reduce vibrations and ensure a concentric hole. The ROP in the pilot hole is compared for all the bits in Figure 6.13. As the actuator velocity is set to 0.2 mm/s during the pilot hole drilling, the maximum achievable ROP is $0.2mm/s \cdot 60s/min = 12mm/min$. From the figure below, one can observe the average ROP for the UiS bit to be close to the maximum limit. The pilot hole drilling gives an indication of the potential of the bits in an unrestricted area where the bit needs to stabilize itself and minimal applied WOB is lost to friction. As the UiS bit performed better than the other bits for this section, but worse for the overall ROP the theory of the bit being too on gauge and inclined for the BHA to fit is strengthened. The ROP of the bits from Alibaba were quite similar and their ROP were reduced at approximately 40 mm where the lack of a cone cutter started to affect the drilling performance. The drill bit designed by Baker Hughes struggled to drill the pilot hole due to lateral vibrations and bit walking as described in the sections above. Indications of reduced lateral vibrations as the first stabilizer enters the wellbore gives the team reason to believe that the bit would perform better had the inserts been installed as the gauge pad clearance could be reduced to 0 mm.
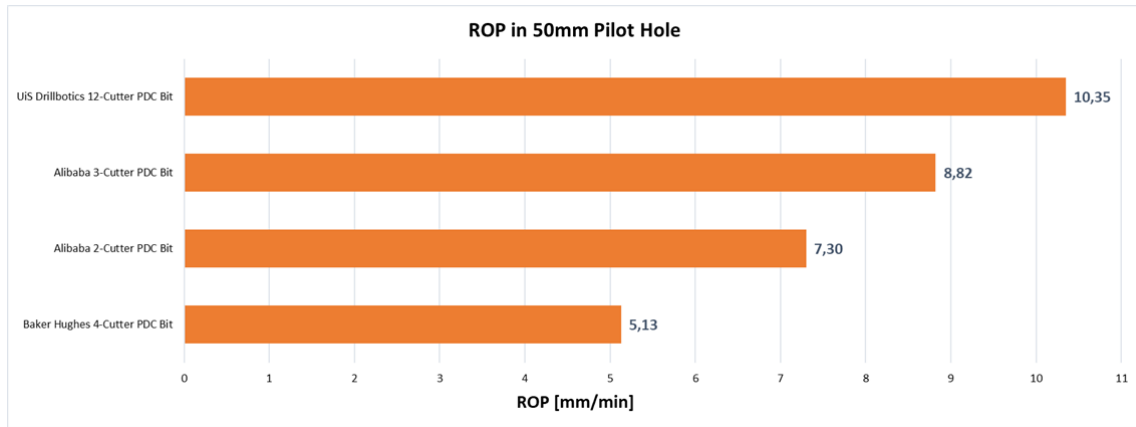
Figure 6.13: ROP in pilot hole for the tested bits.
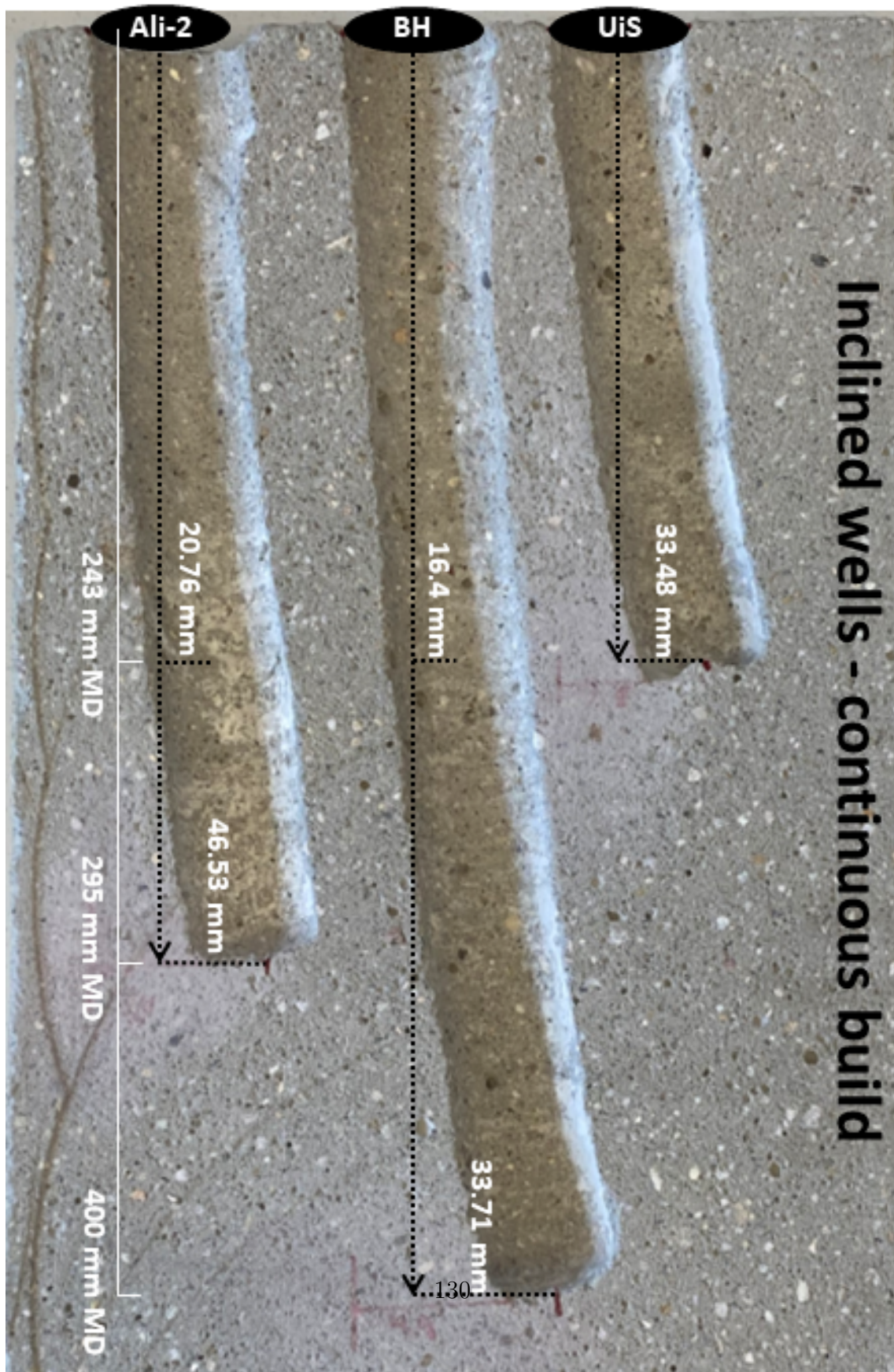
Figure 6.14: Three well profiles in the homogeneous cement using a fixed 8 degrees bend. From the top; UiS 12-Cutter PDC Bit, Baker Hughes 4-Cutter PDC Bit and Alibaba 2-Cutter PDC Bit.

Chapter 7

Conclusion

This report covers the work done by the UiS team for the international Drillbotics competition of 2020. Special attention was given to the implementation of a steerable BHA, bit design for the purpose of directional drilling and the development of a downhole tool to be used in a closed-loop steering model. The improvements and changes made to the drilling assembly for the 2020 rig setup have increased the overall performance of the rig. The current setup is expected to be able to achieve a horizontal displacement of approximately 70 mm horizontal displacement and the maximum ROP has increased from 8-9 mm/min to 20-30 mm/min.

The introduction of actuator velocity control as a drilling parameter greatly improved the performance of the drilling operation. Reduced axial vibrations were achieved by controlling this parameter, in addition the PID controller was more accurate in achieving the desired WOB setpoint than in previous years. This increased the ROP of the drill bit and should be investigate further before the 2021 competition. Finding the optimal actuator velocity for the differing WOB setpoints will be key to optimize the ROP.

The 12-cutter PDC bit which was designed and 3D-printed in stainless steel in-house at the University of Stavanger demonstrated that a customized design has its benefits. The results from testings showed that drilling with the UiS bit reduced the severity of both axial and lateral vibrations, improved hole quality and achieved the

greatest horizontal displacement. Unfortunately, as the scope of the testing changed when the top drive motor was non-operational a pilot hole drilled in rotating-mode (rotation of top drive and downhole motor simultaneously) could not be tested. Drilling in rotating-mode would increase the size of the borehole and would be used for the pilot hole and upon achieving the desired inclination from orienting-mode drilling (stationary BHA and drill pipe). As the whole well had to be drilled in orienting-mode, challenges occurred as the BHA struggled to fit in the inclined wellbore. This issue was avoided for a longer period of time when drilling with the Alibaba 2-Cutter PDC bit and the Baker Hughes 4-cutter PDC bit due to lateral vibrations and bit walking increasing the hole size.

The development of the 9-axis Inertial Measurement Unit (IMU) on a custom flexible Printed Circuit Board (PCB) proved to be a challenge as there were many practicalities that needed to be overcome in order to fit the sensors inside the BHA and close to the bit. Results from the practical testing show that the IMU can measure the orientation and position of the downhole tool by the use of an Attitude and Heading Reference System (AHRS). No drilling operations have been performed with the downhole sensor and further testing is therefore needed to confirm accuracy and robustness of the sensor.

Throughout the semester it was evident that mechanical upgrades to the rig would be necessary to complete the challenge of directional steering to hit multiple targets in more than one direction. These upgrades, in addition to other identified challenges, are documented in this report to assist new UiS Drillbotics team members.

Chapter 8

Challenges and Future Recommendations

Many challenges and limitations were encountered along the way. Manufacturing complicated drilling assemblies, miniature downhole sensors and an autonomous drilling rig come with a lot of practicalities that need to be understood and overcome. This chapter aims to capture the lessons learned from working on the problem statement for this year's competition to improve the understanding of the system for new UiS Drillbotics members. SPE and DSATS released a statement revealing that the problem statement will be similar or identical for the 2021 competition, which is why it is important to capture the learnings from the current team members.

8.1 Drilling rig

An autonomous drilling rig is dependent on a robust and carefully planned design. The current rig design is left as a solid foundation for next year's competition. Nonetheless, improvements have been identified and documented in this section.

8.1.1 Rotational System

One of the key systems for the laboratory-scale drilling rig is the rotational system. The rotational system is divided into the top drive and pneumatic motor, how they

function can be found in Chapter 2. During transportation of the rig back from the 2019 Drillbotics competition the rig was damaged, luckily most of the damage was cosmetic or to non-vital parts of the rig such as the wheels. However, the female connector on the top drive driver was damaged and needed replacement. The driver was been disassembled and the connector was replaced in the best manner possible. Unfortunately, this was not enough to fix the issue as the top drive is unable to rotate in an appropriate manner. Troubleshooting of the motor and countless hours was spent trying to fix the issue as the top drive was supposed to play a vital part to adjust the toolface of the BHA and steer the bit. Rotation of both the pneumatic motor and the top drive simultaneously is yet to be tested due to the damage.

The 2020-2021 UiS Drillbotics team should investigate if a new driver can be acquired as this would likely fix the issue. If the driver cannot be replaced, a new top drive motor should be purchased as soon as possible. The current top drive motor is a hollow shaft brushless motor and allows air or fluids to be pumped through the motor and into the drill string. If a new motor is purchased, new flanges might have to be manufactured in addition. The flanges connect the drill string and motor at the bottom, and the motor and rotary union at the top.

Whilst the pneumatic motor is fit for purpose and the provided torque of 2.1 Nm is sufficient, a shorter motor would improve the directional capabilities of the system. Thorough investigation should be done in order to find a short pneumatic motor with similar specs.

8.1.2 Hoisting System

During the final experiment the team performed, the stepper motors overheated and stopped functioning. The decision was made to let them cool down overnight and testing was resumed the next day. When turning on the power for the system, the stepper motors immediately started moving even though they were not commanded to. The emergency button had to be immediately pushed to avoid damage of the BHA still in the hole from the experiments. All wires for the Arduinos and the stepper motor drivers were unplugged and plugged back in after a few minutes. No sudden movement was observed when powering on the system and the stepper

motors were raised a few millimeters. Stepper motor 2 did not move at the same speed as the two other stepper motors and was investigated further. When going through the wiring for the stepper motor driver, it was found that one of the phase wires were loose. The decision was made to replace the wire connector and attach new pin connectors to the wires. The wires were connected in the same manner as they were detached, however the stepper motor driver started burning as the power was turned on to test the new connection. A grounding issue has caused trouble in the past, and is likely the reason the driver was destroyed.

The suggestion for the 2020-2021 UiS Drillbotics team is to order and replace the stepper motor driver and attempt to fix the grounding issue. If it cannot be fixed, then a new hoisting system consisting of one large servo motor or a hoisting motor that is suited should be installed. Reducing the numbers of hoisting motors from three to one would solve the issue of having to level the top plate routinely and the problem that occur when one stepper motors stops during drilling whilst the other two keeps moving, potentially damaging equipment. To accommodate a new hoisting system, a new top plate or mounting for the top drive would have to be designed. A complete upgrade of the top drive, top plate and hoisting system is advised for the 2021 competition.

8.1.3 PLC

The issues regarding the Measurement Computing PLCs and the Arduinos are described in Chapter 2 and new PLCs should be investigated immediately. Beckhoff Automation Technology have been in contact with the team and has an overview of what the system requires. When installing new PLCs, the electrical cabinet should be stripped of all unused wires and components to minimize the risk of the issues experienced this year in regards to grounding happening again.

8.2 Additive Manufacturing

Additive layer manufacturing has proven to be a very useful technology for this project. Almost every component has been printed in PLA or a composite material in order to test the functionality prior to manufacturing in a CNC-machine or metal

printer. Some of the components designed on this project would have required time-consuming, complex and expensive CNC-machining, but with metal 3-D printing as option one saves a lot of time and effort. Despite being very useful, additive layer manufacturing has not been unproblematic.

8.2.1 Bent Sub

Several problems was observed with the printed bent sub. Since the bent sub experiences quite extensive loads and occasionally vibrations while drilling with sub-optimal parameters, it was supposed to one solid piece. All strength calculations done by the team was based on it being completely solid inside the walls of the bent sub. Unfortunately a mistake were made while setting up the print and it was observed to only have approximately 50% infill. Only having 50% infill gives a noticeable reduction in strength. To avoid failure of the component it should have 100% such that maximum strength is achieved.

Another consideration to keep in mind is printing direction. A printed component is weakest between the printed layers. All the bent subs were printed in an upright position, which makes it more prone to parting if the bit gets stuck and tried to pull out or continuous lateral vibration. Continuous lateral vibration on the bent sub may cause a micro crack between one or several printed layer which will propagate as vibration continues. Eventually it will part where one or several micro cracks started. To avoid this, the bent subs should be printed laying down or at a 45° angle to increase strength. A recommendation would be to do a fatigue test of different printing direction to investigate which performs better for this particular project.

Figure 8.1: Parted bend. One can also see that the bent sub is not solid.

8.2.2 Motor Sleeve

Printing the motor sleeve gave even more knowledge about the challenges with metal 3-D printing. Since the sleeve was designed to be a housing for the pneumatic motor, it needed internal support to avoid the walls of sleeve to collapse during printing. The internal shape of the sleeve is quite complex as it also holds a sensor together with its wires and has conduits to transport air-flow from the exhaust of the pneumatic motor down to the bit for hole cleaning purposes. Due to the complex internal shape of the motor sleeve, creating a support which were easy to remove proved to be a struggle. The sleeve has to be oriented in such a way that the support structure does not fill the slot for the sensor package. If the sensor package slot is filled will the internal support structure have a larger diameter than the open end of sleeve and the support structure will almost be impossible to remove. This problem is especially apparent if the support structure is printed as one a solid rather than in blocks. By printing the support as several blocks it is possible to remove, but not particularly easy. A recommendation based on the experience from this project will be to increase the number of the supporting blocks making each individual block smaller.
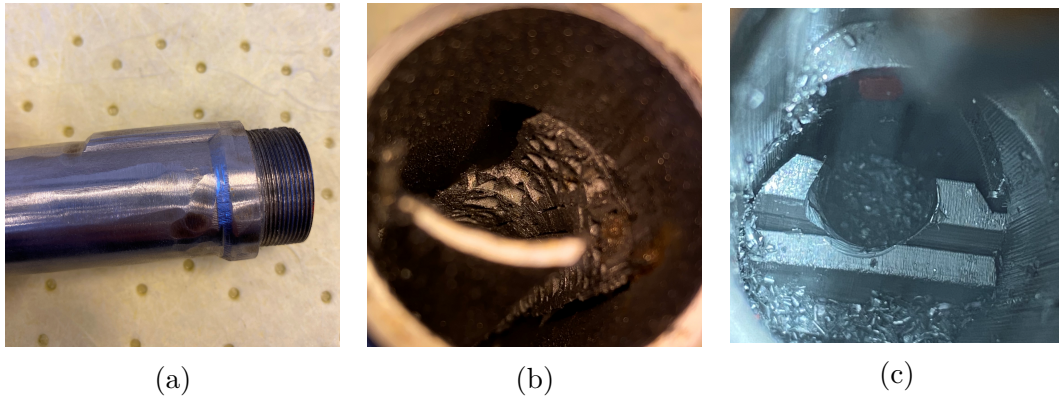
Figure 8.2: Stuck support being drilled.

During one printing iteration of the sleeve, an error occurred during the sintering process. The error caused the sintering furnace to turn off while being in the middle of the process. In order to finish binding the metal, the furnace had to be restarted, i.e. it had to be re-heated and repressurized. Prior to restarting, the sleeve was not inspected. At completion of the sintering process it looked like the sleeve had exploded. It was shattered into multiple pieces with quite clear cracks all over the sleeve. It is reasonable to believe that the support structure expanded inside the already brittle sleeve during the re-heating eventually shattering the sleeve. Naturally this print was dysfunctional and a new printing iteration had to be started.
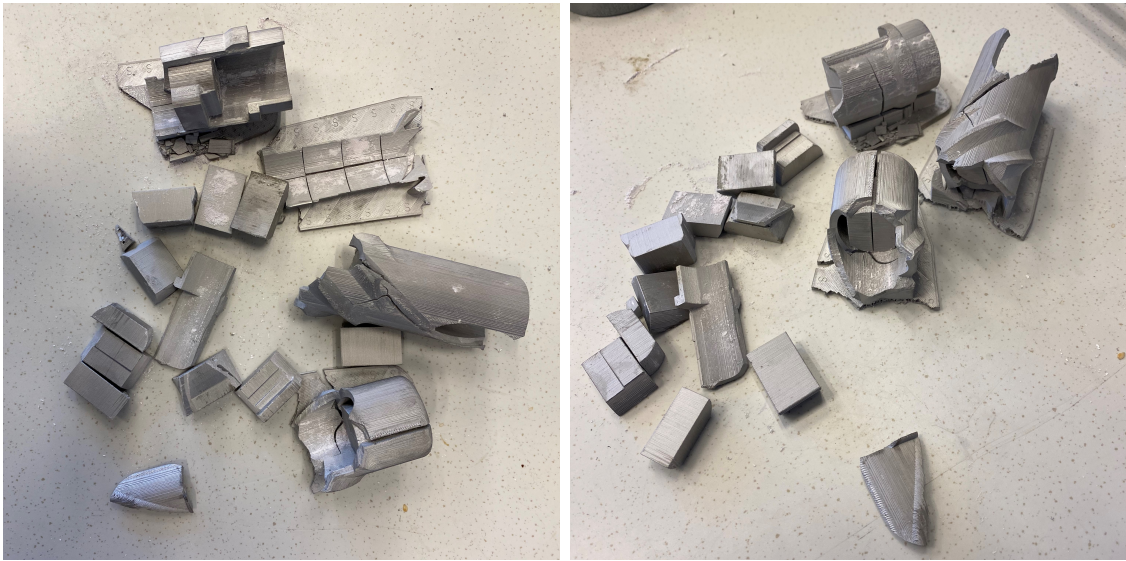
Figure 8.3: Shattered sleeve immediately after sintering.

8.3 Drilling Assembly

Due to time-limitations, some flaws and sub-optimal design features were discovered while testing of the drilling assembly. Usually, these kinds of flaws and sub-optimal design features would have been accounted for prior to performing the final experiments. However, due to the shut down of the university, some crucial components were completed in manufacturing close to the deadline. This meant there was no time to accommodate for the weaknesses of the design, and quick-fixes had to be made in order to perform the experiments.

8.3.1 BHA

The main challenge regarding the BHA was to assemble all components inside the 3-D printed housing and making everything function as desired. That meant all components had to fit perfectly inside their respective printed part which proved to be a challenge. Since all components are supposed to rotate at speeds of 1074 RPM, the precision of the components can not be stressed enough.

Pneumatic motor - Universal joint connection

The connection between the pneumatic motor and universal joint have to be done in a particular way in other to ensure robustness. Keep in mind that the connection needs to be able to transport 1074 RPM and 2.1 Nm of torque from the pneumatic motor. At first, set-screws where used to make the connection. After some attempts to drill, the set-screws broke and no rotational velocity or torque were transported to the bit. It was then decided to try using a pin to make the connection rather than set-screws. Pins were made in copper, brass, steel and stain-less steel. All the different material pins broke after a short amount of drilling. As attempt to strengthen the pins, chemical metal was used to fill voids reducing play in the pin-holes, but it did not help.

Since the pins did not work either, it was decided to make threads on the universal joint then screw the joint inside the pneumatic motor. The threading inside the motor was M8 0.75 which is not a standard pitch on for M8 threads. A M8 0.75 screw die had to ordered in order to make the threads.

Threading of the universal joint proved to be the right solution for this connection. By screwing the universal joint inside motor, enough strength to deliver both rotational speed and torque is achieved. However, it is important to make the length of threads such that the joint will land on its shoulder to avoid stress concentrations at the screw. Another consideration to keep in mind is that the ball of the universal joint should be placed exactly at the bend of the printed bent sub. If there is a misalignment there, will the universal joint tend to grind against the wall of the bent sub and lose some torque to friction.

Just for clarity, the pin shown in Figure 8.4 was only to display the concept. The pins used were manufactured in the lathe with accurate dimensions.
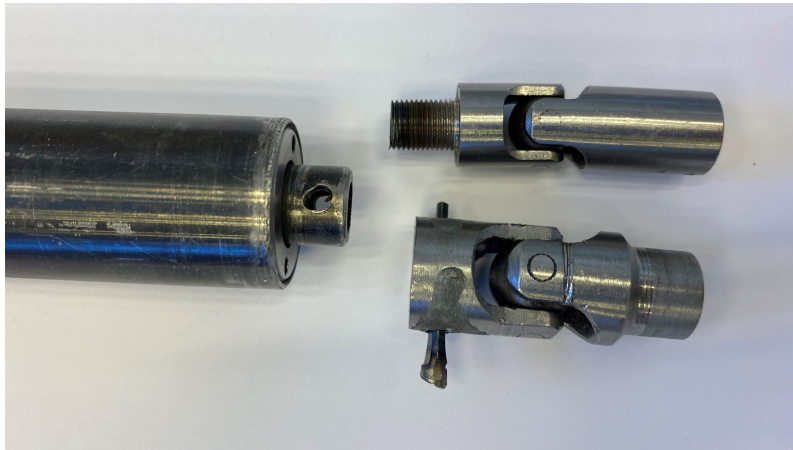
Figure 8.4: Tested connections between motor and universal joint.

Bent Sub Threading

The bent sub is set to have an 8 degree offset. The angled offset made the fastening the bent sub such that it was perfectly level with the shoulder on each side very difficult. It also has a complex external shape which makes it challenging to get an even grip around the bent sub. Due to the offset and complex external shapes, the threading of the bent sub got slightly lopsided. In Figure 8.5, the effect of lopsided threads is shown. From the figure one can observe that one side is landing on the shoulder. However, by turning the BHA 180°, one can observe that there is a gap between the shoulders. This means that the BHA will not be perfectly aligned.
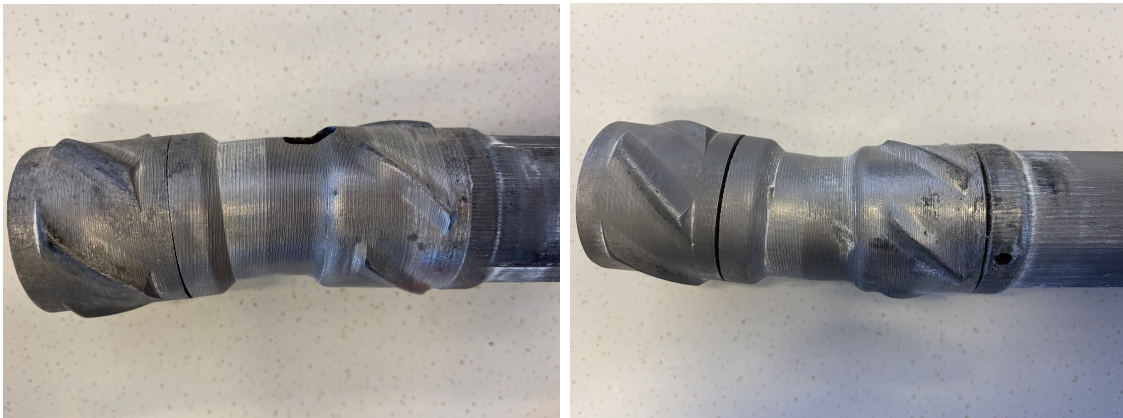
Figure 8.5: The effect of lopsided threads.

Two of the bent subs were printed with a cutout in order to make it straight of the bit got stuck in hole. The two cutout shapes were a helical and a "lego" cutout. The purpose of the "lego" cut was to increase the resistance to twisting, while the helical cut has no additional measures other than material strength. It became obvious that the "lego" cut was necessary to avoid twisting of the bent sub. This became apparent while threading the helical cut bent sub. As shown in Figure 8.6, the bent sub got twisted beyond the bonding strength of the printed layers and eventually parted the bent sub.
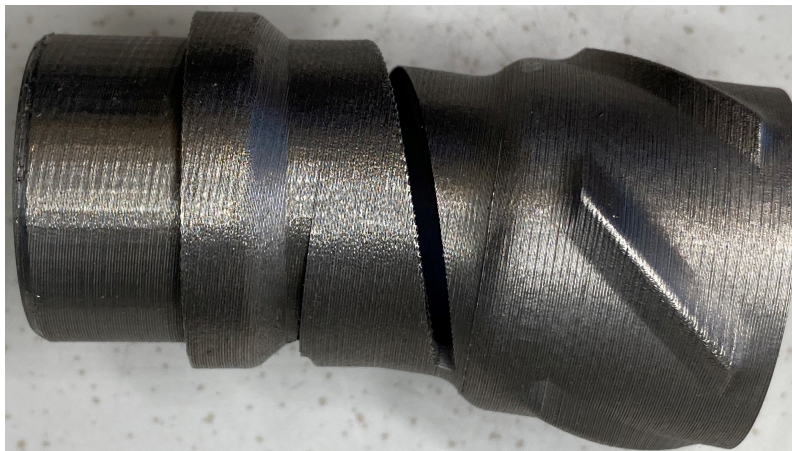
Figure 8.6: Spiral bend untwisting and parting while threading.

Shaft, bushings and bearings

Some noteworthy observations were made with regard to the motor shaft. First of all, the CNC-machining of the piece were not perfectly accurate where the thrust roller bearing should be placed. It is particularly important to have correct tolerances when one uses a hydraulic press to press-fit a bearing. When press-fitting a bearing, one should not exceed more than 0.05 mm discrepancy between the diameter of the shaft and internal diameter of the bearing. On the shafts that were CNC-machined, the diameter was 20.15 mm while the bearing had an internal diameter of 19.99 mm, giving a discrepancy of 0.16 mm which is way too large. On the shafts used for drilling, the diameter was reduced to 20.02 mm in order to safely press-fit the bearing.

Another important observation was on how far the motor shaft could be screwed into the universal joint. If the motor shaft got screwed too far into the joint, it would compress the thrust roller bearing to a higher load than what the bearing is rated for and rotation will not be possible. On the other hand, if it is screwed in too short it will cause the bushings to be compressed increasing the friction effectively losing torque. In addition, more of the shaft will be exposed outside the lower stabilizer leaving the bit more prone to vibrations. Several spacing-length were tested in order the find the optimal distance. After many integration the best suited spacing length was found to be 4.3 mm. A 4.3mm spacing distance was achieved by using three M8 washers as shown in Figure 8.7.

(a) Small

(b) Large

(c) Good

(d) Good=4.3mm spacing.
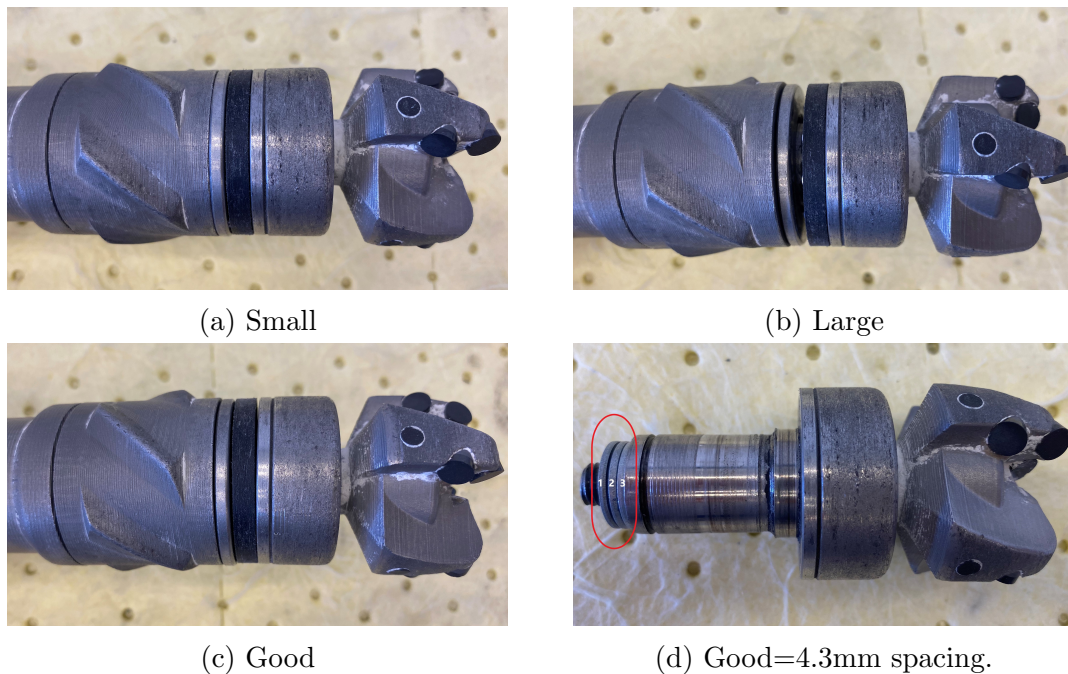
Figure 8.7: The effects on shaft spacing.

As mentioned, precision is key for this solution and the same is true for the bushings. If the brass bushings are too tight around the shaft, a lot of friction will be felt. If they are too loose, the bit will have much play between the bushing and inner wall of lower stabilizer - making the bit highly prone to vibrations. Large play will cause the shaft to get a throw while rotating. The throw may damage the outside of the bushing making it rotate uneven. Therefore, the bushings have to be tested

to ensure they fit perfectly.

Grease vs low viscosity oil

Prior to assembling all components to the BHA, the components were greased up to reduce friction of the rotational components. By inspecting the BHA subsequent of conducting a drilling experiment, it was noticed that the bearing was packed with a mix of grease and dust (cuttings) from the drilling operation. The mix of grease and dust appeared to be almost solidified to a point where the bearing did not move. Since the grease had the tendency to absorb dust, it was decided to change out grease for a light oil. Rather than greasing up the components, roughly 1-2 ml of oil was injected with a pipette through a venting hole located above the components. By testing out the new way of lubricating, it was concluded that the oil evacuated the dust particles much better than the grease. Therefore, it is recommended to use a light oil as lubricant for the internal BHA components. Keep in mind that the friction causes the components to exert heat, so it is important to use an oil which has a sufficiently high flame point.

8.3.2 Drill Bit

Due to limited testing of the bit, there are not many identified challenges. However, if fluid flow through the bit is needed for future projects, the nozzle diameter has to be larger. Currently, the outlet nozzles are 1 mm in diameter, while the inlet channel is 3 mm. With 1 mm nozzle diameter it is even difficult to flow air through them. A future recommendation will be to increase the diameters of the flow channels and nozzles according to Table 8.1 and visualised in Figure 8.8.

	Current Nozzle Design	**Proposed Nozzle Design**
Main inlet channel Ø	3 mm	5 mm
Internal channel Ø	1 mm	3 mm
Nozzle Ø	1 mm	2 mm

Table 8.1: Channel and nozzle diameter for the current and proposed design.

(a) Current design (b) Proposed design
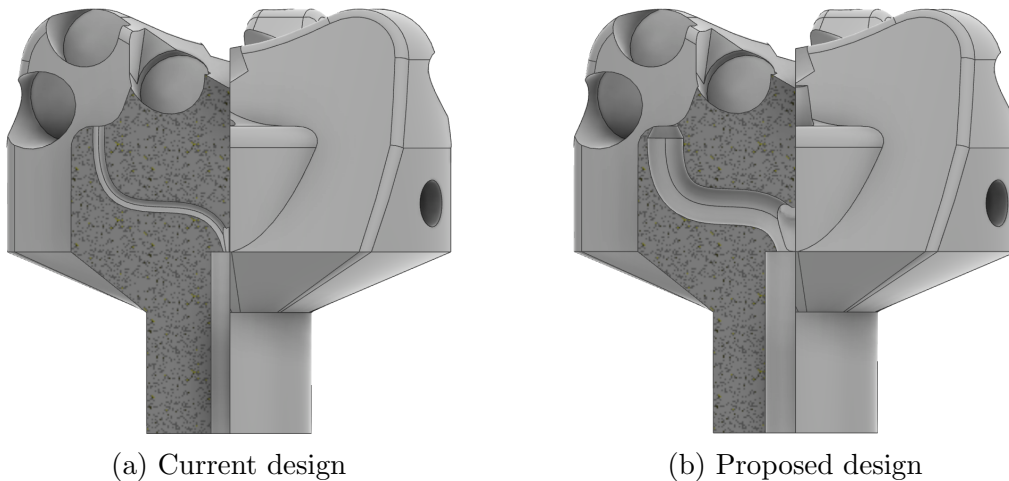
Figure 8.8: Current and proposed nozzle designs.

8.4 Downhole Sensor

Most of the work done on the downhole sensor has been discontinued each year as new designs have been proposed. Changes can be made to the PCB, however the ICM-20948 9-Axis IMU should remain in the design and the well trajectory should be further developed and tested. The code used during testing by this year's team will be uploaded to the UiS Drillbotics GitHub with a readme file with development suggestions.

8.4.1 Printed Circuit Board

A custom flexible PCB was ordered in an attempt to fit the downhole sensor as close to the bit as possible, in an already stacked BHA. The components used and tracing for the current design is presented in Appendix A. Unfortunately, the team was unable to communicate with the IMU on the custom PCB due to unknown issues. Possible explanations are; The IMU needs to be programmed as there is no factory-setting on it or the PCB was damaged during soldering of the various components. As the soldering was done in home office with no access to a heating oven, it is reasonable to believe that the PCB can be damaged.

8.4.2 Sensor Calibration

Factory calibration was deemed sufficient for the accelerometer and gyroscope data used for the IMU. However, the magnetometer needs to be further calibrated in the rig environment to determine the contribution from soft- and hard-iron distortion. Algorithms to dynamically calibrate the sensor should be developed so that the sensor is calibrated before each survey calculation.

8.5 Wiring

Over the years, the electrical components and wires have become a challenge to work with. Reason being that the system has undergone mechanical and electrical upgrades without removing unused components. The number of components in the electrical cabinet is therefore continuously being increased, leaving less space to work with. This makes it complicated to do electric work as some components have to be removed in order to access the faulty component in addition to tracing a thin wire in a cluster of other wires.

Naturally, having a large number of components results in having an even larger number of cables and wires as components usually come with multiple wires. Since there are hundreds of wires inside the electrical cabinet, tracing and troubleshooting are rather time-consuming and challenging. This was experienced several times during this semester as there were multiple errors with the electrical setup and components. A seemingly recurrent incident was grounding issues. The grounding issues experienced caused several of the drivers to get fried. Frying drivers are time-consuming and costly to replaced if it is a recurring incident.

Another observation made during the timeline of this project is that some of the electrical connections are not particularly robust. Some of the electrical connections were observed to have breakage and therefore being loose. Loose connections should be avoided as they can easily disconnect from the component causing a short circuit. Short circuits may cause damage to some components.
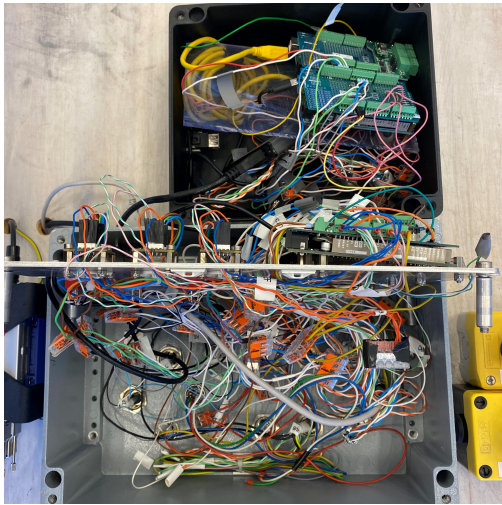
(a) Arduino box   (b) Electric cabinet

Figure 8.9: Cluster of wiring

8.5.1 Remove Unused Components

For future recommendations, it will be beneficial to clean up the electrical cabinet by removing unused components and wires. By removing useless components, one will have more room to work with. Tracing and troubleshooting will also be less complicated due to having a smaller cluster of wires.

8.5.2 Grounding and Short Circuit Issues

To avoid grounding and short circuit issues, a more robust electrical connection should be used for the small electrical components. Some of the connections are self-made rather than off-the-shelf. The self-made connections should be replaced to enhance rigidity.

An updated electrical circuit map should be made such that tracing of wires will be simpler. Having an electrical circuit map gives the advantage of rather following the wire from beginning to end, one can easily see which wire goes where.

8.6 Control System

The control system and machine learning was not the main focus in this year's project scope due to limited time at the laboratories. However, it is important to gather the recommendations and future work from previous years and this section will cover the suggestions to improve the control system of the rig from Løken and Løkkevik [24], and Guggedal and Steinstø. [16].

8.6.1 Control System Improvements

In terms of control algorithms, the suggested practice for a complete closed-loop system is that a database gets developed that contains best practice drilling parameters for the different formation types, so that when a new formation type gets confirmed, the most optimal drilling parameters can immediately get selected. The rig can then make use of various search-algorithms in the reduced state-space (due to previously established most optimal parameters) to identify the point at which the Founder point of the system is found. This point describes the optimal performance point when drilling with optimal conditions related to WOB and RPM. Once the Founder point has been located, for instance by gradient descent method, a series of drilling incident models can be used to not only classify the occurrence of a drilling incident, but also if possible, predict that an incident is imminent (unless measures get taken). Gradient descent method will likely perform significantly better once proper real-time learning rate determination is implemented. While all drilling operations are unlikely to get automated in the near future, in our opinion the first step on the path is to provide the driller with powerful tools to increase safety, operational efficiency and reduce costs. It is therefore our recommendation to build a control system that promotes human-machine integration, where the machine for instance can suggest optimal strategies going forward, and the driller can select one of these or simply override the suggestion. Furthermore, ensuring high quality of data in all steps of the decision making process will increase reliability and ensure consistently high performance. [24]

8.6.2   Machine Learning

The developed approach in 2018-2019 of pre-processing the data, selecting the most optimal features and developing multiple models along with a voting system resulted in reliable results. Future recommendations identified by the team members were:

- Integration of reinforcement learning on the rig, in which the models constantly get improved by correction of the prediction outputs from models,

- developing a larger database containing both different rock formations drilled while varying drilling parameters and a collection of drilling incidents,

- making use of feature dimensionality reduction methods such as principal component analysis, as shown in chapter 6 in order to extract the principal components that explain the variance in the dataset and in order to develop the models,

- develop models and perform principal components analysis based on downhole measurements or surface measurements that accurately describe the bit interaction with the formations.

The models developed by earlier team members should be further tested and implemented by a computer science student.

8.6.3   Toolface Control

No testing was performed to measure and control the toolface of the BHA as the top drive, which would be used to control the toolface, was non-operational during this period. A simple test rig can be built, using one of the spare stepper motors from the whipstock positioning unit. The test rig would simply be a motor, connection to pipe of the same dimensions as the BHA and the downhole sensor attached onto it. A script should be developed for a toolface controller that will orient the downhole sensor in the direction of an external electromagnet. The external electromagnet will create a new local north and the toolface controller should steer towards the new local north. For test drilling, a magnetic ranging setup would have to be installed around the rock sample to control the local north. In order to hit one target the electromagnet can remain stationary at the position required to hit the target, and

if multiple targets need to be hit then the the electromagnet needs to be positioned appropriately.

8.7 Test Drilling

Due to limited time for testing of the laboratory-scale rig, future experiments are suggested in this section. It is recommended to perform these tests prior to making further changes to the drilling rig to develop a better understanding of the system and all its intricacies.

8.7.1 Actuator velocity

The actuator velocity has been a neglected drilling parameter in previous years and set to a default value. During test drilling the parameter was changed in an attempt to stop the WOB measurement from overshooting. Changing this parameter had immediate effect, and a lower actuator velocity than 1 mm/s (the previous default) reduced axial vibrations. Further research should be performed on this drilling parameter and implemented in the closed loop control.

One proposal is to control the actuator velocity instead of actuator distance for the PID controller. In the case of overshooting the WOB setpoint, the system would reduce the actuator velocity instead of moving up and back down, tagging the rock, which creates a lot of vibrations. If initial contact with the rock results in a WOB measurement of 5 kg higher than the setpoint, the actuators would stop and slow down the velocity and the WOB measurement will gradually reduce and stabilize at the setpoint. Drilling at a slightly higher WOB setpoint for a short period of time is less damaging than the vibrations caused by the current method of drilling. This needs to be investigated further as it will have major implications on the performance of the system.

8.7.2 Baker Bit with Inserts

Due to the excessive lateral vibrations and bit walking when drilling with the Baker Hughes bit without the inserts, it would be interesting to perform the same experi-

ment with inserts on the gauge and cone pad. Supposedly, this should improve the stability of the bit, increase ROP and reduce the severity of vibrations. The inserts are shown in Figure 8.10

The bit has provision to let participants adjust the axial and side aggressiveness of the bit before a run by changing the exposure of the blunt tungsten carbide elements on the gauge pads and on the bit face. The elements can be installed at a designed exposure using brazing or a special adhesive to adjust the clearance at the gauge between 0" and 0.150". A tungsten carbide ovoid element will be provided to adjust the depth-of-cut control configuration. The element can be installed on the bit face at a designed exposure using brazing or a special adhesive. [14]
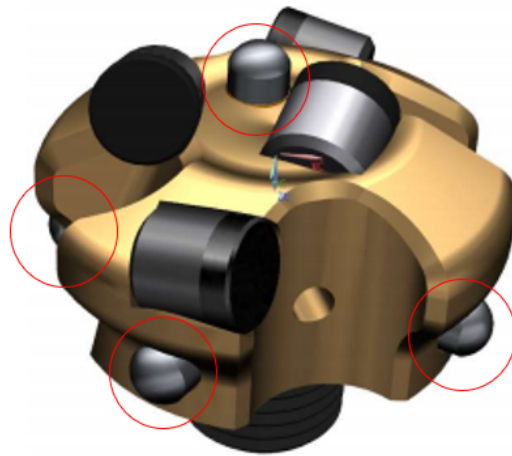
Figure 8.10: Baker Hughes 4-Cutter PDC Bit with inserts.

8.7.3   Optimal Drilling Parameter for PDC bits

The standardized drilling operation performed for the four PDC bits was meant to give the team an indication of which drilling parameters were optimal to achieve the highest ROP. It was assumed (based on previous experience) that the ROP would increase as WOB setpoint increased until the depth of cut would be too deep and the pneumatic motor would stall. The increasing ROP with increasing WOB setpoints can be seen in Figure 6.9, unfortunately the ROP drops before the motor stalls as some of the WOB is lost to friction in the wellbore and accurate WOB measurement cannot be obtained by the load cells, as they are mounted on the top plate.

An experimental setup consisting of either a smaller BHA or a straight bend could be utilized to perform a drilling parameter study. By doing such a study, the PDC bits can be compared to determine which bit performs the best in terms of the drilling speed. A bit female connection (1/4" NPT and M14) to M8x0.75 male connector could be made in the workshop and the bit would be connected directly onto the pneumatic motor. As the pneumatic motor can withstand high axial loads, this simple BHA setup could be used for vertical drilling. The motor sleeve and lower stabilizer could be attached on this setup to help stabilize the bits during the tests.

References

[1] S. K. Arora A. K. Gupta. *Industrial Automation and Robotics; Third Edition.* Laxmi Publications Pvt Ltd, 2007. URL: https://books.google.no/books?id=Y7rgCP7iC18C&sitesec=buy&hl=no&source=gbs_vpt_read.

[2] Mesfin Belayneh Agonafir. "PET 580 Advanced Well and Drilling Engineering". Compendium, University of Stavanger, 2019.

[3] Bjørn A. Brechan et al. *TPG4215 Drilling Engineering, NTNU 2017.*

[4] Chen et al. *A New Theory on Cutter Layout for Improving PDC Bit Performance in Hard and Transit Formation Drilling.* 2013.

[5] Joakim Andrè Alsaker-Haugen. "Design of an Attitude and Heading Reference System for a Laboratory-Scale Drilling Rig". Master Thesis, University of Stavanger, 2020.

[6] Matej Andrejasic. *MEMS Accelerometer.* URL: http://mafija.fmf.uni-lj.si/seminar/files/2007_2008/MEMS_accelerometers-koncna.pdf.

[7] Circuit Basics. *Basics of the I2C Communication Protocol.* URL: https://www.circuitbasics.com/basics-of-the-i2c-communication-protocol/.

[8] Jonatan Kwan-Soo Byman. "Design, Manufacturing, and Optimization of the Drill String Assembly for an Autonomous Miniature Drilling Rig." Bachelor Thesis, University of Stavanger, 2020.

[9] Bodong Li Chinthaka P. Gooneratne and Timothy E. Moellendick. "Downhole Applications of Magnetic Sensors". In: (1989).

[10] Measurement Computing. *USB-1608G Series.* URL: https://www.mccdaq.com/PDFs/specs/USB-1608G-Series-data.pdf.

[11] Gems Sensors & Controls. *Operating & Installation Instructions.* URL: https://docs.rs-online.com/1edd/0900766b80458b63.pdf.

[12] Drillbotics. *Guidelines 2019-2020*. URL: https://drillbotics.com/download/guidelines/2020-Drillbotics-Guidelines.pdf.

[13] FIERCE Electronics. *Compensating for Tilt, Hard-Iron, and Soft-Iron Effects.* URL: https://www.fierceelectronics.com/components/compensating-for-tilt-hard-iron-and-soft-iron-effects.

[14] Kenneth Evans. *PDC Micro-bit for the 2020 SPE Drillbotics Competition.* URL: https://drillbotics.com/download/guidelines/2020-Drillbotics-Microbits-Baker-Hughes.pdf.

[15] Are Funderud. "Presentation: Bit design". Lyng Drilling, a Schlumberger Company. 2020.

[16] Carsten B. Guggedal and Magnus Steinstø. "Control System Architecture and API integration". University of Stavanger, 2019.

[17] HBM. *QuantumX MX840B Data Acquisition Module.* URL: https://www.hbm.com/en/2129/quantumx-mx840b-8-channel-universal-amplifier/.

[18] HBM. *U9C Load Cells.* URL: https://www.hbm.com/en/3926/u9c-miniature-force-sensor-for-tensile-and-compressive-forces/#f34078s.

[19] F.V DeLucia (Smith Intl. Inc. "Benefits, Limitations, and Applicability of Steerable System Drilling". In: *Society of Petroleum Engineers* (1989).

[20] Baker Hughes INTEQ. *Drilling Engineering Workbook.* Baker Hughes INTEQ, 1995.

[21] TDK InvenSense. *ICM-20948 9-Axis MEMS MotionTracking Device.* URL: https://invensense.tdk.com/wp-content/uploads/2016/06/DS-000189-ICM-20948-v1.3.pdf.

[22] Magomed Khadisov. "Directional Drilling: Trajectory design and position uncertainty study for a laboratory drilling rig." University of Stavanger, 2020.

[23] Alexander Trulsen & Erik Andreas Løken. "Construction, Design and Optimization of an Autonomous Laboratory-Scale Drilling Rig". Bachelor Thesis, University of Stavanger, 2017.

[24] Erik Andreas Løken and Jens Løkkevik. "Optimization of an Intelligent Autonomous Drilling Rig". Master Thesis, University of Stavanger, 2019.

[25] MechanicalCalc. *Column Buckling.* URL: https://mechanicalc.com/reference/column-buckling.

[26]   Robert F. Mitchell. *Petroleum Engineering Handbook, Volume 2 - Drilling Engineering.* Society of Petroleum Engineers, 2007. URL: `https://store.spe.org/Petroleum-Engineering-Handbook-Volume-II-Drilling-Engineering-P59.aspx`.

[27]   Mads Bertheussen Nåmdal. "Design and implementation of instrumentation and control system for an autonomous miniature drilling rig." Master Thesis, NTNU, 2019.

[28]   Anuroop Pandey. "Investigation of geosteering in non-trivial geological settings." Master Thesis, Missouri S&T, 2012.

[29]   PetroWiki. *PDC Bits Design.* URL: `https://petrowiki.org/PDC_bit_profile`.

[30]   PetroWiki. *PDC Bits Profiles.* URL: `https://petrowiki.org/PDC_bit_profile`.

[31]   PetroWiki. *PDC Drill Bits.* URL: `https://petrowiki.org/PDC_drill_bits`.

[32]   2000 Schaaf et al. *Application of Point the bit Rotary Steerable System in Directional Drilling Prototype Wellbore Profiles.* URL: `https://www.onepetro.org/conference-paper/SPE-62519-MS`.

[33]   Bürkert Fluid Control Systems. *2-Way Solenoid Control Valve.* URL: `https://docs.rs-online.com/6b20/0900766b81552f54.pdf`.

[34]   Electronics Tutorials. *Hall Effect Sensor and How Magnets Make It Work.* URL: `https://www.electronics-tutorials.ws/electromagnetism/hall-effect.html`.

[35]   Electrical 4 U. *Control System Definition.* URL: `https://www.electrical4u.com/control-system-closed-loop-open-loop-control-system/`.

[36]   Boston University. *Mechanics of Materials: Stress Transformation.* URL: `http://www.bu.edu/moss/mechanics-of-materials-stress-transformation/`.

Appendix A

Technical Drawings

A.1   PDC Drill Bit
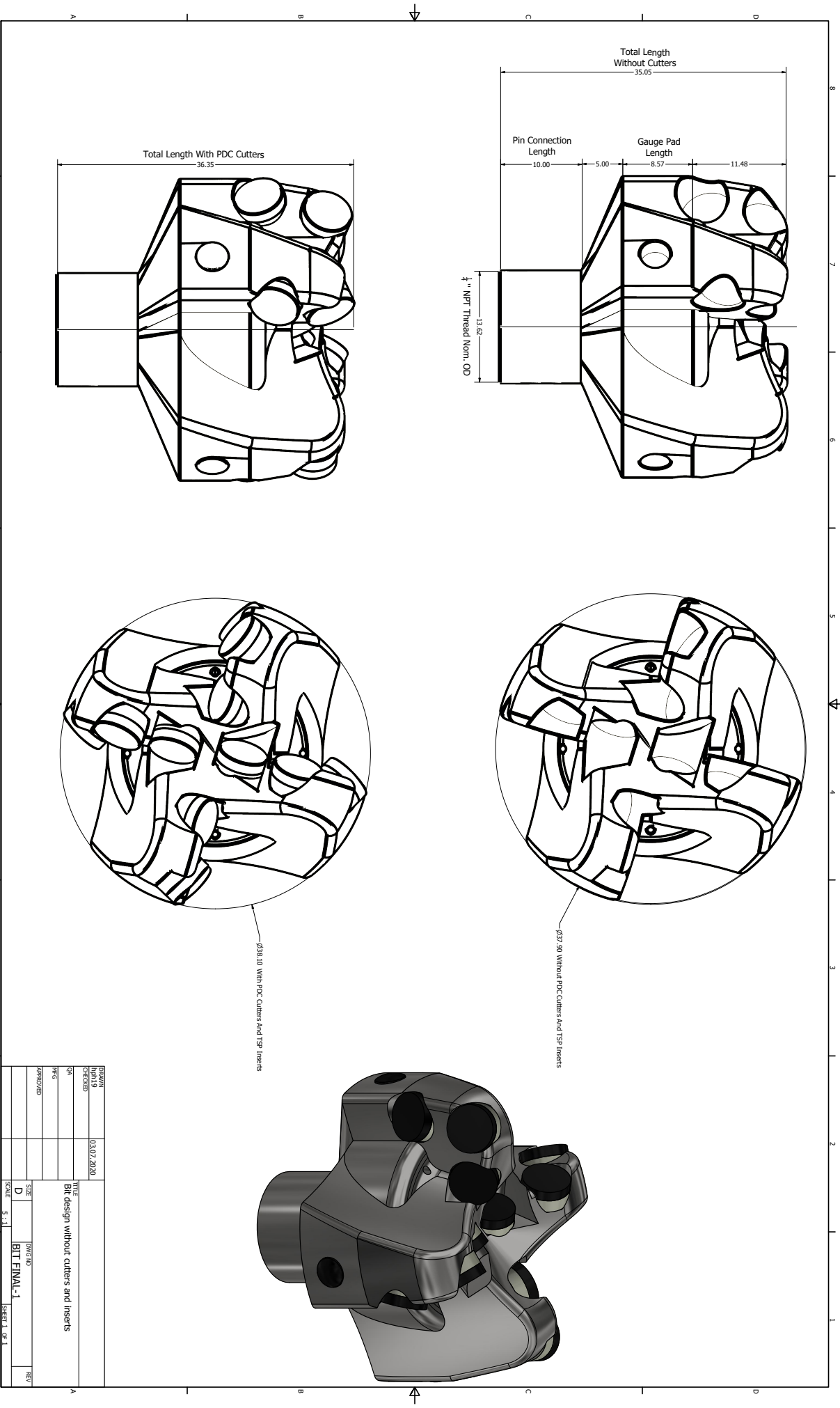
Total Length With PDC Cutters
36.35

Total Length
Without Cutters
35.05

Pin Connection
Length
10.00

5.00

Gauge Pad
Length
8.57

11.48

¼" NPT Thread Nom. OD

13.62

Ø38.10 With PDC Cutters And TSP Inserts

Ø37.90 Without PDC Cutters And TSP Inserts

TABLE

Sequence Number	Blade	Cutter	Back-rake	Side-rake
1	1	1	20	15
2	1	2	20	15
3	1	3	30	15
4	2	1	20	15
5	2	2	25	15
6	2	3	30	15
7	3	1	20	15
8	3	2	20	15
9	3	3	30	15
10	4	1	20	15
11	4	2	25	15
12	4	3	30	15

Four
(4)
side
cutters

Scale 10:1 [mm]

DRAWN andjak
CHECKED
QA
MFG
APPROVED

05.03.2020

SIZE D
DWG NO Cutter_overview
SHEET 1 OF 1
REV
TITLE
SCALE

Blade 1
Blade 2
Blade 3
Blade 4

Appendix B

3D Printing Material

17-4 PH Stainless Steel

Markforged

Composition

Composition	Amount
Chromium	15-17.5%
Nickel	3-5%
Copper	3-5%
Silicon	1% max
Manganese	1% max
Niobium	0.15-0.45%
Carbon	0.07% max
Phosphorous	0.04% max
Sulfur	0.03% max
Iron	bal
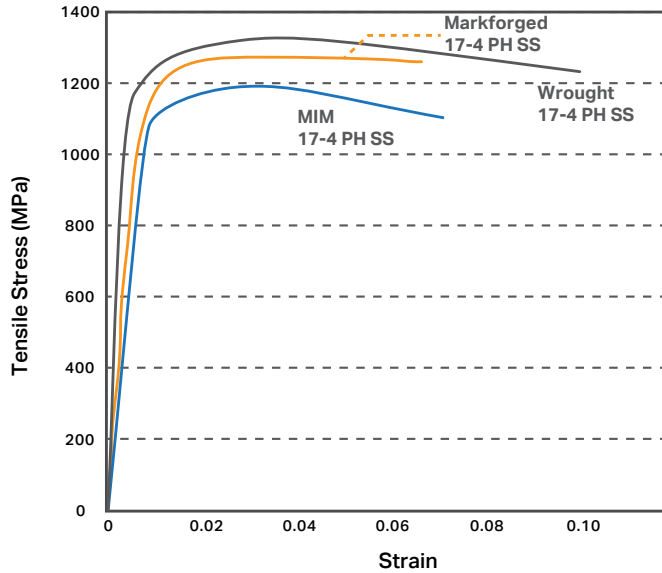
● Markforged H900 Heat Treated

17-4 PH stainless steel processed with the Markforged Metal X system heat treated to H900 specification.

● MIM H900 Heat Treated

17-4 PH MIM standard stainless steel heat treated to H900 specification.

● ASTM A564 H900 Heat Treated

ASTM A564 17-4 PH stainless steel heat treated to H900 specification.

Typical Mechanical Properties
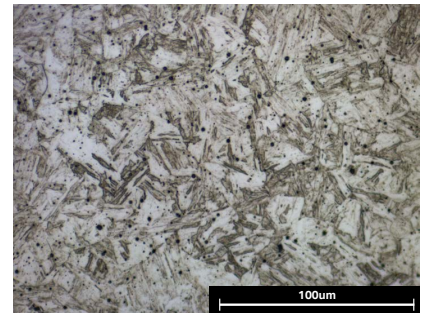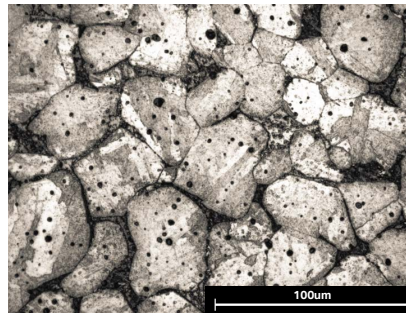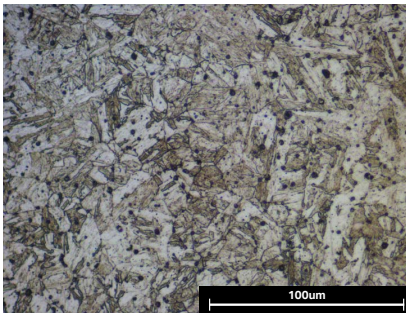
Typical Mechanical Properties	Standard	Markforged H900	MIM H900	ASTM A564 H900
Ultimate Tensile Strength	ASTM E8	1250 MPa	1190 MPa	1310 MPa
0.2% Yield Strength	ASTM E8	1100 MPa	1090 MPa	1170 MPa
Elongation at Break	ASTM E8	6%	6%	10%
Tensile Modulus	ASTM E8	170 GPa	190 GPa	190 GPa
Hardness	ASTM E18	36 HRC	33 HRC	40 HRC
Corrosion	ASTM F1089	Pass	Pass	Pass
Relative Density	—	≥ 96%	95.5%	100%

All data and graphs on front page reflect values of H900 heat treated 17-4 PH SS. Markforged represent typical tested values values, while MIM H900 and Wrought H900 represent typical reference values from MPIF Standard 35. For values of Markforged printed 17-4 PH SS as-sintered and with H1150 heat treatment, please see the reverse side. All composition and "As-Sintered" data verified by a third party test facility. All microstructure images etched and photographed at Markforged.

Appendix C

Downhole Tool

C.1 PCB Footprint
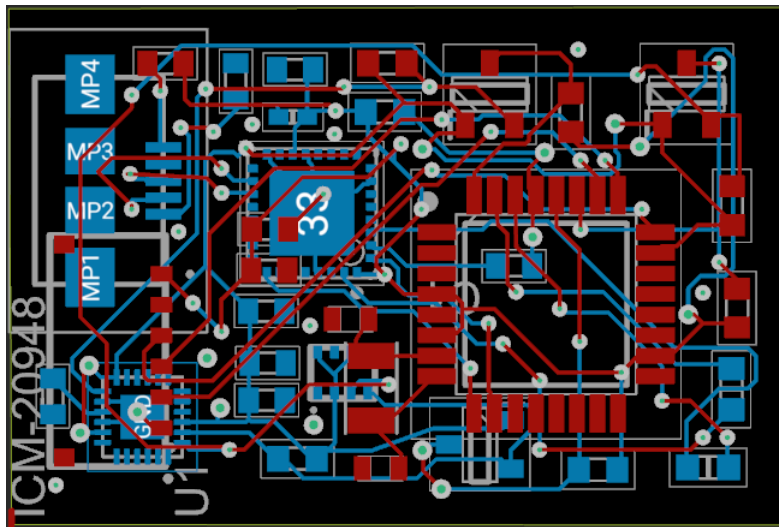
Figure C.1: Printed Circuit Board footprint with component placement and tracing.

C.2 PCB Schematic
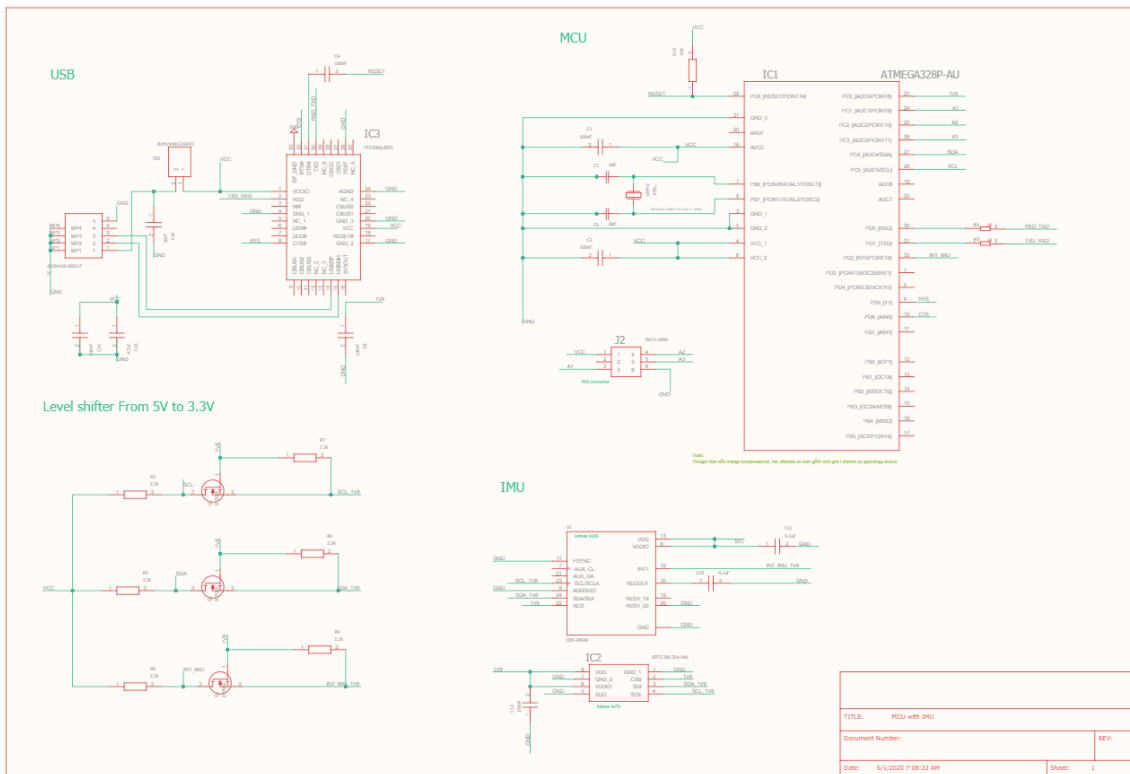
Figure C.2: PCB Schematics of MCU with IMU

C.3   PCB Component Overview

Designator:	Product Name:	Description:
IC1	ATMEGA328P-AU	Microcontroller Unit
IC2	0273.300.354-1NV	Gauge Pressure Sensor
IC3	FT232RQ-REEL	USB to serial UART interface
U1	ICM-20948	9-axis MotionTracking device
XTAL	NX2520SA	16MHz Crystal OScillator
FB1	BLM15HB121SN1D	120Ω Ferrite Bead
C1, C2, C4, C8, C13, C14	C0603C104K4RACTU	100nF Capacitor
C3, C6	CGA1A2C0G1E060D030BA	6pF Capacitor
C10, C11	XXX	0.1uF Capacitor
C15	C0603C475K8PACTU	4.7uF Capacitor
C16	C0603C103J3GACTU	10nF Capacitor
J1	10104110-0001LF	2.0 Micro USB Connector
J2	78171-5006	Vertical PCB Header
Q1, Q2, Q3	2N7002	ON Semiconductor
R1, R2	CRCW06031K00FKEAHP	$1K\Omega$ Power Resistor
R3, R5, R6 R7, R8, R9	CRCW060310K0FKEAHP	$2.2K\Omega$ Power Resistor
R10	CRCW060310K0FKEAHP	$10K\Omega$ Power Resistor

Table C.1: PCB Components and specifications

Appendix D

Finite Element Method

D.1   Bottom Hole Assembly
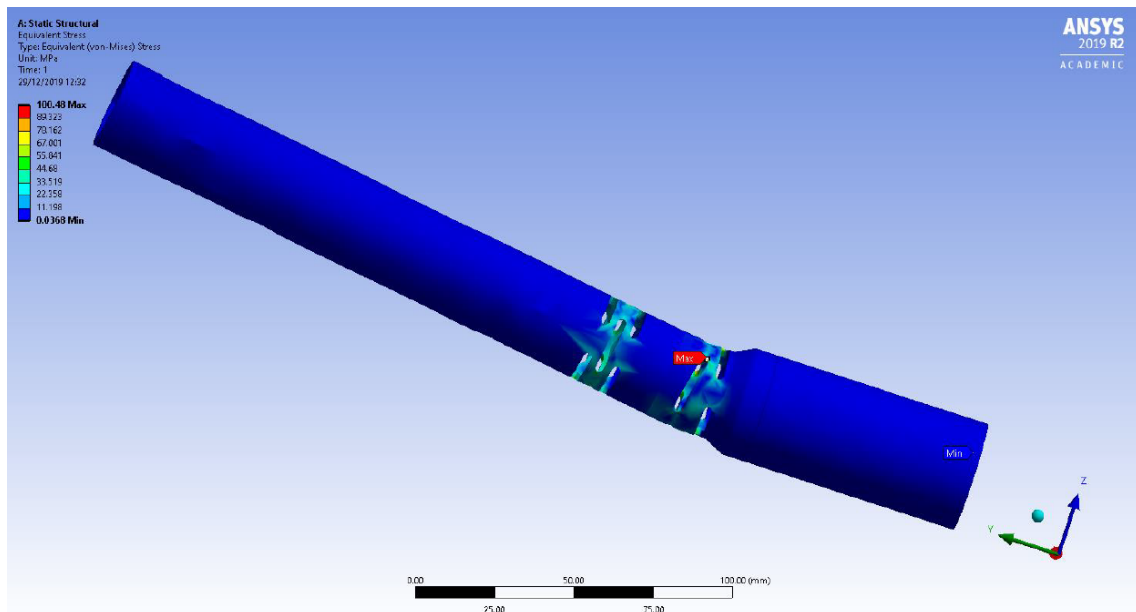
Figure D.1: The preliminary finite element analysis (FEA) (Von Mises). The loading on the Y-axis is set to 500 N, the bottom of the XZ plane is fixed and for the cylindrical support, only radial is set to fixed.

D.2 PDC Drill Bit
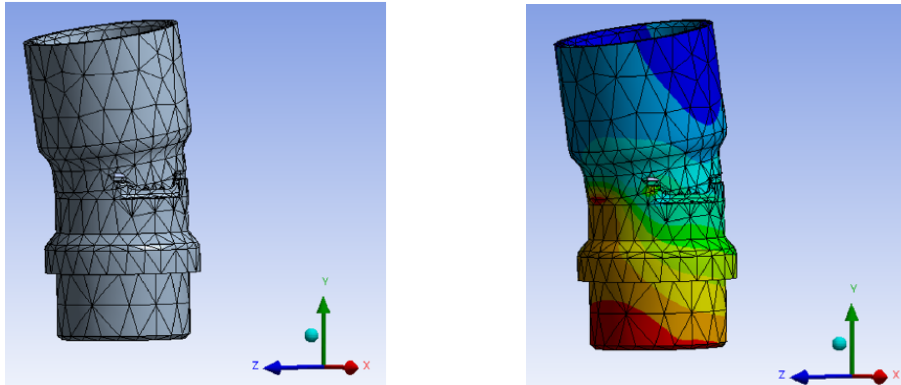
(a) CAD of the bend sleeve with mesh.

(b) Resulted stress distribution, from red to blue area (high to low stress distribution)

Figure D.2: The bend before and after solving the FEM equations

Appendix E

Drillbotics 2019-2020 Guidelines
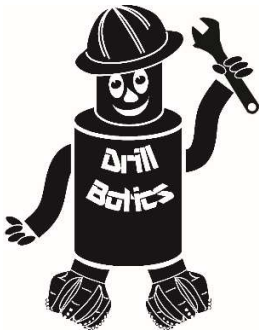
Society of Petroleum Engineers
Drilling Systems Automation
Technical Section (DSATS)
International University Competition
2019 – 2020
Drillbotics™ Guidelines
Revised 18 February 2020

1. Introduction

This year marks the sixth competition for the title of Drillbotics® champion and a chance for students to learn about the drilling process from industry experts and for winning team(s) to travel and present a paper at the next SPE/IADC Drilling Conference and at an event organized by DSATS. The past years involved undergraduates, masters and doctoral students from a variety of disciplines who built innovative drilling machines and downhole tools while developing a deeper understanding of automating the drilling process. The university teams freely share lessons learned, which more rapidly advances the science of drilling automation. Everyone involved claims to have had a lot of fun while learning things that are not in the textbooks or published papers. Students also participated in related events at conferences, workshop meetings and networking with industry leaders in drilling automation. This year's contest promises to be just as challenging and hopefully as much fun.

A new addition to this years' competition is an additional challenge that is focused on drilling system modeling and controls. Students will be able to choose from two challenge groups (Group A and Group B). The challenge Statements for the two groups are:

- Group A: Design and build a miniature drilling rig and autonomously drill a directional well through a homogeneous rock sample to a given plan
- Group B: Design, model, and simulate controls for a miniature directional drilling rig and demonstrate on a virtual drilling system.

How did the competition first come about? The origins began in 2008 when a number of SPE members established the Drilling Systems Automation Technical Section (DSATS) help accelerate the uptake of automation in the drilling industry. DSATS' goal was to link the surface machines with downhole machines, tools and measurements in drilling systems automation (DSA), thereby improving drilling safety and efficiency. Later, at an SPE Forum in Paris, the idea of a student competition began to take shape. A DSATS sub-committee was formed to further develop the competition format and guidelines. Several universities were polled to find out the ability of academic institutions to create and manage multi-disciplinary teams. The Drillbotics® committee began small in 2014-2015 to see if the format could succeed. With fine tuning, we continue along those lines as we start the 2020 process.

Version	Date	Section	Description
2020.01	20 September 2019	All	Update date/location references for 2020 competition. Update challenge guidelines for 2020 competition (drill bit size, drill pipe specs, directional challenge)
2020.02	18 February 2020	9	Added Group B evaluation criteria; judges list

Group A Competition:

The 2020 Group A Competition has a few changes worth highlighting here:

- During previous competitions, the main focus was autonomously dealing with drillstring mechanics. The 2019 challenge introduced a directional drilling component which required teams to attempt to deviate from well center as far as possible in a single given direction. The 2020 challenge will build on the directional drilling element by requiring teams to drill a wellbore to hit multiple targets at varying vertical depths and X/Y coordinates.

- Closed loop control of the rig based on downhole data is mandatory in this year's competition, not integrating this data set into the control algorithm is considered a "F - Failing grade" in this year's competition.

- The drill bit will be increased in diameter from last year's competitions to 1.5". Details will be provided via a post to the Drillbotics® blog once the design is complete.

- DSATS will not be providing tubing to the competition teams, however stainless steel tubing is permitted to be used by the teams.

- First time participating teams can choose to compete in Category II Competition, which would use the prior year's rules/guidelines and will not be competing for the Group A grand prize(s).

- Teams also have the option of competing in the Group B challenge, which is a control systems and modelling challenge. Please refer to the Group B challenge guidelines document posted on the Drillbotics® website for more information.

- To attain a higher rating by the judges, the Phase I report should include a summary paragraph or table in the design report containing details of the control algorithm proposed. See section 3.4. This should be updated for the Phase II presentation to judges at the on-site test.

- The 2020 design should allow for third-party plug and play interface. See section 3.15.5. This is optional for 2020, but it will likely be mandatory in 2021.

Group B Competition:
- The newly added Group B challenge requires teams to develop a drilling system model and corresponding control scheme to virtually drill a directional well to a given plan. The Group B challenge does not involve building a rig or drilling system.
- The teams will design automation and control similar to Group A, but will develop a virtual drilling system (i.e. computer models) to test and demonstrate the controls. Therefore, in addition to the guidelines specified below, Group A Competition Guidelines section in general, and applicable guidelines from Group A, Phase 1 in particular, should be referred. While the teams will have to meet minimum competition requirements, any "above and beyond" work along the main theme will be rewarded additional points to encourage creativity and innovation.

The DSATS technical section believes that this challenge benefits students in several ways. Petroleum, mechanical, electrical and control engineers gain hands-on experience in each person's area of expertise that forms a solid foundation for post-graduate careers. They also develop experience working in multi-disciplinary teams, which is so important in today's technology driven industries. Winning teams must possess a variety of skills. The mechanical and electrical engineers need to build a stable, reliable and functional drilling rig. Control engineers need to architect a system for real-time control, including selection of sensors, data handling and fast-acting control algorithms. The petroleum engineers need an understanding of drilling dysfunctions and mitigation techniques. Everyone must work collectively to establish system functional requirements understood by each team member, properly model the drilling issues, and then to create a complete package working seamlessly together.

The oil and gas industry today seeks lower costs through efficiency and innovation. Many of the student competitors may discover innovative tools and control processes that will assist drillers to speed the time to drill and complete a well. This includes more than faster ROP, such as problem avoidance for dysfunctions like excessive vibrations, stuck pipe, and wellbore stability issues. Student teams built new downhole tools using 3D printing techniques of designs that would be difficult, if not impossible to machine. They used creative hoisting and lowering systems. Teams modeled drilling performance in particular formations and adjusted the drilling parameters accordingly for changing downhole conditions. While they have a lot to learn yet about our business, we have a lot to learn about their fresh approach to today's problems. Good Luck!

DSATS Drillbotics® Committee

Shashi Talya (Chair)	George Michalopulos	Mathew Forshaw
Fred Florence (Co-Chair)	Jana Hochard	Mike Attrell
Aaron Logan (Co-Chair)	Jayesh Jain	Mohamed Ali Ibrahim Hassan
Alex Ngan	Jan Jette Blange	Steven Estvold
Dmitriy Dashevskiy	John Macpherson	Umut Zalluhoglu
Duane Cuku	Kenneth Evans	Victor Soriano
Daan Veeningen	Marco Perez	Vimlesh Bavadiya
	Mark Hutchinson	

WPTS

Jonathan D Lightfoot
David Gutierrez

DUPTS

Salem H Gharbi (Chair)
Jon Curtis
Bader Otaibi
Salaheldin Elkatatny
Vikrant Lakhanpal

Contents

Objectives for the 2020 Competition

1.1. During the school year beginning in the fall of 2019, a team of students will organize themselves to solve a drilling related problem outlined in item 3 below. The team should preferably be a multi-disciplinary team that will bring unique skills to the group to allow them to design and construct hardware and software to demonstrate that they understand the underlying physics, the drilling issues and the usual means to mitigate the issues. We cannot stress enough the need to involve students with different technical training and backgrounds. They will need to develop skills to understand drilling dysfunctions and mitigation strategies, but they must also have the mechanical engineering capabilities to design the rig/drilling package. In past years, some entrants have not adequately considered the control network and algorithms needed for autonomous drilling. They have often misunderstood the need for calibrated sensors and fast, accurate data handling. All of this and more is needed to build and operate a complete automated drilling system.

1.2. The students could produce novel ideas leading to new drilling models, improved drilling machines and sensors, and the ability to integrate the data, models and machines that will hopefully create new, more efficient ways to drill wells in the future. Any such innovation will belong to the students and their university in accordance with the university's written policies. DSATS and SPE waive any claims to students' intellectual property.

1.3. The students, working as a multi-disciplinary team, will gain hands-on experience that will be directly applicable to a career in the upstream drilling industry.

2. Background

2.1. What is DSATS?

2.1.1. DSATS is a technical section of the Society of Petroleum Engineers (SPE) organized to promote the adoption of automation techniques using surface and downhole machines and instrumentation to improve the safety and efficiency of the drilling process. More information is available about DSATS at the DSATS homepage (http://connect.spe.org/DSATS/Home/).

2.1.2. The Drillbotics® website at www.Drillbotics.com includes official updates to the competition guidelines and schedule, as well as FAQs, photos, and previous entrants' submittals and reports. Any updates to the guidelines posted on the Drillbotics® website via blog entries from the Committee is considered to be an official revision to these Guidelines. Questions and suggestions can be posted there, or teams can email the sub-committee at 2020@Drillbotics.com.

2.2. Why an international competition?

2.2.1. DSATS, as part of the SPE, is a group of volunteers from many nations, connected by their belief that drilling automation will have a long-term, positive influence on the drilling industry. This diversity helped to shape the direction of the organization. The group feels that the industry needs to attract young professionals from all cultures and disciplines to advance drilling practices in all areas of the world. The winners of the Group A (Category I) competition will receive a grant for economy class transportation and accommodations to attend the next SPE Drilling Conference and will present an SPE paper that will be added to the SPE archives of One Petro[1]. Winners of Group B will publicly receive recognition of their achievement, and have the opportunity to publish an SPE paper that will be added to the SPE archives of One Petro. DSATS believes recognition at one of the industry's leading technical conferences will help encourage student participation. Also, the practical experience with drilling automation systems increases the students' visibility to the companies that are leading automation activities.

3. *Group A Competition Guidelines*

3.1. Problem statement for the 2019-2020 competition:

Design a rig and related equipment to autonomously drill a well, using downhole sensors, that is able to hit multiple directional targets, as quickly as possible while maintaining borehole quality and integrity of the drilling rig and drillstring.

3.2. 2019-2020 High Level Challenge and Judging Changes

3.2.1. The competition will take place on the same day for all teams in North America, and the same day (likely different from the North American date) for all teams in Europe. (see 3.1.6, 3.5 and 7.0)

3.2.2. Directional steering is a more critical part of the competition for 2020. (see 3.5) The wellbore must be started vertically and then kicked off below a specified depth to hit multiple directional targets (at varying X/Y coordinates and vertical depths). Teams score more points based on how accurately each directional target is hit (see Appendix "A" for scoring details)

3.2.3. Downhole sensors are mandatory, and it is also mandatory to implement their data into the control algorithm of the rig. A severe penalty will be applied to teams who do not use downhole sensors. Closed loop control of the rig based on downhole data is mandatory in this year's

---

[1] Publication is subject to the SPE program committee's acceptance of the abstract/paper. If the abstract is not accepted, DSATS will solicit other SPE events try to get the paper into OnePetro.

competition and not integrating this data set into the control algorithm is considered a "F- Failing grade" in this year's competition.

3.2.4. A homogeneous sandstone Rock Sample will be provided by Drillbotics® at the test sites. (see 3.6)

3.2.5. DSATS to provide a new bit with 1.5" diameter and 2" length. Students are permitted to use their own drillbit for the 2020 competition. (see 3.7)

3.2.6. Groups A&B

3.2.6.1. All returning teams must enter Category I, and are judged according to these guidelines. First time entrants may join Category I or Category II. Category II competitors will be judged by the previous year's guidelines (2018-2019), and will not be competing to receive the Group A grand prize(s).

3.2.6.2. Prizes are described in sections 9 and 10 below.

3.2.6.2.1. The "big prize" will be awarded to the winner of challenge Group A (Category I): an SPE Whitepaper published in OnePetro, economy class transportation and accommodations to attend and present at the next SPE Drilling Conference, with their rig presented at the drilling conference, subject to conference guidelines

3.2.6.2.2. The winning Group B team will have an opportunity to present and publish a SPE Whitepaper, subject to the conference guidelines, and they will also receive recognition of the accomplishment at the conference

3.2.7. Additional information regarding the judging of the competition is detailed in section 3.16.

3.3. Two Project Phases

Fall Semester 2019

The first phase of the project is to organize a team to design an automatic drilling machine to solve the project problem. It is not necessary to build any equipment in this phase, but it is okay to do so. Design considerations should include current industry practices and the team should evaluate the advantages and shortcomings of today's devices. The design effort may be assisted by university faculty, but the students are encouraged to introduce novel designs for consideration. The design should also include consideration for downhole sensor and the control system to automatically control the drilling process. The level of student, faculty and technical staff involvement shall be reported when submitting the design. For returning teams, the Phase I Design should include an analysis of data and learnings from previous ("offset") wells drilled.

Spring Semester 2020

During the second phase, the finalist teams selected by DSATS proceed to the construction and drilling operation will use the previous semester's design to build an automated drilling machine. As per industry practices, it is common during construction and initial operations to run into problems that require a re-design. The team may change the design as needed in order to solve the problem subject to section 4.3.4. Teams may use all or part of a previous year's rig.

See section 7 for detailed timeline information.

3.4. Phase I – Design Competition

Design an automated drilling machine in accordance with the rules below.

3.4.1. DSATS envisions a small (perhaps 2 meters high) drilling machine that can physically imitate the functionality of full-scale rig machinery. (Since the winning machines will be presented at the SPE conference, there may be height restrictions imposed by the conference facility, so machines that are too tall may not be allowed on the exhibit floor.) The machine will be the property of the university and can be used in future research and competitions. New and novel approaches that improve on existing industry designs are preferred. While innovative designs are welcome, they should have a practical application to drilling for oil and gas.

3.4.2. The drilling machine will use electrical power from the local grid not to exceed 25 horsepower. Lower power consumption resulting from energy efficient designs will receive additional consideration.

3.4.3. The design must provide an accurate and continuous measurement of Weight-On-Bit (WOB), inclination, azimuth, and depth; as well as other drilling parameters (see Appendix "A" for directional surveying-specific data requirements), that should be presented as a digital record across the period of the test. All depth related measurements shall use the rig floor as the datum, not the top of the rock (the offset between the rock surface and the rig floor must be adequately processed within the control algorithms). Appropriate statistical measurements should be made at frequencies and with an accuracy and appropriate frequency content for the

dynamics of the drilling system both at surface and downhole. Discussion of such choices should be included in the design report.

    3.4.3.1.   Distinguish in all data and documentation the difference between Weight-On-Bit and Hookload; be specific when referring to these parameters

3.4.4. The proposed design must be offered in Phase I of the project, but changes are allowed in Phase II, as long as they are reported to the Committee via students' monthly reports. A summary of all significant changes, including the reason modifications were necessary, must be included in the students' final report.

3.4.5. Design submittal by the students shall include:

    3.4.5.1.   Engineering drawings of the rig concept, mechanical and electrical and auxiliary systems, if any

    3.4.5.2.   Design notes and calculations

        3.4.5.2.1.   All engineering calculations shall be included in the Phase I report, even if the rig is built using previous years' designs. This ensures that the 2020 team reviewed and understood the previous design assumptions and calculations.

Calculations should include each formula considered in the design, a reference that shows the origins of the formula, why is was chosen, what engineering assumptions were made, a definition of all variables and the values used in the calculation.

    Example

Buckling limit   Euler's Equation   (1) cite a reference here or in the reference section of your design report

The critical buckling load, bcr, is calculated:

$$Pbcr = \pi 2 * E * I / (K * L)^2$$

$Pbcr$:   Critical buckling load

E: Modulus elasticity of the aluminum drill pipe

I: Area moment of inertia

L: Length of the column

K: Column effective length factor (explain how you chose the appropriate k or n factor)

3.4.5.2.2. The report should include a table that summarizes ALL calculations.

Example

Calculations	Formula	Reference	Results
Moment of Inertia	$I = \pi/64\,(dp\,4 - idp\,4)$	Thin wall approx. or ID/OD calc separately or other? List your reference	$0.000546\,in4$
Buckling Limit	$Pbcr = \pi 2 * E * I /(K * L)^2$	Euler's Eq	$18.9\,kg$

3.4.5.3. Control system architecture. (The response time of measurements, data aggregation and control algorithms should be estimated.)

3.4.5.4. Key features for any models and control software.

3.4.5.5. Proposed data handling and display.

3.4.5.6. Specification for sensors, signal processing and instrumentation, (verifying their accuracy, precision, frequency response and environmental stability), including the methods planned for calibration before and after the Phase II testing.

3.4.5.7. Plan for instrumentation of sensors in the BHA, as well as a method to synchronize all measurements and utilize both the surface and downhole sensors for real-time control of the drilling process.

3.4.5.8. An explanation of the implementation of the output of the BHA sensors to improve the trajectory of the wellbore, drilling efficiency and other drilling concerns.

3.4.5.9. An explanation of the algorithm used to autonomously control the drilling rig based on the output of the BHA sensors

3.4.5.10. An explanation of the principles being applied to directionally steer the wellbore and hit the required targets (see Appendix "A") with the intent to score the maximum amount of points

3.4.5.11. Cost estimate and funding plan

3.4.5.12. A design summary video used to outline the design submittal not to exceed five (5) minutes in length. Videos shall be the property of the university, but DSATS shall have the rights to use the videos on its websites and in its meetings or events.

3.4.5.13. All design, construction and operation of the project are subject to the terms and conditions of section 11.

3.4.5.14. A safety case shall be part of the Phase I design (see Appendix B). Include a review of potential hazards during the planned construction and operation of the rig, and for the unloading and handling of any rock samples or other heavy items. An example of a safety case will be posted on the Drillbotics.com website.

3.4.5.15. The Phase 1 design report should include a discussion regarding the major design features proposed (mechanical and otherwise) - are they scalable to today's working rigs? If not, what would be needed to allow implementation?

3.4.5.16. The Phase 1 design report should include a discussion regarding the control scheme and algorithm - How is each individual measurement used in the control code? Are they all given equal weight, and if not, what criteria is used to assign importance? What is the expected response time of the control system's key components? How will this affect equipment selection? The teams are encouraged to perform control simulations to verify the control scheme.

3.4.6. A committee of DSATS members (the Committee) will review the Phase I designs and select the top five (5) teams[2] who will progress to Phase II of the competition.

3.4.7. DSATS shall also award a certificate of recognition and publication on its website for the most innovative design. The design video will also be shown at the DSATS automation symposium at SPE conferences.

3.4.8. DSATS will not fund any equipment, tools, software or other material, including labor, for the construction of the rig. Student teams are encouraged to find external funding from industry participants and suppliers.

---

[2] The number of finalists could be increased or decreased by the DSATS Board of Directors subject to available funding.

3.5. Phase II – Drilling Competition

3.5.1. In the spring term of 2020, qualifying teams will build the rig and use it to drill rock samples provided by DSATS. Drilling a well, deviated to hit the required targets (see Appendix "A"), efficiently though the sample while controlling drilling dysfunctions is the primary technical objective of the competition. Scoring of the directional drilling component will be primarily based on the horizontal distance from the target coordinate at which each target vertical depth was intersected. The use of both surface and downhole measurements to control the drilling process in real-time is mandatory, failure to do so will result in a failing grade. To avoid disqualification due to a downhole sensor failure, redundant or immediately replaceable items should be part of the design and implementation. Time to replace a sensor will be added to the drilling time for calculation of ROP.

3.5.2. The teams are to use manual control to pre-drill a vertical pilot hole not more than 1" deep measured from the rock's top face. This hole is to be drilled using the competition drilling rig. Location of this pilot hole will be marked on each sample by the committee at the intersection of two lines drawn from opposite corners of the rock sample.

3.5.3. Teams may use glue or use a mechanical fastener to attach a bell nipple or diverter housing to the top of the rock to allow connection of a flowline for return mud flow. The maximum allowable length of the bell nipple is 8 inches. If you use a fastener, be careful not to break the rock.

3.5.4. When the competition drilling begins, teams competing in Category I & II will be required to continue to drill the pilot hole vertically to the kick off point. The kick off point may be at any depth greater than 4" below the surface of the rock.

3.5.5. Navigation shall be done autonomously

    3.5.5.1. Manual intervention to add and/or remove a steering mechanism (e.g. whipstock) is permitted, however the determination/calculation of the orientation setting of the mechanism is required to be autonomous and must be shown on the rig floor display during each steering mechanism manipulation activity

3.5.6. No lateral forces are allowed to be applied above the rocks top face

3.5.7. No forces are allowed to be applied external to the rock that will force the drillbit in a particular direction

3.5.8. External magnetic field effects from the drilling rigs will be present on the directional sensors used to drill the wellbore. The industry has accepted practice of magnetic ranging, this may be a technique worth investigating to improve the signal to noise of magnetic measurements

3.5.9. Once drilling commences, the test will continue until the drillbit exits the rock sample, or three (3) hours, whichever comes first

3.5.10. Drilling performance will be observed and measured by Drillbotics® judges invited to attend and witness the test.

3.5.11. DSATS will judge the competitors primarily on their ability to hit the required targets as accurately (i.e. as close to target center at the given target vertical depth) as possible (see Appendix "A" for details)

3.5.12. DSATS will run a flexible "casing" into the wellbore, and use this to gauge the borehole quality

    3.5.12.1. Casing will be nearly equal in diameter to the 1.5" drillbit

    3.5.12.2. An over gauge, and under gauge Casing will also be used as a no-go measurement

3.5.13. The final test will be scheduled late in the school year or soon after graduation. The test will occur at two locations, so teams must allow time to ship their rig from their university in accordance with the timeline per section 7 below.

3.6. Rock Samples

3.6.1. DSATS will prepare a set of nearly identical homogeneous sandstone samples appx. 12"W x 24"L x 24"H (30 x 60 x 60 cm) that will be shipped to each test site. It will not be sent to the schools. A smaller sample could be provided (no smaller than 12"W x 12"L x 24"H), which will be announced not later than March 1st.

3.6.2. The rock sample will be homogeneous sandstone, and rock compressive strength values will be provided for the sandstone samples furnished by DSATS. The Drillbotics® committee will mark the surface of rock to indicate the well center where drilling will start. It will be located at the intersection of two lines drawn from opposite corners of the rock sample.

3.6.3. The university and/or students may acquire or produce at their own cost rock samples as needed to verify the design and allow students to practice using their machine prior to the test. Drilling of the samples provided by DSATS prior to Phase II testing is not allowed and could lead to disqualification, except for the pilot hole to be drilled at the test location.

3.6.4. The sandstone sample will be oriented during drilling so that it rests on a 12"x24" face so that the drilled depth will be 24".

3.7. Bits

3.7.1. Upon request, DSATS will send a bit to the finalist teams for use in Phase II. It is expected that the BHA and pipe will cause some difficulty, both for causing drilling dysfunction and for sensor integration and data telemetry. The judges will look for creative concepts supported by sound reasoning showing an understanding of how the BHA, bit and drillstring function together, and how the downhole system measures, samples and transmits the drilling data.

3.7.2. Upon request, the bit shall be returned to the Committee following Phase II testing for reconditioning for use in future competitions.

3.7.3. One (1) PDC bit will be provided by DSATS to be used during the Phase II tests. For 2019-2020 the bit will be:

3.7.3.1. A micro-bit 1.5" in (38.1 mm) diameter and 2.0" in total length.

3.7.3.2. Low axial aggressiveness and high side aggressiveness (i.e. high bit anisotropy).

3.7.4. Students are encouraged to consider bit wear prior to the final test and its impact on drilling performance during the onsite testing. Based on prior competitions, bit wear should be minimal but some cutter damage is always possible.

3.7.5. Student teams may build or buy similar drill bits to test their design with the rock samples they sourced. The students must not engage any third parties or receive professional assistance in designing their own bit, however manufacturing can be performed by a third party.

3.7.6. For the final competition, the students may use the directional drill bit provided by DSATS, or use their own bit design. However, the dimensions of their bits must not exceed 1.5 inches in diameter and 2 inches long. This provision is made to enable students to fully optimize the bit design for their specific directional system.

3.8. Drillpipe

3.8.1. Stainless steel tubing will be permitted for the competition. Preliminary typical tubing specifications are listed below to assist with the mechanical and electrical design of the rig.

3.8.2. The drill pipe specifications for the 2019-2020 competition are subject to change, but should be:

3.8.2.1. Round Aluminum Tube 3/8 inch diameter x 36 inches long; 0.049 inch wall or equivalent

3.8.2.2. The material from KS Precision Metals is a typical low alloy material: "Our Aluminum tubing with wall thickness of .035 or .049 is 6061 T6"

3.8.3. DSATS will not be providing tubing to the competition teams.

3.8.4. The use of a metric equivalent of the tubing is permitted.

3.8.5. Tubing is usually available from various hobby shops such as K-S Hobby and Craft Metal Tubing and via Amazon and other suppliers.

http://www.hobbylinc.com/htm/k+s/k+s9409.htm

ROUND ALUMINUM TUBING		
OUTSIDE DIAMETER INCHES	WALL THICKNESS	ID
3/64 (.047)	.014	.019
1/16 (.0625)	.014	.035
5/64 (.078)	.014	.050
3/32 (.094)	.014	.066
	.016	.062
7/64 (.109)	.014	.081
1/8 (.125)	.014	.097
9/64 (.141)	.014	.113
5/32 (.156)	.014	.128
11/64 (.172)	.014	.144
3/16 (.187)	.014	.159
	.022	.143
	.035	.117
	.049	.089
13/64 (.203)	.014	.175
7/32 (.219)	.014	.191
	.022	.175
	.035	.149
15/64 (.235)	.014	.207
1/4 (.250)	.014	.222
	.016	.218
	.022	.206
	.035	.180
	.049	.152
9/32 (.281)	.014	.253
	.016	.249
5/16 (.312)	.014	.284
	.016	.280
	.035	.242
	.049	.214
11/32 (.344)	.016	.312
3/8 (.375)	.016	.343
	.035	.305
	.049	.277
13/32 (.406)	.016	.374
7/16 (.437)	.016	.405
	.035	.367
15/32 (.468)	.016	.436
1/2 (.500)	.016	.468
	.035	.430
17/32 (.531)	.016	.499
9/16 (.562)	.016	.530
5/8 (.625)	.016	.593

3.9. Tool joints

3.9.1. Students may design their own tooljoints as long as the design concept is included in the Phase I proposal.

3.9.2. Alternately, students may use commercially available connectors/fittings attached to the drillpipe using threads, epoxy cement or other material, and/or may use retaining screws if desired, as long as the design concept is included in the Phase I proposal.

3.9.2.1. A fitting used somewhat successfully in 2017 is available from Swagelock. In 2018, the winning team used a fitting from Vertex.

3.9.2.2. A fitting used successfully in 2016, but which did not work well in 2017, is available from Lenz (http://lenzinc.com/products/o-ring-seal-hydraulic-tube-fitting/hydraulic-straight-connectors) that uses a split-ring to allow a torque transfer across the fitting.

3.9.3. Students must state <u>WHY</u> they choose a tooljoint design in the Phase I proposal.

3.10. Bit sub/drill collar/stabilizers

3.10.1. It is expected that each team will design and build their own bit sub, instrumentation of the bit sub is ideal for directional sensors

3.10.2. Additional weight may be added to the bit sub, or surface weight/force (above the rock sample) may be applied to provide weight on bit and drillpipe tension

3.10.3. Stabilizers are permitted but will be limited in length. Advise the committee of your choice and why and include this in the Phase I design for committee consideration.

3.10.4. Students must add sensors to the drillstring, but are not permitted to instrument the rock samples. They must have a smaller diameter than the stabilizers and bit by at least 10%. Please include design concepts in the Phase I design.

3.10.5. The addition of along-string sensors to measure vibrations, verticality and/or tortuosity or other parameters will receive extra consideration. They must have a smaller diameter than the stabilizers and bit by at least 10%.

3.11. Automated Drilling

3.11.1. Drilling automation should be considered a combination of data, control AND dynamic modeling so that the control algorithm can determine how to respond to differences between the expected and actual performance. Process state detection can often enhance automation performance. Refer to documents posted on the DSATS website for more information.

3.11.2. Once drilling of the sample commences, the machine should operate autonomously. Remote operation and/or intervention is not allowed.

3.11.3. All directional control operation should be autonomously controlled by the drilling rig

3.11.3.1. Manual intervention to add and/or remove a steering mechanism (e.g. whipstock) is permitted, however the determination/calculation of the orientation setting of the mechanism is required to be autonomous and must be shown on the rig floor display during each steering mechanism manipulation activity

3.11.3.2. Length and timing of drilling modes (e.g. switching from slide drilling to rotational drilling, initiating the directional surveying procedure at the appropriate survey interval), must be autonomously determined/calculated and controlled

3.11.3.3. Directional surveys acquired by the system need to be used as feedback for the steering control (and/or calculation of the steering requirements) logic.

3.11.4. Set-point commands for drilling parameters (WOB, RPM, ROP, etc.) should be optimized such that drilling dysfunctions are avoided, and drilling can be completed within the given time frame. Real-time optimization should be done automatically. The controllers need to ensure that the drilling parameters respond once the set points are altered.

3.12. Sensors

3.12.1. The team may elect to use existing oilfield sensors or may look to other industries for alternate sensors.

3.12.2. The team may develop its own sensors if so desired.

3.12.3. Sensor quality differs from data quality. Both are important considerations in this competition.

3.12.4. The final report shall address which sensors were selected and why. The sensor calibration process shall also be explained.

3.13. Data collection and handling

3.13.1. The team may elect to use standard data collection and recording techniques or may develop their own. Data handling techniques and why they were chosen should be described in the Phase I submittal.

3.13.2. The final report shall address which data systems were selected and why.

3.13.3. The observed response time of measurements, data aggregation and control algorithms should be compared to the Phase I estimates.

3.13.4. Describe how data is measured, aggregated, stored and retrieved. Describe calibration and data validation techniques used.

3.14. Data visualization

3.14.1. Novel ways of presenting the data and progress of drilling in real time while drilling will receive particular attention from the judges.

3.14.2. Visualization of the processes (automation, optimization, drilling state, etc.) should be intuitive and easily understood by the judges, who will view this from the perspective of the driller operating a rig equipped with automated controls.

3.14.3. Data must be presented in a format that allows the judges to easily determine bit depth, elapsed drilling time, ROP, MSE, verticality/inclination, vibration, and any other calculated or measured variable used to outline the drilling rigs performance to the judges. Lack of an appealing and usable Graphic User Interface (GUI) will be noted to the detriment of the team.

3.14.4. All depths shall use the industry-standard datum of rotary/kelly bushing interface (RKB), which should be the top of the rig's "drill floor."

3.14.5. And End of Well (EOW) report should be provided to the judges at the conclusion of drilling.

3.14.6. See Appendix "A" for directional surveying-specific data visualization requirements

3.15. Measure and analyze the performance

3.15.1. The drilling machine should react to changing "downhole" conditions to select the optimal drilling parameters for improved performance, as measured by the rate of penetration (ROP), mechanical specific energy (MSE), verticality, cost per foot or meter, and other standard drilling measures or key performance indicators. Adding parameters such as MSE, or similar features, to the control algorithms will receive special attention from the judges.

3.15.2. Design limits of the drilling machine shall be determined and shall be incorporated in the programming of the controls during the construction phase.

3.15.3. Downhole measurements from directional sensors are to be used for adjusting drilling parameters and control of drilling machines used to aid in directional drilling

3.15.4. The final report (see Clause 3.19) shall outline drilling performance and efficiency criteria and measured results.

3.15.5. One of DSATS' goals is to promote plug and play capability to accelerate the implementation of drilling automation. A DSATS committee is preparing definitions and examples of proposed data communication protocols and interfaces. Once this is available, the Drillbotics® competition will require the use of these standard protocols. This will not be a requirement for 2020 but it will be included in future competitions. Links to these standards will be added to the Drillbotics.com website when they are published.

3.16.   The test well:

3.16.1. The competition will take place on the same day for all teams in North America, and the same day (likely different from the North American date) for all teams in Europe. The competition will take place at a facility capable of hosting all drilling rigs at the same time, and capable of having all drilling rigs start drilling at the same time (Category I and II). Location of drilling to be conducted indoors, in a location that does not have an unusually distorted magnetic field.

3.16.2. Prior to the commencement of the test, teams will attach a bell nipple per 3.5.3. They will then manually drill the pilot hole not to exceed 1" deep.

3.16.3. When the test begins, the teams will start drilling autonomously by continuing to drill the pilot hole, keeping the wellbore as vertical as possible until reaching the kick-off point. All rigs start the drilling competition at the same time (Category I and II)

3.16.4. The teams will kick off from vertical at any depth below the 4" vertical surface hole

3.16.5. The teams will attempt to hit multiple targets (varying X/Y coordinates and vertical depths) by following a provided directional plan/trajectory. Directional objective scoring will be based on the accuracy of the target depth intersection (i.e. horizontal distance from the target coordinate at the given target vertical depth). Refer to Appendix "A" for additional directional objective details.

3.16.6. No lateral forces may be applied above the rock.

3.16.7. Drilling will stop at 3 hours or when the last team exits the rock sample.

3.16.8. Should be drilled with a maximum allowable Weight-On-Bit dependent on the rig and dynamic drillstring integrity.

3.16.9. Will not require a closed-loop fluid circulation system, but could be of advantage for directional drilling, the bit and machinery should be cooled with air or fluid/water if needed. The design of the fluid system, if any, should be included in the Phase I design.

3.16.10. The rock sample will be homogeneous and will be capable of aiding in closed-loop fluid circulation. Note that the rock samples will leak once the drillbit punctures a rock face, so a rig design that includes a containment system is required.

3.16.11. Will require casing to fit in the directional wellbore. The ability to "run casing" is the secondary judging metric. Judges will run a "flexible" casing used as a gauge of borehole quality

3.16.12. Will not require a rig move, walking or skidding, but the mobility of the rig will be considered in the design phase.

3.17. Not included in the 2019-2020 competition

3.17.1. The drilling will not include automating the making or breaking of connections. If connections are necessary due to the rig and drillstring design, connections should be made manually, and the time involved with the connections will be included with respect to its effect on drilling performance (rate of penetration reduction).

3.18. Presentation to judges at Phase II Testing

3.18.1. The judges will arrive at the centralized test site facility to meet with the student teams and advisors immediately prior to the Phase II testing. DSATS will provide a suitable meeting room for discussion lasting about two hours.

3.18.2. The students will present a BRIEF summary of their final design, highlighting changes from their Phase I design, if any. Include an explanation of why any changes were necessary, as this indicates to the judges how much students learned during the design and construction process. Explain what measurement and control features have been deployed. Describe novel developments or just something learned that was worthwhile. Also include how actual expenses compared with the initial estimate. (Previous teams used a short PowerPoint presentation of about ten slides or so. Use any format you like.) Be sure to include all your team members as

presenters, not just one spokesperson. At some time during your talk, let us know who the team members are and what background they have that pertains to the project.

3.18.3. Judges will ask questions to ascertain additional details about the design and construction process and to see if all team members have a reasonable understanding how all the various disciplines used for the rig design and construction fit together.

3.18.4. All teams may sit in for the presentations and Q&A of the other teams. The order of presentation will be determined by drawing lots.

3.19.   Project report

3.19.1. The student team shall submit to DSATS a short monthly project report that is no more than one page in length (additional pages will be ignored) due on or before the last day of each month that will include:

3.19.2. Phase I

- Key project activities over the past month.
- Rig design criteria, constraints, tradeoffs, and how critical decisions were determined
- Cost updates
- Significant new learning, if any

3.19.3. Phase II

- Construction issues and resolution
- Summary of recorded data and key events
- Drilling parameters [such as WOB] and how they impact the test
- Other items of interest

3.19.4. Report content

3.19.4.1.   To teach students that their work involves economic trade-offs, the monthly report should include at a minimum a summary estimate of team member labor hours for each step in the project: design, construction, testing, reporting, and a cost summary for hardware and software related expenditures. Also include labor for non-students that affect the cost of the project. Labor rates are not considered, as to eliminate international currency effects. Labor is not considered in the cost limits of item 6.1, but should be discussed in the report and paper.

3.19.4.2. Design reports must contain the following tables and place them in their design report appendices:

A. Student Biographies

- Name

- Previous degree attained – major

- Current degree and expected graduation date (month/year)

- Main area of contribution to the project

- Other information as deemed appropriate by the team

B. Summary of Calculations (list these at a minimum, list other is a similar format)

Parameter	Symbol	Calculated Results		Safety Factor	Max Allowable		Reference	(Other as needed)
		Field Units	Metric Units		Field Units	Metric Units		
Critical buckling load								
Burst limit								
Torque limit								
… Other								

C. Power Consumption (rename devices as appropriate)

Device	Voltage	Current	Estimated		Single or Three φ	(Other as needed)
			HP	Watts		
Rotation						
Hoist						
Pump						
… Other						
Controls						
Displays						
…						
Total						

D. Diagram showing maximum dimensions of rig when operational (Include all auxiliaries) [Needed to determine size of display area as the Drilling Conference and confirm the height is within the limits imposed by the conference organizers]

E. Chargeable Weight of Rig (include shipping crates/boxes for rig and auxiliaries)

- The Chargeable Weight of Freight shipments are calculated as the Actual Weight (Gross Weight) or the Volumetric (also called Volume or Dimensional) Weight of the shipment, whichever is the greater. This uses an estimated weight that is calculated based on the dimensions (length, width and height) of a package (shipments are always shown in the order of L x W x H). Typically, large items with a light overall weight take up more space on an aircraft than a small, heavy item. That's why the shippers charge according to Chargeable Weight.
- Multiply the length by the width by the height (L x W x H) in inches to obtain the cubic inches, then:
- To obtain the dimensional weight in pounds using inches, divide the cubic inch result by 166
- To obtain the dimensional weight in kilograms using inches, divide the cubic inch result by 366
- Using Dimensions in Centimeters: To obtain the dimensional weight in kilograms using centimeters, multiply the length by the width by the height (L x W x H) in centimeters and divide the result by 6000

F. Finances

Teams are responsible for estimating the cost to attend the nearest local test site and the next SPE/IADC Drilling Conference. The cost is not used to evaluate the team's design. It is simply to help the Drillbotics® committee estimate the total expense to hold the competition. Items that should be included are:

- Rig transportation costs
- Student and supervisor travel: transportation
- Visas (also include a statement if visas applications must be made well in advance)
- DSATS will estimate hotel and per diem costs

3.19.5. File naming convention

    3.19.5.1. To avoid extra work by the committee to rename all files, please use this convention for:

        3.19.5.1.1. Monthly reports

                Year-Month# University Name (abbreviated)

                (note this is the competition year (spring term))

                Example 2020-09 UDC

        3.19.5.1.2. Design reports

                Year University Name (abbreviated)

                (note this is the competition year (spring term))

                Example 2020 University of Drillbotics® Competition

3.20. Final report and paper

3.20.1. The finalists shall prepare a project report that addresses the items below. We suggest you use the format of most SPE papers. For reference, please see http://spe.org/authors/resources/

3.20.2. The winning team of Group A and Group B shall update the report as needed to comply with SPE paper submittal guidelines to write a technical paper for publication by the SPE at its Annual Drilling Conference. SPE typically requires that the manuscript is due in the fall following the Phase II test. While the Drillbotics® committee will make every effort to have the paper presented during the Drilling Conference, the SPE Program Committee has authority over which papers will be accepted by the conference. If the paper is not accepted by the conference, the Drillbotics® committee will endeavor to have it presented at the DSATS Symposium and will use its contacts to have the paper published via other related SPE conferences.

3.20.3. The report, paper and all communications with DSATS shall be in the English language. The presentation will be made by at least one member of the student team.

3.20.4. The timing for submittal of the abstract and paper will be the published deadlines per the call for papers and conference guidelines as posted on the SPE's website (www.spe.org).

3.20.5. The abstract must generate sufficient interest with the SPE review committees to warrant publication, although DSATS will help promote acceptance where possible

3.20.6. The paper should address at a minimum

3.20.6.1. The technical and economic considerations for the rig design, including why certain features were chosen and why others were rejected.

3.20.6.2. The setup of the experimental test, the results and shortcomings.

3.20.6.3. Recommendations for improvements to the design and testing procedures.

3.20.6.4. Recommendations for improvements by DSATS of the competition guidelines, scheduling and provided material.

3.20.6.5. Areas of learning gained through the competition not covered in the university course material.

3.20.6.6. A brief bio or CV of the team members and their sponsoring faculty.

4. *Group B Competition Guidelines*

    4.1. Challenge overview for the 2019-2020 competition: The newly added Group B challenge requires teams to develop a drilling system model and corresponding control scheme to virtually drill a directional well to a given plan. The Group B challenge does not involve building a rig or drilling system. The teams will design automation and control similar to Group A, but will develop a virtual drilling system (i.e. computer models) to test and demonstrate the controls. Therefore, in addition to the guidelines specified below, Group A Competition Guidelines section in general, and applicable guidelines from Group A, Phase 1 in particular, should be referred. While the teams will have to meet minimum competition requirements, any "above and beyond" work along the main theme will be rewarded additional points to encourage creativity and innovation.

    4.2. Design: Since the challenge does not require rig construction, the scope of the design portion is limited – the teams are not expected to carry out detailed mechanical design of the rig, but are expected to perform basic calculations for a realistic system. The scope includes selecting essential elements such as drive mechanism, BHA, surface systems for application of WOB and RPM, and other required components for the virtual system. Please refer to Group A Challenge, Phase 1 guidelines for the drilling system requirements and the target.

    4.3. Modeling:

        4.3.1. The drilling system model should predict bit trajectory for given WOB, RPM, drive mechanism parameters (e.g. steering force, AKO angle), and rock strength – as a function of time, measured depth, or true vertical depth. While the teams are empowered to decide on the complexity of the simulation model, the minimum requirements are stated below.

        4.3.2. Bit model: The bit model can be as simple as the equivalent model of Pessier et al. (1992) with appropriate framework for steerability such as bit anisotropy and bit tilt such as Menand et al. (2012). Effect of key parameters such as gage length, drilling efficiency (MSE-DOC relationship) should be included. Inclusion of bit wear effects is not mandatory.

        4.3.3. Rock/wellbore: The rock model should be defined by rock type, UCS, and could vary with depth. At each simulation step increment, the bit drills and extends the wellbore. While calculation of explicit contact forces with the wellbore are not mandatory, the build rate could still change due to newly formed wellbore geometry and changing rock strength.

4.3.4.<u>BHA</u>: The resulting behavior of drive mechanism should be modeled (e.g. resulting tilt, side force, etc.) The drive mechanism should take commands from a control system and change parameters accordingly. The BHA should also (virtually) measure certain parameters and return to the surface or the control system. The bit-to-sensor distance as well as measurement frequency (i.e. intermittent vs continuous survey) should be a configurable parameters in the design.

4.3.5.<u>String</u>: A simple spring model is sufficient for modeling the string elasticity effects. Wellbore friction should be included.

*4.3.6.*In addition to predicting the wellbore trajectory in 3D (inclination and azimuth), calculations for buckling and tool face disorientation should be performed. Any additional considerations such as dynamics of bit/BHA/string will be rewarded.

*4.3.7.*The modeling assumptions should be clearly stated. The implementation (or sub-models) should be verified against published data such as Menand et al. (2012).

4.4. Controls: The control system may include the following elements

*4.4.1.*Drilling Optimization: Optimize set point commands for drilling parameters such as WOB, RPM, etc. such that drilling performance and steering are optimized. Such real-time optimization should be done automatically.

*4.4.2.*Trajectory Control: Steer the well according to the given well plan trajectory. The objective is both to minimize trajectory error and wellbore tortuosity. Virtual surveys should be acquired and be used as feedback for the steering control logic. Appropriate steering control scheme for the chosen mechanism (e.g. RSS, AKO motor, etc.) should be developed.

*4.4.3.*The steering model should include considerations for how often the survey is taken and how far from the bit the sensors are placed (e.g. projecting from the survey depth to the bit, and the control system using survey information to decide steering parameters).

*4.4.4.*The system should be able to achieve up to 30 degrees inclination, 15 degrees azimuth, and 10" displacement (departure from the vertical axis) while drilling through a moderate strength rock within 24" TVD.

*4.4.5.*Real-time display of the drilling parameters and wellbore positioning during the final testing is mandatory. End of well report immediately after the competition is mandatory.

*4.4.6.*Set Point Control: Although set point control, i.e. automatic control of drilling parameters as per optimal set points, is an integral element of the drilling systems, this competition does not make

it mandatory to reduce complexity. It can be assumed that the surface parameters such as WOB and RPM reach the BHA, making quasi-static modeling sufficient. However, the teams are encouraged to go "above and beyond" and demonstrate set point control independent of trajectory drilling. For example, the WOB and RPM control could be implemented for the virtual drill rig with a suitable mechanism for applying WOB (e.g. dead weight and drawworks), RPM (e.g. top drive), etc. Characteristics for each sub-system could be assumed realistically (e.g. top drive motor characteristics with RPM-TRQ relationship). Other examples include slide/rotate mode control.

4.5. Coding:

4.5.1. The entire code should be written with a modular design with functions/subroutines for each sub-system. The drilling system model should be a separate application that interacts with the control system. Appropriate interfaces (APIs) should be developed for interoperability and deployment.

4.5.2. Teams are encouraged to share their code to promote the learning spirit. Such sharing can occur during or after the final presentations, or after securing any IP protection, at the discretion of the teams. However, release of codes is not mandatory and will not count towards the final score.

4.6. Evaluation:

4.6.1. The drilling plan will be presented to the teams on the day of competition. The plan will involve up to 30 degrees inclination, 15 degrees azimuth, and 10" displacement (departure from the vertical axis). The rock properties will be provided as a function of true vertical depth or measured depth. The teams are given maximum of three hours to virtually drill the well. Students are allowed to debug/modify the code and use multiple attempts within the allotted time.

4.6.2. An RSS or AKO motor BHA will be specified on the day of the competition. Thus, the model should be capable of simulating both steering systems.

4.6.3. On the day of the competition, Drillbotics may provide data to calibrate sub-models such as the bit model. Additional details will be released during Phase 2.

4.6.4. While sharing of code is not mandatory, the presentations should include the details of the control schemes. Organizers can be contacted in case of any confidentiality requirements.

4.6.5. The set point control is not a mandatory item for the competition. Any demonstration of such capability will attract extra points in "above and beyond" category.

4.7. Deliverables:

4.7.1. <u>Phase 1</u>: A report containing detailed literature review, the selected drilling system per Group A, Phase 1 guidelines, overall plan of the virtual system with definition of sub-systems and sub-models, mathematical framework for modeling and control schemes, a plan for implementation, and relevant details.

4.7.2. <u>Phase 2</u>: A deployable application that drills a directional well to a given plan using autonomous control of a virtual drilling system.

4.8. Useful resources:

4.8.1. Pessier, R. C., & Fear, M. J. (1992, January 1). Quantifying Common Drilling Problems With Mechanical Specific Energy and a Bit-Specific Coefficient of Sliding Friction. Society of Petroleum Engineers. doi:10.2118/24584-MS

4.8.2. Menand, S., Simon, C., Gerbaud, L., Ben Hamida, M., Denoix, H. J., Cuillier, B., Sinardet, H. (2012, January 1). PDC Bit Steerability Modeling and Testing for Push-the-bit and Point-the-bit RSS. Society of Petroleum Engineers. doi:10.2118/151283-MS

4.8.3. Pehlivantürk, C., D'Angelo, J., Cao, D., Chen, D., Ashok, P., & Van Oort, E. (2019, March 4). Slide Drilling Guidance System for Directional Drilling Path Optimization. Society of Petroleum Engineers. doi:10.2118/194096-MS

4.8.4. Marck, J., Detournay, E., Perturbation to Borehole Trajectory across an Interface, ARMA-2014-7479, 48th US Rock Mechanics/Geomechanics Symposium, Minneapolis, Minnesota, June 1-4, 2014.

4.8.5. Zalluhoglu, U., Marck, J., Gharib, H., & Zhao Y. (2019) Borehole Propagation with Undergaged Stabilizers: Theory and Validation. ASME Journal of Dynamic Systems, Measurement and Control, vol. 141, no. 5: 051013. doi: 10.1115/1.4042380

4.8.6. Perneder, L., Marck, J. and Detournay, E., 2017. A model of planar borehole propagation. SIAM Journal on Applied Mathematics, 77(4), pp.1089-1114. doi: 10.1137/16M1094518

4.8.7. Zalluhoglu, U., Demirer, N., Marck, J., Gharib, H., & Darbe, R. (2019) Steering advisory system for rotary steerable systems. SPE/IADC Drilling Conference and Exhibition, 5-7 March, The Hague, The Netherlands. SPE-194090-MS, doi: 10.2118/194090-MS

4.8.8. Zalluhoglu, U., Gharib, H., Marck, J., Demirer, N., & Darbe, R. (2019) Steering advisory system for mud motors. SPE/IADC Drilling Conference and Exhibition, 5-7 March, The Hague, The Netherlands. SPE-194077-MS. doi: 10.2118/194077-MS

4.8.9. Franklin, G. F., Powell, J. D., Emami-Naeini, A., & Powell, J. D. (1994). Feedback control of dynamic systems, 3rd Edition, Reading, MA: Addison-Wesley.

4.8.10. Ogata, K. (2003). System dynamics, 4th Edition, Upper Saddle River, NJ: Prentice Hall.

4.8.11. Ogata, K. (2009). Modern control engineering, 5th Edition, Upper Saddle River, NJ: Prentice Hall.

4.8.12. Li, Y., Ang, K. H., & Chong, G. C. (2006). PID control system analysis and design. IEEE Control Systems Magazine, 26(1), 32-41.

4.8.13. Rawlings, J. B. (2000). Tutorial overview of model predictive control. IEEE control systems magazine, 20(3), 38-52.

4.8.14. Webinar: Machine Learning and Physics-based Solutions for Drilling Automation by SPE Distinguished Lecturer Prof. John Hedengren, Brigham Young University Link: https://www.youtube.com/watch?v=trW7MwDx77M

4.8.15. Note: A more complete and live webinar with a demo will be available in May 2020: https://webevents.spe.org/products/drilling-automation-and-downhole-monitoring-with-physics-based-models

4.8.16. Video and Webinar Series: Understanding Control Systems by Mathworks Link: https://www.mathworks.com/videos/series/understanding-control-systems-123420.html

5. *Team Members*

5.1. DSATS envisions that the students would be at least senior undergraduate or Masters level, well versed in the disciplines needed for such a project. The maximum number of students per team is five (5) and the minimum shall be three (3). Any team that loses team members during the project can recruit a replacement.

5.2. At least one member of the team must be a Petroleum Engineering candidate with sufficient coursework completed to understand the physics relating to the drilling problems and the normal industry practices used to mitigate the problem.

5.3. Students with a background in mining, applied mathematics, mechanical and electrical engineering, as well as controls, mechatronics and automation or software development, are the most likely candidates, but students with any applicable background is encouraged.

5.4. A multi-disciplinary team simulates the working environment in the drilling industry today, as most products and services are produced with the cooperation of technical personnel from differing backgrounds and cultures.

5.5. A university may sponsor more than one team but must submit only one team/design for Phase II evaluation.

5.6. Students shall register their team not later than 30 November using the registration form on the Drillbotics® website. Any changes to the team members or university supervisor over the course of the competition should be reported in the monthly reports.

6. *Expenditures*

6.1. Teams selected to advance to the second phase must limit the cost of the rig and materials to US$ 10,000 or its equivalent in other currencies. The students shall find a source of funding and report the source in the Phase I proposal. All funding and procurement should comply with university policy. These funds are intended to cover the majority of expenses for hardware, software and labor to construct and operate the team's equipment. DSATS shall not be liable for any expenditure other than DSATS provided material and specified travel expenses.

6.2. DSATS will assist when possible to obtain free PLCs or similar control devices from suppliers affiliated with the DSATS organization. Such "in-kind" donations shall not be included in the team's project costs.

6.3. Students and universities may use other "in-kind" contributions which will not be included in the team's project costs. Such contributions may include modeling software, laboratory equipment and supplies, and similar paraphernalia usually associated with university laboratory projects.

6.4. Any team spending more than US$ 10,000, or its equivalent in other currencies, may be penalized for running over budget.

6.5. DSATS reserves the right to audit the team's and university's expenditures on this project.

6.6. Any devices built for the project will become the property of the university and can be used in future research and competitions. Any maintenance or operating costs incurred after the competition will not be paid by DSATS.

7. *Other Considerations*

7.1. The design concepts shall be developed by the student team under the supervision of the faculty. Faculty and lab assistants should review the designs to ensure student safety (see Appendix B).

7.2. Construction of the equipment shall be supervised by the student team, but may use skilled labor such as welders and lab technicians. The use of outside assistance shall be discussed in the reports and the final paper. DSATS encourages the students to gain hands-on experience with the construction of the rig since this experience will be helpful to the career of individuals in the drilling industry.

7.3. University coursework and credit: Each university will decide whether or not this project qualifies as a credit(s) towards any degree program.

8. *Project Timeline*

Phase I - Design:	Fall 2019
Submit monthly reports	On or before the final day of each month
Submit final design to DSATS	30 Nov 2019, midnight UTC
Submit an abstract to DSATS*	30 Nov 2019, midnight UTC

*DSATS will submit an abstract to the SPE that will include excerpts from the student abstracts by the conference paper-submittal deadline, typically in mid-summer, for consideration of a paper by the conference program committee.

Phase II – Construction and Testing	Spring 2020
DSATS to announce finalists	On or about 15 Jan 2020
Construction	Spring 2020
Monthly reports	On or before the final day of each month
Drilling Test	Specific on-site test locations and dates for the North American and European locations to be arranged not later than 31 March 2020. The testing will typically occur in late May or early June.
The timeline for the Phase II tests:	Day 0 Students arrive
	Day 1 Students rig up; judges arrive
	Day 2 Students present to judges
	Day 3 Performance tests
	Day 3 pm/Day 4 Students rig down and depart

Shipping of rig to test site	The rig should be shipped to arrive no earlier than 10 days before the test date. Each team will coordinate with the committee and provide any documentation necessary.
NOTE:	Teams must consider shipping delays that can occur due to Customs clearance or shippers re-routing vessels.
Prepare and submit paper	Per SPE deadline*
Prepare and submit presentation	Per SPE deadline
Present paper at the Drilling Conf	Per SPE and DSATS schedule

9. *Evaluation Committee*

9.1. DSATS will select an evaluation committee from its membership

9.2. Criteria/Weighting for Group A (see chart):

Criteria	Parameter	Weighting
Phase I:		
a. Safety	Safety: construction and operation	10
b.Mobility of rig	Rig up, move, rig down	5
c.Design considerations and lessons learned		10
d.Mechanical design and functionality, versatility		25
e.Simulation/Model/Algorithm		25
f.Control scheme	Data, controls, response times	25
	Total	100%
Phase II:		
a.Creative Ability	Analysis, concepts, development	10
b.Engineering Skills	Problem/Goal, design criteria, feasibility	10
c.Construction Quality		10
d.Cost Control		10
e.Performance		30
Various parameters such as:	ROP, MSE, Landing Bit, Inclination, and other	
Are these used within the control algorithms		
Accuracy of drilled wellbore trajectory (see Appendix "A" for details)	Proximity of drilled wellbore to required target X/Y coordinates and vertical depths	
f.Quality of wellbore	Tested using the Go-No-Go flexible 'Casing'	10
	Verticality, tortuosity, caliper, other	
g. Data	Data handling, data visualization, data comparison to judges' wellbore logs, and other	20
h. Downhole Sensor Data Used in Control Algorithm	Pass/Fail	Pass/Fail
	Total	100%
Intangibles	Additional score may be added or subtracted by the judges at their discretion	

Criteria	Metrics	Weight
Drilling system model	Does the bit-rock interaction model consider rock properties, basic bit design parameters (aggressiveness, gage configuration), etc.? Does steering model consider steering method, geometry (e.g. projection-to-bit algorithm), bit side force/tilt, new wellbore, etc.? Are string elasticity, wellbore friction modeled?	30
Control scheme	Does trajectory control algorithm use realistic constraints? Does it use of realistic virtual-measurements? Does it consider surveying uncertainties and noise? Does the model utilize a re-planning to target process based on as-drilled surveys? Is basic drilling optimization algorithm implemented? Are rig controls simulated? (e.g. slide vs rotate)	30
The Virtual Drilling App	Features, modularity, and robustness of the app, real-time display, end of well report	10
Ability to calibrate the model	Calibration against the provided data	10
Performance	Demonstration of the app and the degree to which drilling objectives are met	20
Bonus	Considerations above and beyond the minimum requirements that demonstrate thoroughness and creativity	10
	Maximum achievable score out of 100	110

Group A Prizes

9.4. The winning team of Group A (Category I) will be sponsored by DSATS to attend the next SPE/IADC Drilling Conference to present a paper that explains their project in detail.

9.4.1. The program committee of the Drilling Conference awarded the Drillbotics® subcommittee a permanent slot in one of the drilling sessions at the conference. As per SPE's customary procedures, the paper will be archived in OnePetro. In addition, SPE has agreed to furnish a booth in the exhibition area during the conference where the team can erect their rig and describe its operation to the conference attendees. This is an excellent opportunity for students to network with the industry.

9.5. Upon submittal to DSATS of a valid expense statement (typically a spreadsheet supported by written receipts) of covered expenses will be reimbursed by the treasurer of DSATS for the following:

9.5.1. Reasonable shipping costs of the Drillbotics® rig to and from the conference as long as charges are pre-approved by the chair or co-chair of the Drillbotics® subcommittee.

9.5.2. Round trip economy airfare for the team and one university sponsor/supervisor to the gateway city of the next SPE/IADC Drilling Conference. Entrants should use the SPE approved carrier where possible to minimize cost. Airfares that exceed the SPE rate must be pre-approved by the committee or the reimbursement will be limited to the SPE rate. Information of reduced fare flights is available on the conference website. Please note that reservations must be made before the SPE published deadline. The departure point will be a city near the university, the student's home, or current place of work, subject to review by the Committee. Alternately, a mileage reimbursement will be made in lieu of airfare should the entrants decide to drive rather than fly to the conference. The reimbursement is based on current allowable mileage rates authorized by the US Internal Revenue Service.

9.5.3. One rental car/van at the gateway city for those teams that fly to the conference.

9.5.4. Lodging related to one hotel room per team member will be reimbursed at a rate not to exceed the SPE rate. Note that the room reservations are limited, so entrants must book their rooms early. Room and taxes for the night before the DSATS symposium, the night of the symposium and for the nights of the conference are covered. Charges for the room on the last day of the conference need to be pre-approved by the Committee as most conference attendees depart on the last day of the conference unless there are unusual circumstances.

9.5.5. A per diem will be pre-approved by the Committee each year, which will vary with the cost of living in the gateway city. The per diem is intended to cover average meals (breakfast, lunch and dinner) and incidentals.

9.5.6. ATCE registration will be reimbursed. Students should register for the conference at the student rate. Early registration is appreciated.

9.6. Individual award certificates will be presented to all participants upon request, with special certificates given to all finalists.

9.7. DSATS may provide additional awards, at its sole discretion.

9.8. The evaluation and all decisions on any matter in the competition by the DSATS judges and DSATS board are final.

10. Group B Prizes

10.1. The winning team of Group B will submit a SPE Whitepaper that explains their project in detail. If the quality of the abstract is approved by the SPE Conference Program Committee, as per SPE's customary procedures, the paper will be archived in OnePetro

10.2. Individual award certificates will be presented to all participants upon request, with special certificates given to all finalists.

10.3. DSATS may provide additional awards, at its sole discretion.

10.4. The evaluation and all decisions on any matter in the competition by the DSATS judges and DSATS board are final.

11. Terms and conditions

11.1. In no event will SPE, including its directors, officers, employees and agents, as well as DSATS members and officers, and sponsors of the competition, be liable for any damages whatsoever, including without limitation, direct, indirect, special, incidental, consequential, lost profits, or punitive, whether based on contract, tort or any other legal theory, even if SPE or DSATS has been advised of the possibility of such damages.

11.2. Participants and Universities agree to indemnify and hold harmless SPE, its directors, officers, employees and agents, as well as DSATS members and officers, and sponsors of the competition, from all liability, injuries, loss damages, costs or expenses (including attorneys' fees) which are sustained, incurred or required arising out of participation by any parties involved in the competition.

11.3.   Participants and Universities agree and acknowledge that participation in the competition is an agreement to all of the rules, regulations, terms and conditions in this document, including revisions and FAQs posted to the DSATS and Drillbotics® websites (see section 2.1).

11.4.   Winning teams and finalists must agree to the publication of their names, photographs and final paper on the DSATS web site.

11.5.   All entries will be distributed to the Drillbotics® Committee for the purpose of judging the competition. Design features will not be published until after all teams have been judged and a winner is announced. Previous years' submittals, reports, photos and similar documentation will be publicly available to foster an open exchange of information that will hopefully lead to faster learning for all participants, both new and experienced.

11.6.   DSATS and the SPE cannot provide funding to sanctioned individuals and organization per current US law.

11.7.   Participants must comply with all local laws applicable to this contest.

12. Marketing

12.1.   Upon request, DSATS will provide a link on its website to all participating universities.

12.2.   If university policy allows, various industry journals may send a reporter to witness the tests and interview students to publicize the project.

12.3.   Drillbotics is now a registered trademark. According to international law, the proper reference is to use Drillbotics® instead of Drillbotics™. The trade mark reference is only needed the first time Drillbotics is referenced.

12.4.   Any team that wishes to use the trademark on signs, tee shirts, technical papers or for other purposes may receive a no-cost license upon request. Send the request by email to the committee at 2020@Drillbotics.com. Upon completion of the license agreement, access to the files with the logo will become available.

- End -

Appendix

A. Directional Objective Requirements

The following attached pages describe the directional objectives as well as the data/deliverables requirements. Scoring for the directional competition objective will be primarily based on how accurately the directional targets are intersected by the calculated well trajectory.

Objectives

- Hit one or more targets at one or more vertical depth(s) and X/Y coordinates
- The starting directional plan to hit the targets will not require wellbore inclinations in excess of 30° from vertical, 15° change in azimuth, or 10" displacement (departure from the vertical axis at well center)

Automation Requirements

- Drilling mode/survey mode switching must be automated (i.e. built-in survey interval and drill string movement for on/off-bottom, slide/rotation mode switching)
- Steering requirements (e.g. toolface direction, slide length) must be calculated autonomously
  - NOTE: Steering mechanism can still require human intervention for placement and/or retrieval (e.g. whipstock) but orientation of steering mechanism must be calculated by the system and shown on the rig floor display.
- Directional surveying process must be entirely autonomous
  - Survey qualification must be done autonomously, however secondary qualification/verification/override can be made by a human
- Dogleg severity required to hit target(s), distance/direction to plan must be autonomously calculated at each survey station and shown on the rig floor display

Deliverables Requirements (Magnetic surveying)

- All teams are required to provide a definitive directional survey (TXT, LAS, or CSV format) meeting the following minimum requirements:
  - Header info to include:
    - Team/school name
    - Directional Survey Date
    - Well Center Coordinates (WGS84 Latitude & Longitude)
    - True Vertical Depth Reference (in depth units above block level)
    - Grid Convergence
    - Geomagnetic model used (if applicable)
    - Magnetic declination applied (Geomagnetic model or in-field referenced)
    - Total Azimuth Correction
    - Magnetic field dip reference (Geomagnetic model or in-field referenced)

- Total magnetic field strength reference (Geomagnetic model or in-field referenced)
- Error model associated with well trajectory (ISCWSA/OWSG error model or otherwise)
  - If non-standard error model is being used (i.e. formulas being modified and/or coefficients being changed), error model description (using standard variable/coefficient naming conventions) and justification must be included in project design
- Minimum Curvature calculated trajectory (using appropriate survey station interval to accurately represent the drilled wellbore position)
  - Each survey station is to include the following data:
    - Measured Depth
    - Inclination
    - Azimuth (referenced to "block north")
    - True Vertical Depth
    - Northing (from well center)
    - Easting (from well center)
    - Dogleg Severity
  - Final survey station is to be an extrapolation to total depth at the bit
- All teams are required to provide plan vs. actual plots containing the following minimum requirements:
  - As-drilled trajectory and original planned trajectory shown on same TVD vs. Vertical Section plot
    - Vertical section direction to be determined by well center-to-target bearing
  - As-drilled trajectory and original planned trajectory shown on same X/Y plot
    - Grid north reference to "block north"
    - [0,0] at well center
- All teams are required to provide directional survey raw data logs containing the following minimum requirements:
  - Each log entry is to include the following data:
    - Time stamp (containing year, month, date, hour, minute, second)
    - Sensor measured depth
    - Downhole sensor value(s) recorded
      - Sensor axes values
      - Calculated survey qualifier values
    - Accepted survey indicator (if log entry is an intended survey station)
      - If secondary (i.e. human) qualification is also used, both acceptance indicators must be shown

B. Safety

The team's safety plan should consider all foreseeable hazards and methods to mitigate them. Personal protective equipment is part of a safety plan but is far from sufficient. Teams must consider risks due to handling the rock, rotating machinery, electrical shock and others. How the team communicates with each other before and during rig operations is also important. Judges will grade each team on its comprehensive safety case.

Because most of the rigs have equipment spinning at high RPMs, some form of protective cover must be included in the team's rig design. A broken coupling, a loose screw or similar item becomes a projectile that can lead to serious injury to the team members, judges or visitors. Judges may decide to deny a team from competing if their design is unsafe.

The following links are a good starting point, but is by no means a comprehensive list of links:

- OSHA Pocket Guide, Worker Safety Series:
  https://www.osha.gov/Publications/OSHA3252/3252.html
- OSHA Checklist for General Industry: http://www.scosha.llronline.com/pdfs/genind.pdf